國 立 交 通 大 學

應用化學系 博士班

博士論文

無機螢光粉在提升矽基太陽能電池轉換效率之應用

Enhancing the Performance of Si-Based Photovoltaic Cells Using Inorganic Phosphors

研究生：陳彥吉

指導教授：陳登銘 博士

中華民國 100 年 6 月

摘要

如何提升太陽能電池的轉換效率向來為極具挑戰的課題，矽基材太陽電池的轉換效率與矽半導體對太陽光譜中不同波長的響應呈現密切相關，如何改善矽基材對不同波長的吸收，以提高太陽能電池的轉換效率一向為熱門研究趨勢。本論文的研究之主旨為以太陽光譜轉換技術，利用網印塗佈技術結合上/下轉換螢光粉與各型元件結構之太陽電池，期望有效改善矽太陽能電池之轉換效率。

本研究利用 X-光繞射進行螢光粉晶相鑑定、激發、發射與反射光譜探討螢光粉發光特性、掃描式電子顯微鏡術分析螢光粉微結構與太陽光譜模擬機進行光電轉換參數與電流-電壓曲線之量測。

此外，成本低廉、簡易可行的網印技術則被使用於將下轉換螢光粉 $Na_2CaPO_4F:Eu^{2+}$ 與 $KMGd(PO_4)_2:Eu^{3+}$ (M =Ca, Sr)塗佈於太陽能電池正面，利用螢光粉將太陽光譜紫外波段轉換成可見光，藉以增加矽基板轉換效率。實驗證實：經 $Na_2CaPO_4F:Eu^{2+}$ 塗佈後，太陽電池之效率由 15.93%增至 16.59%；而經三種 $KCaGd(PO_4)_2:x\%Eu^{3+}$ 螢光粉分別塗佈後，太陽電池之轉換效率增加值分別為 $0.66\pm0.01\%$ (x = 10)、$0.71\pm0.01\%$ (x = 50)與 $0.52\pm0.01\%$(x = 100)。

此外，本研究亦將上轉換螢光粉 $La_2Mo_2O_9:Yb, R$ 與 $KCaGd(PO_4)_2:Yb,R$ (R = Er, Ho)分別網印塗佈於太陽能電池之背層，

實驗證實，不同化學組成的螢光粉可以提高太陽能電池轉換效率不等，結果顯示：上轉換螢光粉塗佈太陽能電池中，以 $La_2Mo_2O_9$:Yb,R 塗佈者，其效率分別增加 0.25-0.29± 0.01% (R = Er)與 0.44± 0.01% (R = Ho)。另一方面，以 $KCaGd(PO_4)_2$:Yb,R 塗佈者，其轉換效率分別增加 0.44± 0.01% (R = Er)與 0.59± 0.01% (R = Ho)。

本研究已掌握具有高效率頻譜轉換螢光材料、穩定且可靠的漿料與不同元件結構太陽電池之供應，經初步試驗證實太陽電池轉換效率之增幅最高可達5%，預期可望縮減矽太陽電池轉換效率提升所需之成本。

Abstract

Given the challenges associated with global warming, the development of green energy materials has been recognized as an important issue in materials research. The solar cell is one of the devices that can be used to generate sustainable energy. The power conversion efficiency (η) from light to electricity in the silicon-based photovoltaic (PV) cells is highly dependent on the wavelength of the incident sunlight, and the η–λ relationship is characterized by the spectral responsively. In this research, we have utilized the solar spectral conversion principle and predesigned device structures to investigate the enhancement of efficiency by coating PV cells with down-conversion or up-conversion phosphors using low-cost screen-printing technique. In addition, X-ray diffraction, fluorescence and reflection spectra, and SEM imaging as well as solar simulator were used for characterizations and measurements of phosphor-coated PV cells.

Composition-optimized down-conversion phosphors (i.e., $Na_2CaPO_4F:Eu^{2+}$ and $KMGd(PO_4)_2:Eu^{3+}$ (M =Ca, Sr)) and upconversion phosphors (i.e., $La_2Mo_2O_9$:Yb,R and $KCaGd(PO_4)_2$:Yb,R (R = Er, Ho)) were selected to investigate their potential in efficiency enhancement. With coating of $Na_2CaPO_4F:Eu^{2+}$ on the front side of PV cells, the η value was found to increase from 15.93% to 16.59%; whereas the

experimental $\Delta\eta$ values were found to be 0.66±0.01% (x = 10), 0.71±0.01% (x = 50), and 0.52±0.01% (x=100), respectively, when $KCaGd(PO_4)_2:xEu^{3+}$ was screen-printed on the surface of PV cells. Furthermore, with the coating of $La_2Mo_2O_9$:Yb,R (R = Er, Ho) on the back side of PV cells, the experimental $\Delta\eta$ values were found to be 0.25-0.29± 0.01% (R = Er) and 0.44± 0.01% (R = Ho), respectively; whereas those were found to be 0.44± 0.01% (R = Er) and 0.59± 0.01% (R = Ho), respectively, when $KCaGd(PO_4)_2$:Yb,R was screen-printed on the back side of PV cells.

In this work, by using spectral conversion principle we have demonstrated the feasibility of efficiency enhancement in Si-based PV cells through screen-printing various phosphors onto the front/rear sides of the commodity PV cells. We have prepared phosphors with different functionalities and secured quality-reliable binders and PV cells with predesigned structures and achieved an optimal enhancement rate of 5% in experimental $\Delta\eta$ value. Our pioneering research may serve as a guide and a promising alternative in reducing the cost of enhancing conversion efficiency of PV cells for the PV industries.

Keywords: Photovoltaic cells; Spectral conversion; Upconversion phosphors; Screen printing technique; $Na_2CaPO_4F:Eu^{2+}$; $KCaGd(PO_4)_2:Eu^{3+}$; $La_2Mo_2O_9$:Yb,R (R = Er, Ho); $KCaGd(PO_4)_2$:Yb,R (R = Er, Ho)

誌謝

時間飛逝，轉眼間已經七年，博士班的訓練可真是扎實，能夠順利畢業首先得感謝我的恩師陳登銘教授，在老師的細心指導與提攜下，終於能夠完成博士學位，這七年來在生活與課業上得到老師莫大的啟發。此外，也要謝謝實驗室夥伴的陪伴：德茹學姊、靜萍學妹、阿豪學弟、怡親學妹、依蓉學妹、婉妤學妹…等，由於有大家陪伴，這七年過的很精彩。另外我想特別感謝我的家人，我的爸媽，我的岳父母，還有我可愛的老婆與兒子，非常感謝大家這七年來對我的支持與鼓勵，讓我能夠順利完成我的學業。

在此刻的心情是開心的，因為即將進入職場邁入下一階段，迎接新的未來，人生有夢、築夢踏實。

總目錄

圖目錄

表目錄

第一章 緒論

1.1 螢光體簡介

螢光的定義最早是在西元1852年斯托克斯(G. G. Stokes)用分光計觀察奎寧和葉綠素溶液時，發現其發光波長較入射光波長稍長，由此推論此係由物質吸收能量並發射不同波長光所致，而非由光的漫射作用所造成，斯托克斯稱這種光放射為螢光。而螢光體(Phosphor)一詞源來自拉丁文 *phosphorus*，而其來自希臘文*phōsphoros*，其字面上的意義為light bringer或 light-bearing之意思。

簡單來說，螢光體就是物質經由激發原激發之後能夠放光的一種物質。絕大多數分子在室溫時均處在電子的最低振動能階，稱為基態。如下圖1所示：當物質吸收了與它所具有的特徵頻率相一致的光子時，其電子由原來的能階躍遷至第一電子激發態或第二電子激發態中各個不同振動能階(a 點、b點)。其後，大多數分子常迅速降落至第一電子激發態的最低振動能階，在過程中它們和周圍的同類分子或其他分子撞擊而消耗了能量，因而不發光(c點)。分子在第一電子激發態的最低振動能級停留約10^{-9}秒之後，直接下降至電子基態的各個不同振動能階，此時以光的形式釋放出多餘的能量，所發生的光即是螢光。[1]

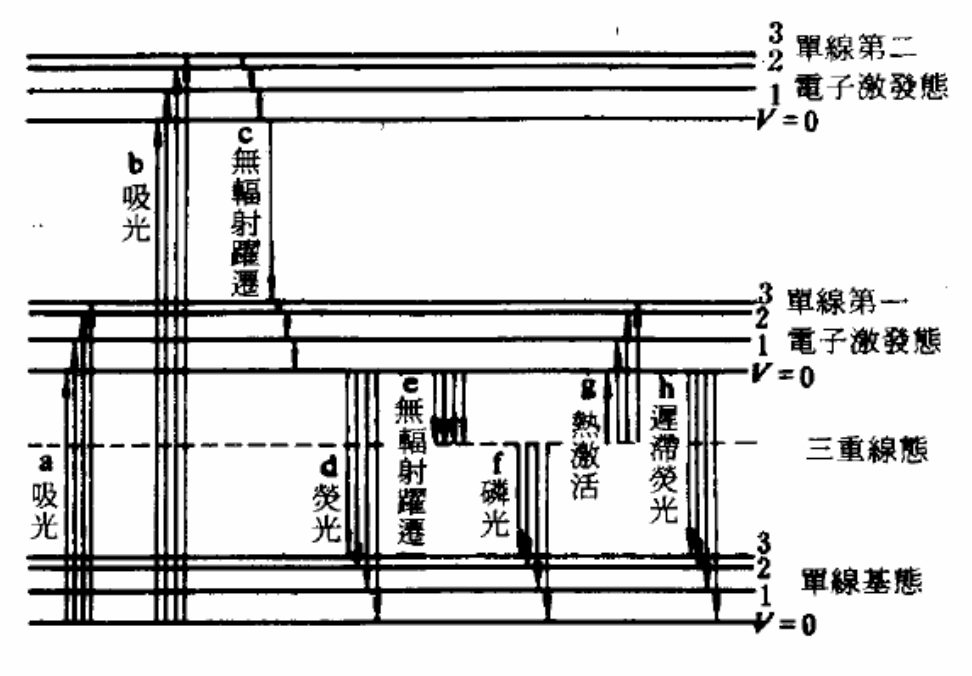

圖 1 物質能階躍遷與放光形式示意圖

一般而言螢光體可分成有機及無機兩大類。很多的有機分子，本身就具有放射螢光的能力。例如深海裡就有一些浮游生物如：水母，體內含有螢光物質，能夠發射螢光。無機螢光體通常是由主體化合物及活化劑組成，主體化合物本身通常不會發光，而是靠活化劑摻雜活化之後才會發光。無機螢光體的優點，就是可以精確地控制主體化合物與活化劑的比例，利用活化劑含量的改變，可以改變螢光發光的強度、波長與效率。只要少量的活化劑就能改變主體發光特性。此外，若能改變主體化合物的組成，則能有效調控螢光發光的光色。此外，也有一些化合物，不需活化劑就能發光，這類螢光體稱為「自發光螢光體」。螢光體的用途十分廣泛，舉凡日常生活中使用的日光燈管、電視機到新穎平面顯示器、新世代二極體照明光源，甚至生物科技，

都不能缺少它，螢光體早已以各種不同的形式存在於日常生活中，儼然是現代人生活的一部分。

1.2 機螢光材料之特性

一物質經由適當方式激發，提供其能量，可能產生一些能量吸收和轉換的過程。若此材料在吸收能量後，最後經由光輻射的方式，將能量釋放，則稱為發光材料。

按照激發能量以及方式的不同，一般可將發光類型分為下列幾類：

(1) 光致發光（photoluminescence）。

(2) 陰極射線發光（cathodoluminescence）。

(3) 電場發光（electroluminescence）。

(4) 熱發光（thermoluminescence）。

(5) 摩擦發光（triboluminescence）。

(6) 化學發光（chemiluminescence）。

(7) 生物發光（bioluminescence）。

(8) X 射線發光（x-ray luminescence）。

無機螢光材料是由一個材料主體（host）以及摻雜少量雜質作為活化劑（activator）所組成，有時須摻雜另一種雜質作為敏化劑

（sensitizer），而活化劑及敏化劑部分取代主體晶格中原有格位的離子，形成雜質缺陷，由這些缺陷所引起的發光稱為激活發光，而活化劑在發光材料中所扮演的角色為發光中心，其受到外來的能量激發後會產生特徵的可見輻射，圖2螢光體發光過程中能量傳遞示意圖[2]。而敏化劑的加入，可將所吸收之能量傳遞給活化劑，使能量能更有效地以發光的形式釋放，圖3螢光體中主體、活化劑與增感劑三者交互作用示意圖。[3]

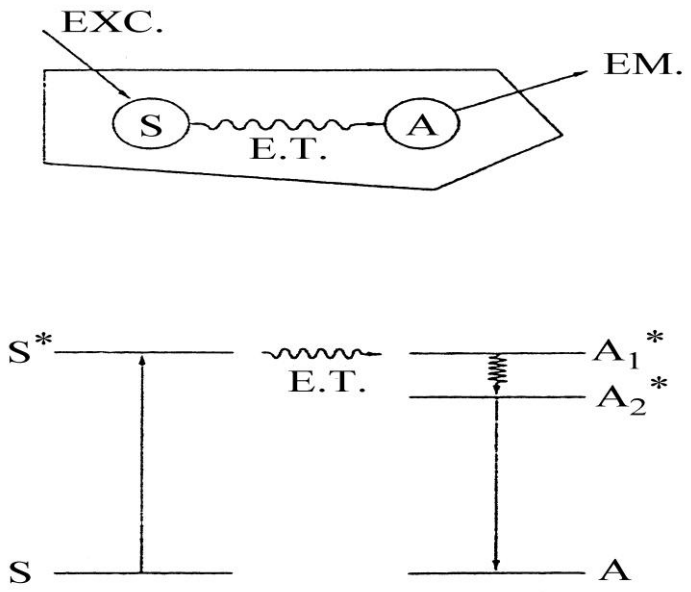

S：敏化劑　S^*敏化劑激發態 ET：電荷轉移

A_1^*：活化劑激發態，A_2^*活化劑低激發態，A：活化劑

圖 2 螢光體發光機制與能量傳遞示意圖[2]

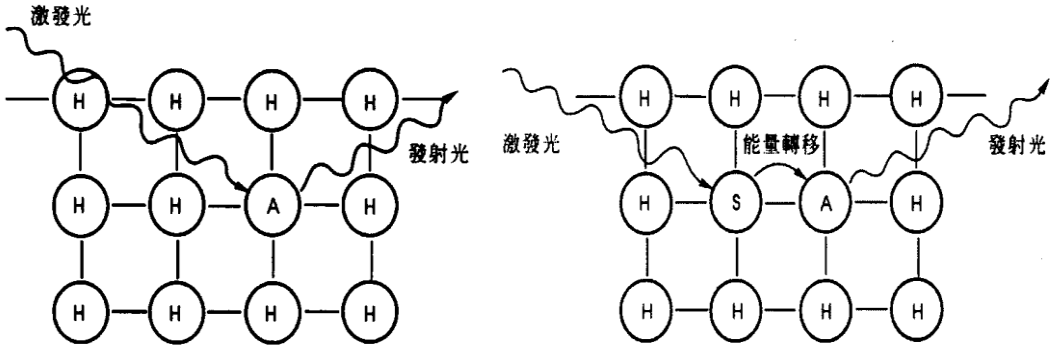

圖 3 螢光體中主體、活化劑與增感劑三者交互作用示意圖[3]

1.3 螢光材料的設計

一般而言，無機螢光體主要由主體晶格(host lattice)及活化劑(activator)構成，有時可摻加適當增感劑(sensitizer)。化學式以 H:A 或者 H:A,S 表示，如：$Y_2O_2S:Tb^{3+}$、$SrAl_2O_4:Eu^{2+},Dy^{3+}$等。兩個中心間的能量傳遞可為通過發光的再吸收或激發能量的無輻射傳遞兩種，如果兩個中心之間具備以下條件，就可能發生高效的能量傳遞。

(1) 活化劑和增感劑的基態和激發態之間的能量差是否相等，以及活化劑和增感劑之間是否互相共振，可根據增感劑的發射光譜和活化劑的吸收光譜是否重疊加以判斷。

(2) 活化劑和增感劑之間存在著適當的相互作用，相互作用可以是交換作用(如果活化劑和增感劑相距很近，波函數重疊)，也可以是電多極或磁多極之間的相互作用(如果相距較遠，彼此只

能藉助庫侖力相互作用)。

能量轉移的程序曾分別被 Forster.與 Dexter.以下列的式子描述：

$$P_{SA} = 2\pi/h \mid \langle S, A^{*} \mid H_{AS} \mid S^{*}, A \rangle \mid^{2} \cdot \int g_S(E) \cdot g_A(E) dE \quad [6]$$

其中，方程式中的積分值表示光譜重疊程度，P_{SA} 表示敏化劑到活化劑的能量傳遞概率，H_{AS} 表示利用哈密頓增感，S 和 S^{*}分別表示電子的基態和激發態的波函數。活化劑和敏化劑必須有共振的條件和存在相互作用，才可能有較高的能量傳遞機率，即較大的 P_{SA} 值。

1.3.1 主體晶格

無機螢光體的主體晶格通常為一個或數個陽離子與一個或數個陰離子團結合而成，通常主體在激發的過程中所扮演的角色為能量的傳遞者，而主體中的陽離子或陰離子通常不具光學活性，如此一來，能量的吸收與放射皆由活化劑進行。圖 4 的陰離子團則分為兩部分：一是不具光學活性的陰離子團，另一則是具有光學活性可充當活化劑之陰離子團，後者通稱為自身活化(self-activated)的螢光體，如 $CaWO_4$、YVO_4，圖 5 為週期表中可作為螢光體主體晶格的陰離子[4,5]。而作為主體陽離子的條件通常具有如鈍氣的電子組態(如 ns^2np^6 或 d^{10})或具封閉的外層電子組態(如：f^0、f^7、f^{14})，如此才不具光學活性，圖 6 為週期表中可作為螢光體主體的陽離子[4,5]。

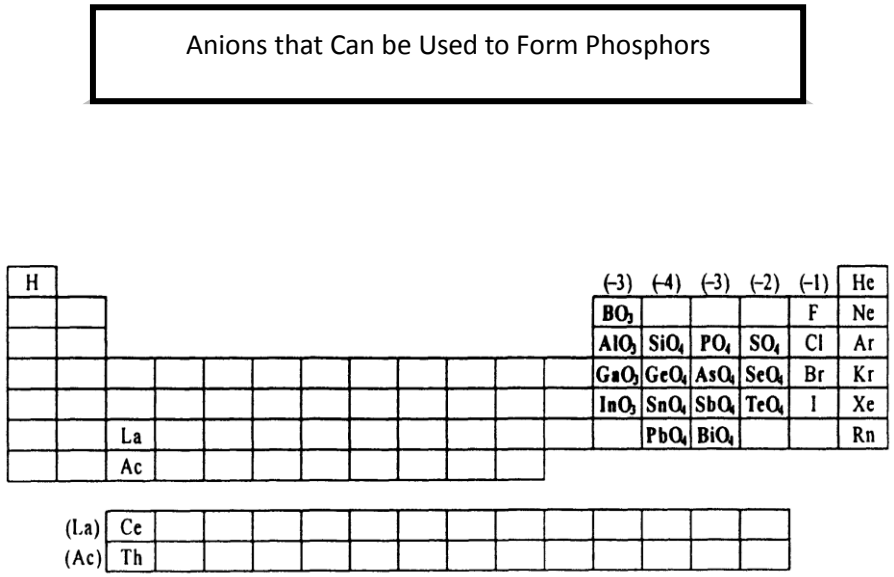

圖 4 週期表中可作為螢光體主體之陰離子團

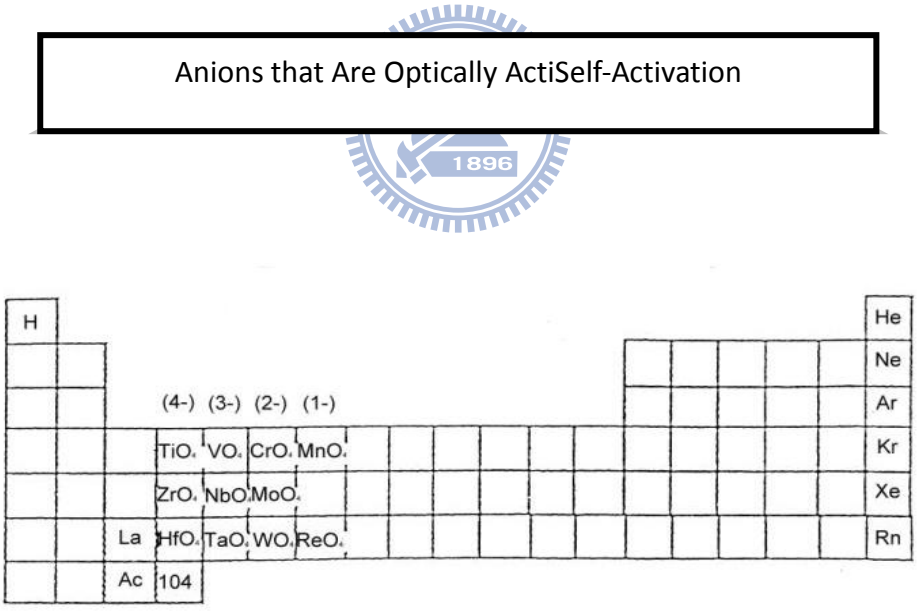

圖 5 週期表中可作為螢光體主體晶格的陰離子

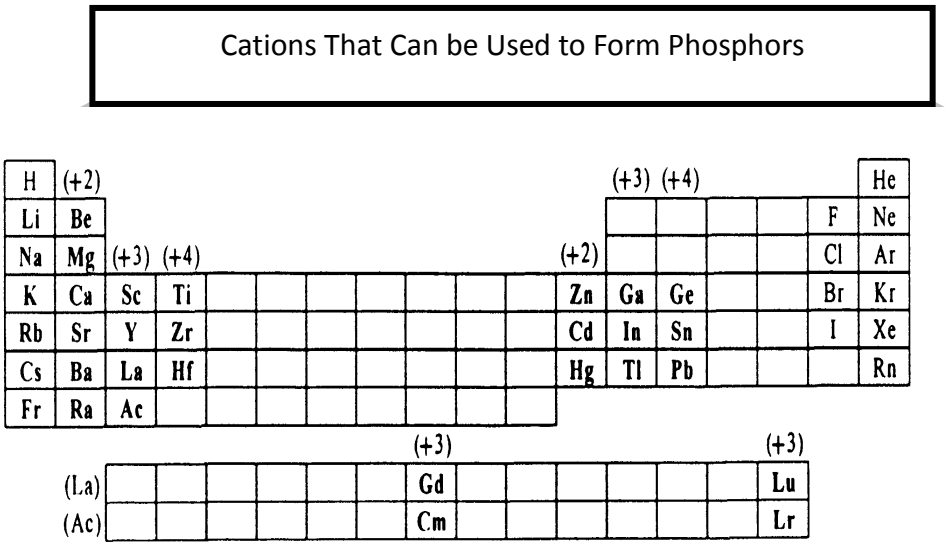

圖 6 週期表中可作為螢光體主體之陽離子

1.3.2 活化劑之選擇

一個適當的活化劑通常具有 $nd^{10}(n+1)s^{2}$ 的電子組態或是未填滿的外層電子之價態，而最重要是在主體晶格中，能穩定且以特定價數存在的離子，如圖 7 [4,5]所示。此外，摻雜至晶格中的活化劑的價態，在晶格中的位置、活化劑的配位環境，是否有增感劑存在，這些都會影響發光中心的結構和它的性質。下列規則可以提供我們選擇適當活化劑的參考，如：活化劑離子與主體晶格離子其離子半徑大小之搭配，若兩者離子半徑差異過大，則易造成晶格扭曲與殘留應力(residual stress)於晶格中，活化劑在主體晶格中的溶解度亦因此受限，進而降低螢光體發光效率。此外，當兩離子之價數不同，亦會造成電荷補償問題，也會使發光效率降低。在多數情況下，發現當活化劑的濃度達到並超過一定數值之後，發光效率不再繼續提高，反而開始下降，這

種現象稱之為濃度焠滅。其成因為活化劑濃度過高時，能量在活化離子之間的傳遞機率超過了發射機率，激發能量重複地在活化離子之間傳遞所造成。

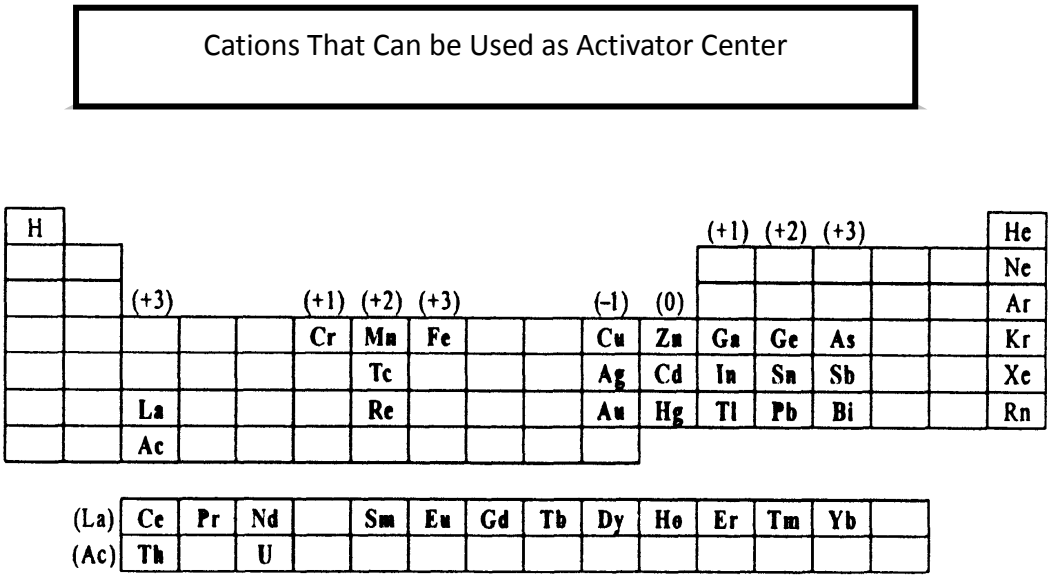

圖 7 週期表中可作為螢光體活化劑之陽離子

製備無機螢光體材料之控制要素，可區分為兩部分來探討：獨立性變因（independent variables）和依賴性變因（dependent variables）。

(一) 獨立性變因：

獨立變因計有：(1)材料的純度、(2)活化劑與主體離子大小差異程度、(3)主體晶格的選擇、(4)主體晶格內的電荷補償、(5)活化劑的選擇、(6)反應物的比例等六項，其中最重要的是螢光體的純度，螢光體之製程應儘可能避免其遭受到雜質污染。

(二) 依賴性變因：

依賴性變因可分為：(1)燒成溫度、(2)燒成時間、(3)燒成顆粒的大小、(4)燒成時的氣體環境、(5)活化劑濃度、(6)主體晶格結構的影響、（7）合成方法的影響、(8)反應物的比例與(9)助熔劑的使用等九項，由於這些變因之間，有相當的相互關聯性存在，不太容易直接歸究於何因素，需看個別情況而定。

1.4 無機螢光材料之分類

1.4.1 下轉換螢光體

一般而言，無機螢光體絕大多數為吸收高能的激發光(如:紫外光(UV)或是能量更高的真空紫外線(VUV))，造成電子躍遷到激發態後經由緩解而回到基態，其過程中放出的能量大部分會以光的形式釋放；此類的無機螢光粉種類繁多，例如:螢光燈粉，發光二極體螢光粉。通常我們以高能量光子激發螢光體，螢光體放射螢光的能量較激發光能量低、波長較長。例如，當我們用波長254 nm的紫外光激發螢光體，螢光體內的電子吸收激發能量後，會躍遷到高能量的激發態，經過一連串的非輻射緩解過程，電子會釋放部分能量、躍遷至另一能量較低的激發態，最後放射可見光返回基態。可見光能量較紫外光低、波長比紫外光長。螢光體發光因經一系列非輻射緩解過程，故放射的光能量會較原來吸收的能量低。

1.4.2 上轉換螢光體

是否所有螢光體放射的螢光，能量一定會比原來吸收的能量低？是否波長一定會比激發光波長為長嗎？答案是不一定。其實，有一種很有趣的物質，它可以放出能量比激發光高、波長比激發光短的螢光。此現象稱之為「上轉換」(Up-conversion)，其發光原理機制如圖8所示。以低能量紅外光光子激發上轉換螢光體，處於基態電子會吸收激發能量躍遷至激發態E1，若電子不立刻釋放出所吸收的能量，亦即位於E1能態的生命期夠長，則電子可能再吸收激發能量，繼續躍遷至更高能量的E2能階。經兩次能量吸收，此時電子具有高於20,000 cm^{-1}的能量，此為激發紅外光子能量的兩倍。當位於E2能階的電子釋放能量返回基態時，會釋放波長是原本紅外光的一半的可見光光子。利用此原理，可藉由觀察螢光體所產生的可見光，以偵測肉眼無法看見的紅外光，較著名的上轉換螢光體為$NaYF_4$:Yb,R (R = Er, Ho)。[10]

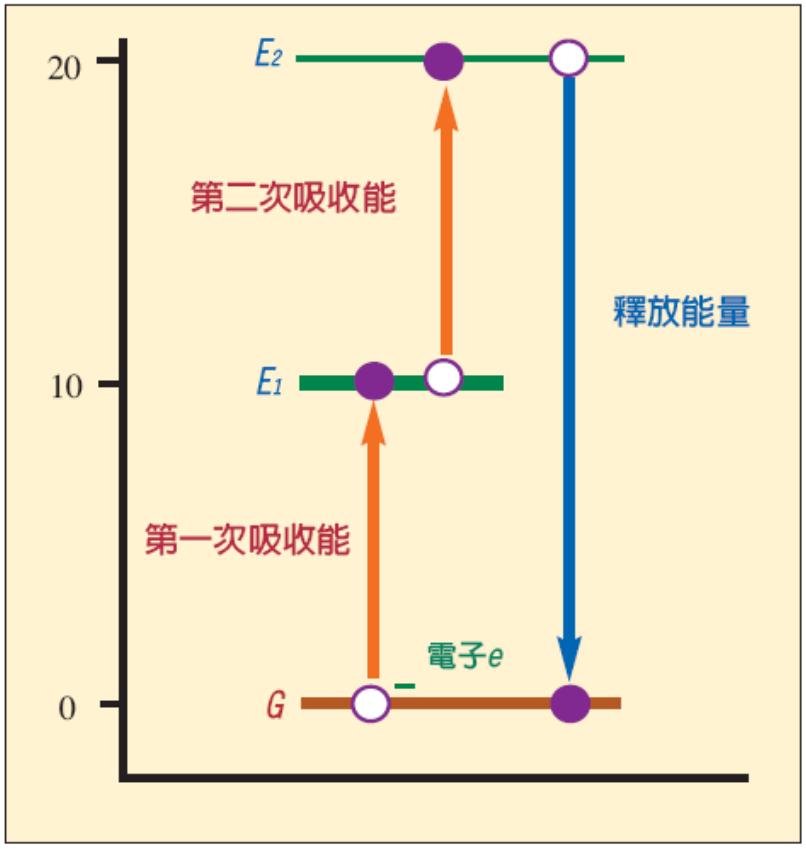

圖 8 上轉換原理示意圖：基態電子吸收能量躍遷至 E1 後，再吸收能量躍遷至 E2。從 E2 返回基態 G，放出的能量為單一激發能量的二倍。[6]

1.5 螢光體製備方法

螢光體的製備方法發展至今，由傳統的固態燒結法，到使用溶劑製備的濕化學方法(Wet chemical method)，其主旨不外乎是希望能發展出高均勻度、粒徑適中、高純度、高亮度以及高發光效率的螢光產物。以下將簡介一些常用且常見的螢光體製備法：

(1) 傳統固態法（Solid-state method）

傳統固態法通常使用金屬氧化物（metal oxides）或金屬碳酸鹽類(metal carbonates)為起始物，依所需比例混合研磨後，再進行後續的熱處理動作。此為一簡單且廣為應用的方法，但其缺點是產物的組成均勻度不佳，所以需要比濕化學方法更長的燒成時間及更高的燒成溫度，而且此法並無法有效的控制產物的粉體粒徑。

(2) 溶膠–凝膠法 (Sol–gel method)

此法主要是利用二元有機酸(dicarboxylic acid）與金屬鹽類混合均勻，以多元醇(polyol，通常為乙二醇 ethylene glycol)為溶劑，加熱攪拌或者是直接將金屬鹽類與多元醇加熱混合以形成金屬醇鹽錯合物(metal alkoxide)，經部分水解後，即可形成黏稠狀的凝膠(gel)，再經過熱裂解（pyrolysis）後，即可得到粉末狀前驅物。此法製程簡易、具有量產的潛能。溶膠溶膠法最大的優點在於能獲得組成均勻，粒徑大小可控制在一定範圍內，且再現性極佳。此外，此法並具有能塗佈（spray coating）於大面積基材上的特點，但是其缺點為金屬醇鹽錯合物取得成本較高，不利於商業化量產。

(3) 共沉澱法 (Coprecipitation Method)

共同沉澱法的基本原理，乃利用適當的沉澱劑(通常為有機酸、鹼)，如：草酸根(oxalate)、檸檬酸根（citrate）與碳酸根（carbonate）等，將各種不同的金屬離子從溶液中以相近的速率形成沉澱，再經過

過濾、乾燥等動作形成組成均勻的前驅物。此法的優點為合成容易，不需要特殊的設備或者昂貴的原料即可進行。此外，本法尚有程序的控制、原料的取得容易、製程再現性高、具量產潛能等優點。

(4)化學溶膠法 (Chemical colloid method)

此法為共沉澱法經修正後之製備方法，內容為分別配製陽離子及陰離子溶液，混合後所得之沉澱即為其前驅物，再經過後續的高溫熱處理即可得到所欲的螢光粉體，而上述溶液的混合速度及攪拌均勻的程度均可用以控制產物粒徑的大小與分佈。

(5) 氣溶膠熱解法(Aerosol pyrolysis method)

製程方法為將溶有離子的水溶液經噴霧器噴灑預先裂解，再於高溫爐中進行後熱處理以合成螢光體，其優點為簡便並可應用於量產。

(6) 微乳液法 (Microemulsion method)

利用油相（oil）、水相（water）兩個互不相溶的相態，加上界面活性劑，使得油相–水相界面的表面積擴張，表面張力下降；當表面張力下降到一定程度時，系統的表面活化能（或張力）之增加量相當小。因而產生乳化現象(Emulsification)，而當表面張力幾乎趨進於零或暫時為負值時，便會形成我們所稱的微乳液（micromusification）。

由於微乳液中的液滴直徑約在 0.01μm 至 0.1μm 之間，且粒徑分佈均勻，在 W/O 相微乳液中，水相被油相包覆在內，形成所謂反微胞

（reverse-micelle），化學反應如氧化、還原、水解等均可在微胞內進行，因此又可叫做“奈米反應器”（nanoreactor），此即為微乳液法的最大優點。

(7)水熱法 (Hydrothermal method)

此法適用於合成高溫不穩定相–即低溫相或次穩定相（metastable phase），以及含有特殊氧化態的化合物。水熱反應是在密閉反應器內進行，依反應溫度可區分為兩類：

(a)中溫高壓型：溫度範圍在 100℃～275℃間，所以適用於以鐵氟龍當內容器的 Parr acid digestion bomb(高壓反應器)，其容量約為 23 ml，材質的溫度及壓力上限分別為 260℃與 100 bar，一般使用 65 %的溶液填充度，將高壓反應容器置於高溫爐中加熱至反應溫度即可。此法雖然能承受的溫度與壓力有限，但是若能選擇適當的酸鹼 PH 值，亦能利用此反應器合成新穎化合物。

(b) 高溫高壓型(＞275℃)：此系統中，水熱反應是在密閉的高溫反應器內進行，水的臨界溫度與壓力分別是 374.1℃與 217.6 atm，在高溫高壓水熱反應系統中，水的性質變化包括：密度變低、表面張力變低、黏度變低等。所以當處於超臨界狀態時，水中離子的滲透速率會大幅增加，使得其中晶體的生長速度增快。

1.6 螢光體之應用與發展

發光材料的發明改變了人類傳統日出而做、日入而息的習性，使夜晚不在是那麼漆黑無光，而螢光體的發明更將夜晚修飾得更加璀璨繽紛。螢光體的研究歷史已經相當悠久，市面上處處可見應用螢光體所發展出的產品，如日光燈或顯示器等，為人類帶來便利的生活。人類日常日常生活上，以陰極射線管當做顯示裝置的產品琳瑯滿目，如電視、電腦螢幕、監視器等，其顯像的方式是經由電子槍所發射出的電子束撞擊屏幕上塗佈的螢光體，使其受激發而發光，達到顯像的目的。組成不同的螢光體會發射出不同顏色的光，經由紅、藍、綠三色光的調變，呈現螢幕上所看見的各種顏色。

第二章 文獻回顧與研究動機

2.1 太陽能電池簡介

在「能源危機」與「環保問題」的雙重訴求下，開發能自產的綠色能源，已成為人類的最重要課題，而太陽能具有同時具有普遍性、自產性及環保性，為最佳的再生能源之一。太陽能電池直接將太陽能轉換成電能，其運作不產生毒性物質、溫室氣體及噪音，其操作相當安全，亦僅需低廉的維護成本，況且太陽能為取之不盡、用之不竭的理想再生能源，發展太陽能電池應用的相關材料及技術，為解決現今能源及環保問題的最佳方法及策略。但是，以目前太陽能電池的發展大致上還是分為兩大類，第一類是以矽為基礎材料，第二類就是非矽基礎材料。第二大類目前比較多開發為：CdTe、染料敏化（Dye Sensitized Solar Cells, DSSC）、有機電池等，現階段的太陽能電池幾乎以第一類為主要發展，因為以矽為基礎材料的太陽電池轉換效率較高，其又可以分為：單晶、多晶、非晶矽、矽薄膜等，這些種類的優缺點就稍微整理為表1中。

目前的太陽能市場以單晶和多晶矽的太陽能電池為主，目前市售的單晶轉換效率約在20%，至於多晶的轉換效率約在17%。此均與理想目標的轉換效率差距甚遠。揭開太陽能發展歷史，1954年美國貝爾

實驗室首次研發能將光能轉換成電能的半導體元件-太陽能電池，其基本構造是運用P型與N型半導體組合而成。由基本的矽元素(能隙1.12 eV)摻入鋁或磷等元素，形成P(電洞)型與N(自由電子)型半導體，當太陽光照射時，光能將矽原子中的電子激發，而產生電子和電洞對流，上述電子和電洞均會受到內建電位影響，分別被N型及P型半導體吸引，而聚集在兩端。其操作原理如圖9所示。

表 1 各類太陽能電池的優點、缺點、發展方向

種類	優點	缺點	發展方向
單晶矽太陽電池	發電力與電壓範圍廣，轉換效率高，使用年限長(一般可達20-25年)	製作成本較高，及製作時間冗長	1. 高效率大面積之PEAL結構 2. 增加可利用的光波長範圍的新結構 3. .提升安全性
多晶矽太陽電池	製作步驟簡單， 不需使用成長單晶圓，故成本較單晶矽太陽電池低約20%，	效率較單晶矽低	1. 新材料的製造 2. 大面積、高效率、安定性提升 3. 新結構
非晶矽太陽電池	非晶矽電池為目前成本最低的商業化太陽能池，使用廣，多用於消費性電子。a-Si 薄膜太陽電池可解決大面積太陽電池所需材料不足問題	a-Si 戶外設置後輸出功率減少了約15~20% 的光劣化現象	1. 改善光劣性 2. 低成本化 3. 採用tandem cell結構、薄層化層
碲化鎘	易製作大面積薄膜且能再較便宜的玻璃與金屬基板上製作多晶薄膜，可構成hetero接面太陽電池	製作成本高	1. 新材料的製作 2. 新結構 3. 低成本化 4. multi-junction

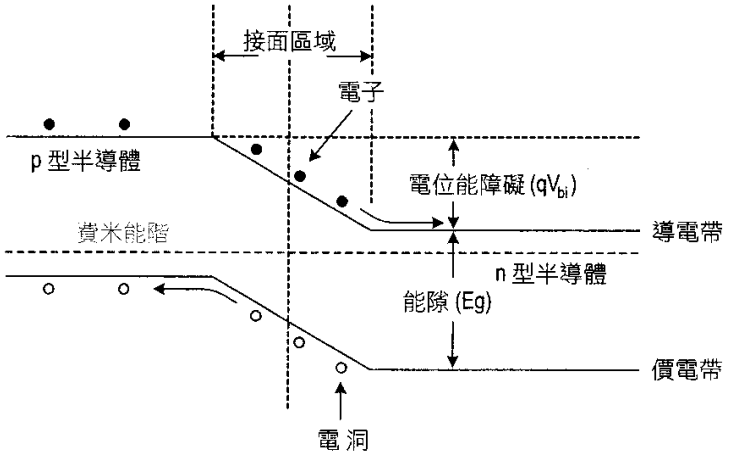

圖 9 p-n 接面型矽太陽電池元件之能帶示意圖

由就 p-n 接面型矽晶型太陽電池(圖 10(a))而言，其基本結構與組成上而下依次為電極、抗反射膜(Si_3N_4 或 SiO_2)、手指狀的歐姆接觸導電薄膜層、n-型矽基板、p-n 接合層、p-型矽基板與背面歐姆接觸導電薄膜層，其餘各類型 p-n 接面型矽太陽電池元件基本結構與組成如圖 10 所示。

在進一步探討太陽電池之前必須先了解其基本物理特性，一般最受關注為輸出特性、光譜響應感度 (spectral response)特性、照度特性、溫度特性、非相配(miss match)特性與二極體(diode)特性等六項[4]。圖 11 顯示太陽電池典型電流/電壓(I-V)輸出特性，I-V 關係會受溫度與照度影響。

.

.

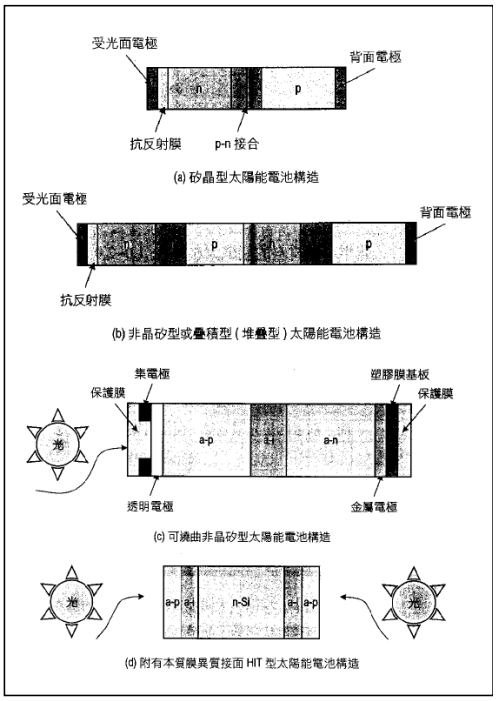

圖 10 各種 *p-n* 接面型矽太陽電池元件基本結構與組成：(a) p-n 接面型矽晶型太陽電池。(b)非矽晶型或積疊型太陽電池。(c) 可撓曲非矽晶型太陽電池。(d)具本質膜異質接面雙面受光 HIT(Heterojunction with Intrinsic Thin layer)型太陽電池。[4]

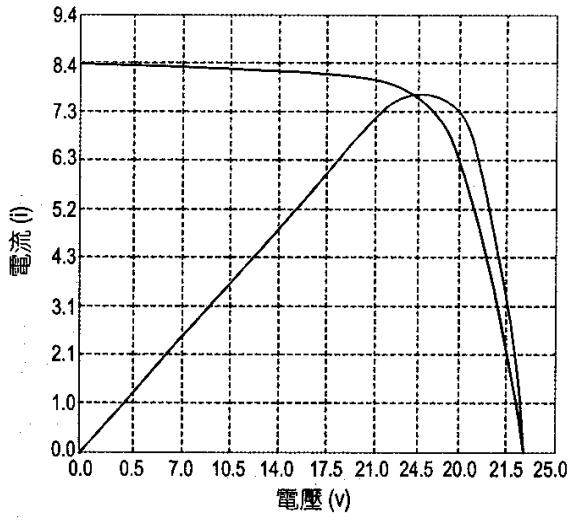

圖 11 太陽電池標準電流/電壓(I-V)關係

一般而言，太陽電池元件的理想 I-V 特性可以下列關係式表示

$$\mathbf{I} = I_s[\exp(q\mathbf{V}/kT)-1]-I_L$$

其中 V 為電壓、I_s 為二極體飽和電流、而 I_L 為電源電流，此一公式所繪製之曲線分布於圖 12(a)直角座標系統之第四象現所圍成的區域，此相當於此一電池元件所輸出之功率，圖 12 (a)中所顯示之四方形面積即為該元件之最大輸出功率，圖 12(a)與(b)亦顯示短路電流(I_{sc})、斷路電壓(V_{oc})、最大電流值(I_{max})與最大電壓值(V_{max})之意義。

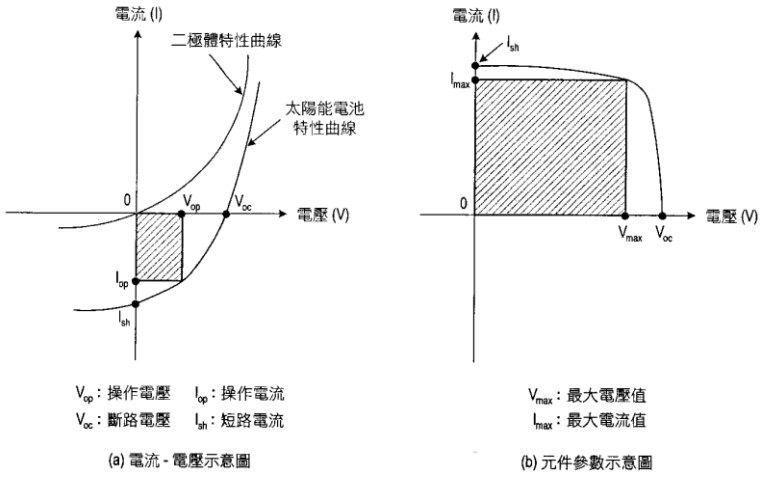

圖 12 (a) 太陽電池元件 I-V 關係曲線。(b)短路電流(I_{sc})、斷路電壓(V_{oc})、最大電流值(I_{max})與最大電壓值(V_{max})之比較

此外，太陽電池光譜響應感度特性可以由圖 13 加以說明，圖中顯示電池中光電能量轉換僅發生於特定波長範圍，而在此範圍之外則不具光電能量轉換之特性。而日光輻照光子流通量分佈曲線則顯示入射太陽光譜將受到大氣的吸收、反射、散射等效應以及此一元件表面入射角之影響而產生不同程度之變化。

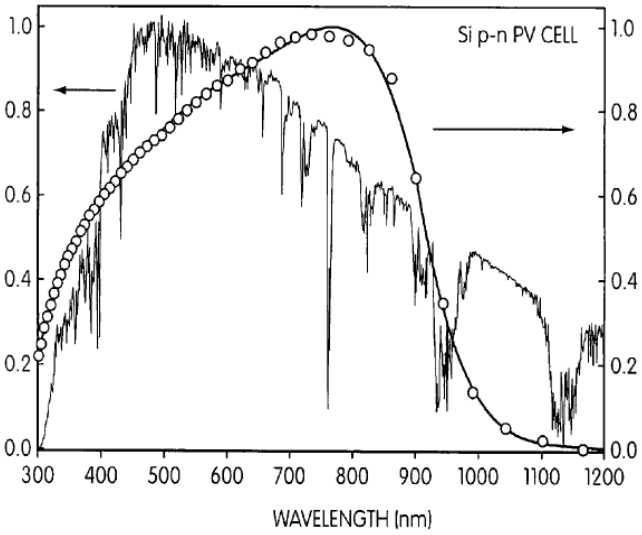

圖 13 AM1.5G 日光輻照光子流通量分佈曲線與典型矽太陽電池之內部光譜響應

此外由於太陽電池為兩種不同屬性半導體所組成的二極體元件，其典型的 I–V 曲線如圖 14 所示。

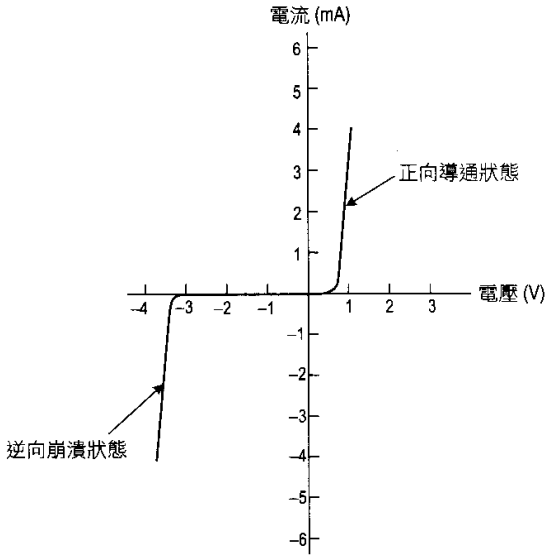

圖 14 太陽電池二極體 I-V 特性示意圖

了解上述太陽電池基本物理特性之後，如何正確評估太陽電池效率則必須了解太陽電池運作時所涉及重要物理參數之意義，特加以簡介如下：

1. 最高輸出功率 (P_m)

太陽電池可在不同電壓(V)與電流(I)之下操作，最高輸出功率可定義為「當光轉換成最高最大電能輸出時之功率(P_m)」，其中 $P_m = V_m \cdot I_m$ (V_m、I_m 分別為在最高輸出功率時之電壓與電流)。

2. 能量轉換效率 (Energy conversion efficiency, η)

能量轉換效率定義為「進入太陽電池之輻照光能量(P_{in})與太陽電池輸出之電能(P_m)之比值」

$$(P_m/P_{in}) \times 100\% = (V_m I_m/P_{in}) \times 100\% = (V_m I_m/A_c E) \times 100\%$$

其中 E 為標準條件下之日照輻射量($Watt/m^2$)，A_c 為太陽電池面積。目前太陽電池最高效率為：單晶矽 24.7%、多晶矽 19.8%、非晶矽 14.5%、砷化鎵 25.7%、CIGS 18.8%與多接面串疊型 33.3%。

3. 填充因素 (Fill factor, FF)

填充因素(通常< 1)一般定義為「最高輸出功率(P_m)除以開放電壓(V_{oc})與短路電流(I_{sc})之乘積」即

$$FF = (Pm/V_{oc}I_{sc}) = (V_m I_m / V_{oc}I_{sc}) = (A_c E/ V_{oc}I_{sc})$$

在太陽電池 I-V 關係圖(參閱圖 11)中，填充因素通常用來描述 IV 曲線和一個矩形類似的程度，因此 FF 值越高即顯示 IV 曲線越接近

矩形，此外 FF 值不因溫度或日照率之改變而改變。此時能量轉換效率可重新改寫為$\eta = FF \cdot I_{sc} \cdot V_{oc}/P_{in}$

4. 量子效率 (Quantum efficiency, QE)

當太陽電池表面被光照射時，可以有效轉換為電子-電洞對之光子數百分比。一般而言，每個光子能量下之量子效率通常是在不同波長範圍加以量測。

2.2 太陽光譜簡介 [14]

太陽表面溫度接近6000K，因此其放射光譜幾乎等同於該溫度下的黑體輻射，且太陽光照射並無方向性，地球與太陽相距約1億5千萬公里遠，能到達地球表面的光子，幾乎只有正向入射至地球表面的光譜所貢獻，到達地球大氣圈表面的光譜輻射能量定義為太陽常數(Solar Constant)，其數值大約1.353 kW/m^2 ，因此大氣圈外的太陽光譜定義為AM0 ，其中大氣質量(Air Mass)用來估量因為大氣層吸收後，所導致影響太陽光譜表現與總體能量值，而這些能量值亦是地球表面應用的太陽電池元件所能運用的，圖15敘述大氣質量的計算方法，大氣質量數值常使用Air Mass =$1/\cos\theta$ 來計算，其中$\theta = 0$ 所代表為太陽光從頭頂上方直射下來，而由上述的計算式中可知，地球表面用以衡量太陽光譜的大氣質量值$\geqq 1$ ，目前慣用的太陽光譜值

AM1.5 ，即是太陽光入射角偏離頭頂46.8^{o}，當太陽光照射到地球表面時，由於大氣層與地表景物的散射與折射的因素，會多增加20% 的太陽光入射量，抵達地表上所使用的太陽電池表面，其中這些能量稱之為擴散部份(Diffusion component)，因此針對地表上的太陽光譜能量有AM1.5G (Global)與AM1.5D (Direct)之分，其中AM1.5G 即包含擴散部分的太陽光能量，而AM1.5D則沒有。圖16表示的即是大氣圈外(AM0)與地表上(AM1.5)太陽光能量光譜。太空用太陽電池元件電性量測所使用的標準光譜是採AM0，而地表所應用的太陽電池元件電性量測所使用的標準光譜，依其應用性之不同，可採用AM1.5G 或是AM1.5D ，其中AM1.5G 光譜的總照度為963.75W/m^2 ，而AM1.5D光譜的總照度為768.31W/m^2，在量測計算應用上方便，常會將此二值做歸一化至1000 W/m^2 。

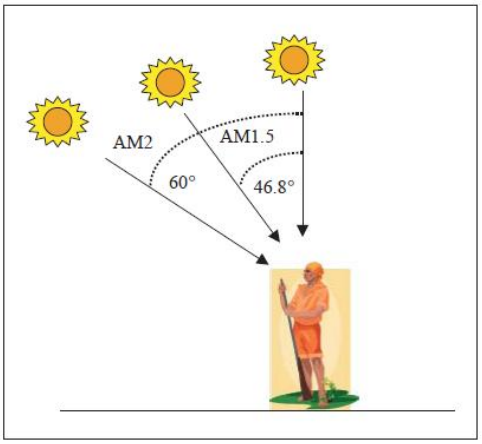

圖 15 大氣質量的計算方法示意圖 [14]

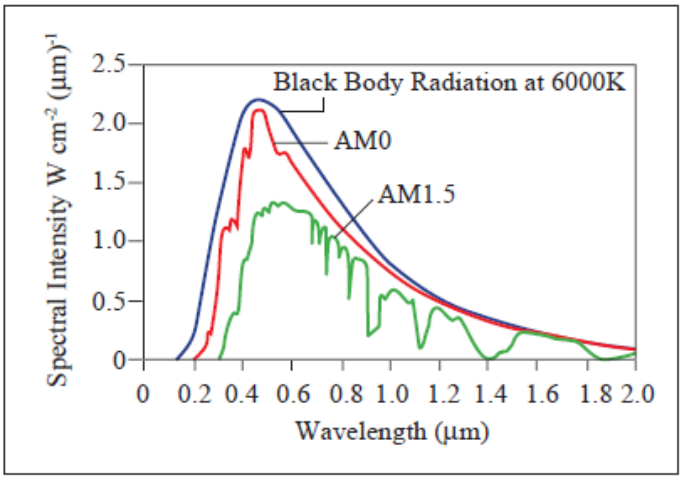

圖 16 大氣圈外(AM0)與地表上(AM1.5)太陽光能量光譜 [14]

太陽電池元件的電性量測可分別於戶外或是室內來進行，而太陽電池元件容易受到溫度、照度與地利位置等因素影響，所以在戶外進行量測所得到的數據不易有再現性與可比較性，雖不利於太陽電池的研究開發之用，但對於已完成的太陽電池模組的實際發電效率監控卻有莫大的助益。基於前述理由，目前主要的太陽電池元件量測工作大都於室內進行，元件電性量測過程所需的太陽光線，是利用太陽光模擬器來提供近似太陽光譜的光源，同時因為太陽電池元件的電力輸出，與太陽光頻譜有著密不可分的關係，因此太陽光模擬器的優劣，即會大大影響元件的測試結果，因此有美國標準量測規範ASTM E927 、IEC 60904-9與 JIS C8912 等標準來規範太陽光模擬器的等級區分，綜合光源的照射強度均勻性(Non-uniformity of Total Irradiance)、照射不穩定性(Temporal Instability of Irradiance)、光譜合

致度 (Spectral match)，將太陽光模擬器等級分為A、B與C三個等級，如表2所示。

表 2 太陽光模擬器分級標準 [7]

特　　性	太陽光模擬器級別		
	A	B	C
照射強度不均勻性 (Non-uniformity of Total Irrandiance)	≦±2%	≦±5%	≦±10%
照射強度不穩定性 (Temporal Instability of Irradiance)	≦±2%	≦±5%	≦±10%
光譜合致度 (Spectral Match)	0.75~1.25	0.6~1.4	0.4~2.0

進行太陽電池量測工作前，為了確保太陽光模擬器符合所需的AM1.5G或AM1.0的照射強度，通常都會使用標準參考太陽電池來監控或藉以調校太陽光模擬器，而一般的參考太陽電池可分為：

一次太陽電池(Primary reference cell)與二次標準參考電池(Secondary reference cell)，目前主要參考電池僅有少數研究單位有能力調校，例如： 美國國家再生能源實驗室(NREL)、日本獨立產總研究院(AIST)等，而不論是主要標準參考電池或二次標準參考電池都是採用單晶矽太陽電池，著眼其本身的輸出特性穩定，儘管如此二次標準參考電池亦須定時地送回標準公正機構重新校正，才能確保太陽電池元件量測的準確度。

2.3 螢光粉應用於太陽能電池之原理

目前市售單晶和多晶的太陽電池轉換效率都離理想轉換效率甚遠，因為實驗室理想的轉換效率分別可達30~40%，該如何提升轉換效率就是一個很重要的發展目標。在2002年由M.A.Green等人提出了一個第三代太陽能電池提昇效率探討，其中提到了一項利用上、下轉換螢光粉來提昇效率如圖17所示，這是因為以矽為基礎材料的太陽能電池，受限於矽元素本身能矽大小所致，所以只能吸收太陽光中400-1000 nm的光來進行光電轉換如圖18所示，是以一般的太陽光的頻譜來看，太陽光涵蓋的範圍從紫外光(UV)到紅外光(IR)，所以矽的吸收光範圍明顯比較狹窄；因此，如果可以增加紫外和紅外兩大頻寬區塊的利用，將可以可觀提升其光電轉換效率（圖19）。

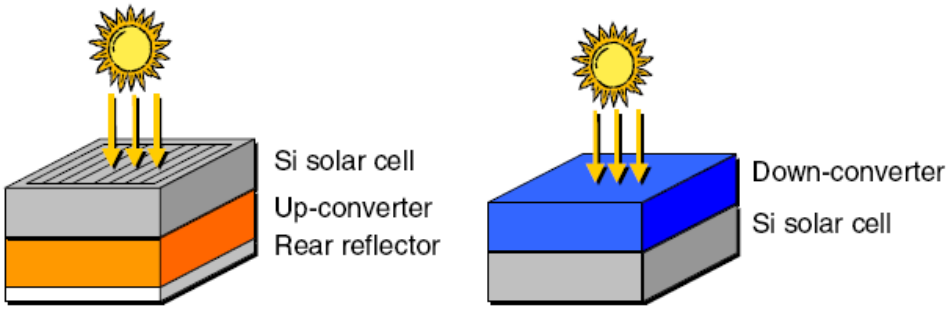

(a) Up conversion (b) Down conversion

圖 17 上轉換與下轉換螢光粉應用於太陽能電池示意圖[8]

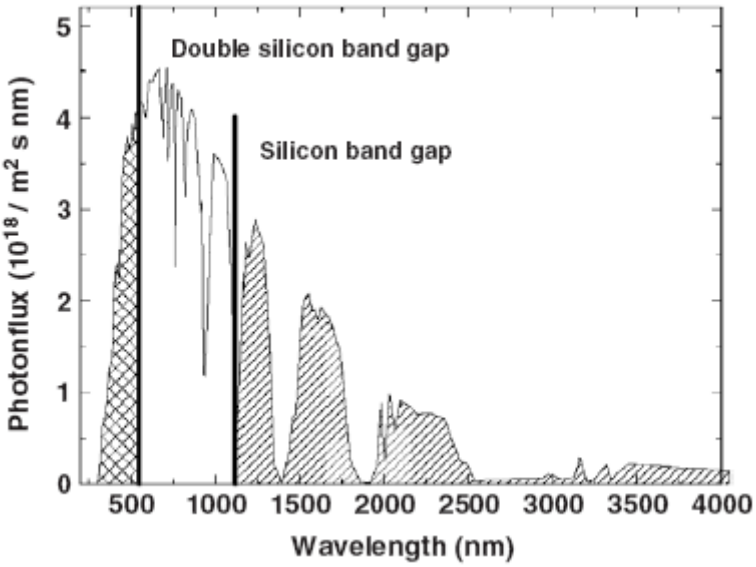

圖 18 在 AM 1.5 的太陽光譜下，矽元素的能階與吸收波長[9]

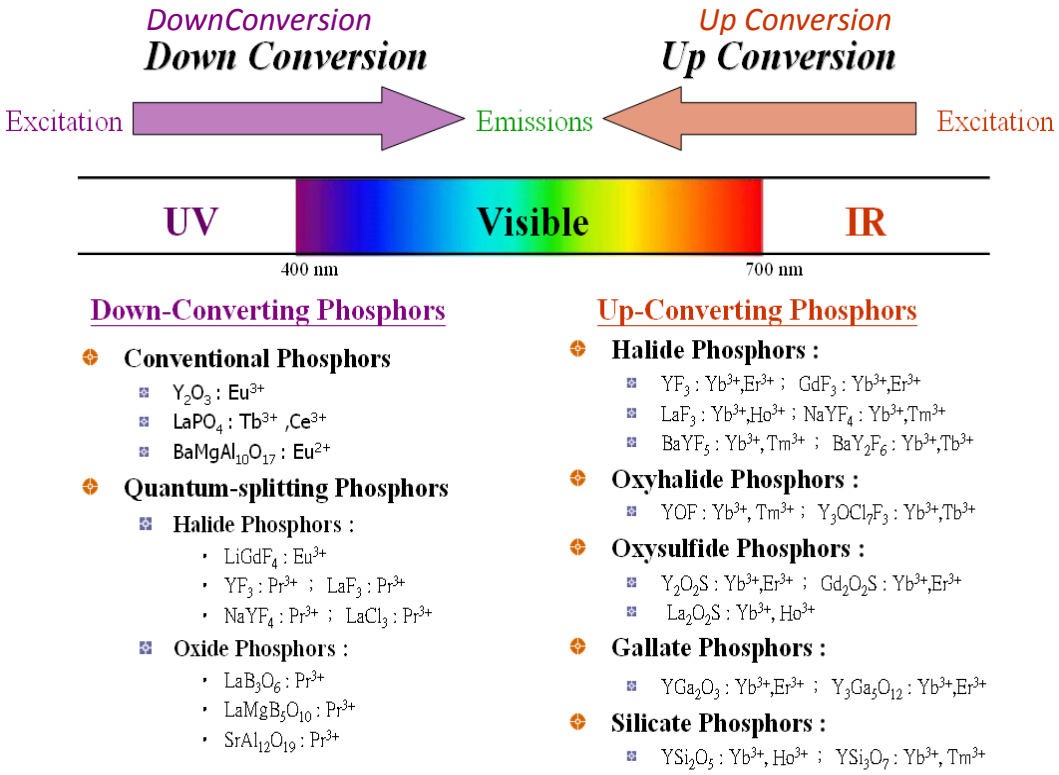

圖 19 利用紫外和紅外的波段可以提升轉換效率示意圖

一般而言，頻譜或光譜轉換可搭配適當螢光材料，可以下列三種方式實行：上轉換(up conversion; 結構如圖 17 (a)所示)、下轉換(down

conversion；結構如圖 17 (b)所示)與集中轉換(spectral concentration)。太陽光譜上轉換之原理，主要是將能量小於太陽電池材料能隙的入射光子，轉變為能量大於能隙之光子，然後經由反射鏡反射所產生的高能光子，供太陽電池再次吸收而產生電子/電洞(electron-hole pair)對，其最高理論光電轉換效率為 47.6%，而太陽光譜下轉換之原理係將螢光材料 down converter 製作於太陽電池表面上，利用能量大於太陽電池材料能隙二倍以上的一個入射光子，轉變為能量大於能隙的兩個光子，之後供太陽電池再次吸收而產生兩組電子/電洞對，其最高理論光電轉換效率為 30.9%。第三種選擇則為頻譜集中轉換，其原理主要整合上/下轉換兩者之優點，將入射太陽光之光譜轉換集中於稍大於太陽電池材料能隙之附近，則能量小於能隙的入射光子被上轉換，亦即能量小於能隙的入射光子被上轉換為高能光子，而能量高於二倍能隙的入射光子被下轉換為低能量光子，最終可以有效提升光轉換效率，其最高理論效率則決定於上/下轉換材料之種類與兩種結構之耦合。

2.3.1 上轉換螢光粉應用於太陽能電池之相關研究

目前文獻所揭露較常見可用於太陽能電池的上轉換螢光粉的有 $NaYF_4:Er^{3+}$；此為2005年澳洲Shalav、Richards與Trupke等人所提出[10]，該文提及利用 $NaYF_4:Er^{3+}$ 塗佈於雙面受光型太陽能電池(Bifacial

silicon solar cell)提升約2.5%的光電轉換效率。此外，2007年由Shalav、Richards與Green等人在Solar Energy Materials & Solar Cells期刊中所提出，利用$NaYF_4$:Er和上轉換$NaYF_4$:Yb,Er確實可以增加其光電轉換效率[11]，其理由為氟化物的聲子振動能量較小，所以上轉換的效果明顯優於氧化物、鹵化物或硫化物，其觀點如圖20所示：

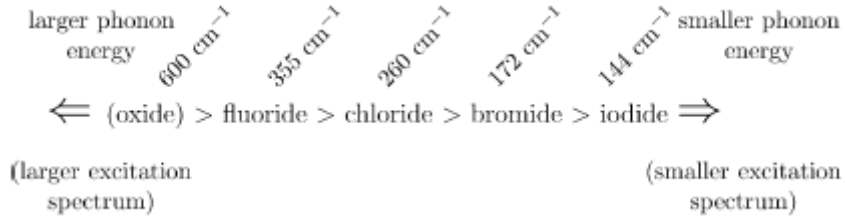

圖 20 不同化學組成主體聲子振動能大小順序

2.3.2 下轉換螢光粉用於太陽能電池之相關研究

在下轉換螢光粉應用在太陽能電池上的文獻，目前比較詳細的為在2007年J. Vac. Sci. Technol. 期刊上由Chung、Chung與Holloway等人所提出，該團隊利用$Y_2O_3:Eu^{3+}$與$Y_2O_2S:Eu^{3+}$以提升太陽能電池的光電轉換效率[12]，該研究利用與高分子3,9-perylenedicarboxylic acid bis(2-methylpropyl)ester (PE),and tetraphenylporphyrin （TPP）.結合塗佈於小尺寸(2x2 cm^2)的太陽能電池上。

最近 Shpaisman 等人[13]更詳細分析了光子上轉換與光子誘發形

成多激子的條件之下，非集中型(non-concentrated)單接面(single junction)矽太陽電池之理論光電轉換效率上限為 49%，相較於無光子上轉換或光子誘發形成多激子條件存在時的 31%。

2.4 本研究相關專利之探討

美國 Intematix 公司 Li、Shan、Cheng 與 Ko 等人在 WO 2007/1333445 專利中[14]，揭露將一系列能吸收 280-460 nm 波長之奈米與微米級 $(Sr,Ba,Eu)_2SiO_4F_x$ 螢光粉塗佈於矽太陽電池表面，以有效提升其轉換效率之構想。荷蘭 Eindhoven 理工大學 Hintzen 教授研究團隊在 US2009/0044859A1 專利公告揭露，將不同系列的氮化物 $Sr_2Si_5N_8:Eu^{2+}$、$LaSi_3N_5:Eu^{2+}$與 $CaSiAlN_3:Eu^{2+}$整合於矽太陽電池中，可以將 350-550 nm 波長之太陽光轉換為波長 550-950 nm 可以供矽太陽電池吸收之輻射。[14]

2.5 研究動機

國內太陽光電產業自 1980 年即已由工研院在能源基金支助下展開，1999 年起政府積極推動太陽能電池發電產業，2005 年產值達 55 億元(即 90 MW 全球市佔率 6.4%)，2006 年產 130 MW(全球市佔率 8.5%以上)，未來預期於 2012 年產 300 億元(全球市佔率 21%以上)。在以太陽光譜轉換技術，試圖改善太陽能電池之轉換效率之相關研究

甚少，1993 年成大微電子所張守進教授與益通光能科技合作，成功地以網印技術結合螢光粉，在調整最適的 firing 溫度與速度之後，最終可以完成效率 16.23%的量產型高效率矽太陽電池[15]。近五年來文獻已多次揭露「可利用下轉換、光致發光(將光譜中光子波長調變至太陽電池可有效利用之範圍)或上轉換等機制皆可以有效提升太陽電池轉換效率」，Strümpel 等人[9]則蒐集並系統化詳盡分析了具有上述三種功能的多種材料如：稀土或過渡金屬離子摻雜之上或下轉換材料、量子剪裁材料、波長 1000 nm 以上可激發有機上轉換材料。理論已證實利用「光轉換材料」(各類型螢光材料)為提昇太陽能電池之光電轉換效率的可行方法之一，其主要可能具有特點為：方法簡單、成本低廉、較不影響原本太陽能電池的製作，理論上亦可適用於各種不同類型的太陽能電池。是故，可應用於太陽能電池之光轉換材料的尋求及實用化，相信對於太陽能電池的推廣及未來發展，將會具有深遠的影響。本研究也著重於利用各種螢光粉於太陽能電池的效率提升，希望能夠以簡單的方式來提升轉換效率。本研究著重在磷酸鹽類的螢光粉，因為期盼磷酸鹽類可以跟抗反射層接合性較好。

第三章 研究方法

3.1 實驗藥品

1.碳酸鎂 (Magnesium carbonate) 化學式：$MgCO_3$ 純度：99%

廠牌：Showa Chemicals, Japan

2.碳酸鋇 (Barium carbonate)化學式：$BaCO_3$ 純度：99.98%

廠牌： Aldrich Chemicals, U.S.A.

3.氧化鋁 (Aluminium oxide) 化學式：Al_2O_3 純度：99%

廠牌：Acros Chemicals, Belgium

4.碳酸鉀 (Potassium carbonate) 化學式：K_2CO_3 純度：99%

廠牌：Showa Chemicals, Japan

5. 碳酸鈣 (Calcium carbonate) 化學式：Ca_2CO_3 純度：99.99%

廠牌： Aldrich Chemicals, U.S.A.

6.氧化釓 (Gadolinium(III) oxide) 化學式：Gd_2O_3 純度：99.9%

廠牌： Aldrich Chemicals, U.S.A.

7.磷酸二氫銨 (Ammonium dihydrogen phosphate)

化學式：$(NH_4)H_2PO_4$ 純度：99.9% 廠牌： Merck, Germany

8.氧化銪 (Europium(III) oxide) 化學式：Eu_2O_3純度：99.99%

廠牌：Strem Chemicals, U.S.A.

9.碳酸鍶 (Strontium Carbonate) 化學式：$SrCO_3$純度：99%

廠牌：Showa Chemicals, Japan

10.氧化鑭 (Lanthanum(III) oxide) 化學式：La_2O_3純度：99.99%

廠牌： Aldrich Chemicals, U.S.A.

11.氧化鐿 (Ytterbium(III) oxide) 化學式：Yb_2O_3純度：99.9%

廠牌：Aldrich Chemicals, U.S.A.

12.氧化鈥 (Holmium(III) oxide) 化學式：Ho_2O_3純度：99.9%

廠牌： Aldrich Chemicals, U.S.A.

13.氧化鉺 (Erbium(III) oxide) 化學式：Er_2O_3純度：99.9%

廠牌： Aldrich Chemicals, U.S.A.

14.氧化銩 (Thulium(III) oxide) 化學式：Tm_2O_3 純度：99.9%

廠牌： Aldrich Chemicals, U.S.A.

15.氧化鐠 (Praseodymium(III) oxide) 化學式：Pr_2O_3 純度：99.9%

廠牌： Aldrich Chemicals, U.S.A.

16.氧化鉬 (Molybdenum trioxide) 化學式：MoO_3純度：99.5%

廠牌： Sigma Chemicals, U.S.A.

17.硫粉 (Sulfur powder) 化學式：S 純度：99%

廠牌：Showa Chemicals, Japan

18. 聚甲基丙烯酸甲酯 (Poly(methyl methacrylate)) 化學式：

$[CH_2C(CH_3)(CO_2CH_3)]_n$，簡寫：PMMA ；分子量：90,000

廠牌：Aldrich Chemicals, U.S.A.

19. 聚甲基丙烯酸甲酯漿料(Poly(methyl methacrylate, PMMA Binder)：台北市尚利科技

20. 太陽能電池(Solar cells): 台彎茂矽、昱晶能源科技或

新日光能源 科技所提供 156mm*156mm (6吋) 市售a級規格效率16%以上

3.2 儀器設備

(1)高溫爐組 (High Temperature Furnaces)

使用台北市陵勝企業公司生產的箱型爐，加熱空間約為 7,056cm^3，配備 Eurotherm 818P 型溫控器及矽化鉬加熱元件，最高溫度可達 1600℃及美國 Lindberg 公司生產的程式控溫箱型爐，加熱空間約為 9,880cm^3，溫度上限為 1500°C。

(2) 高溫管狀通氣爐

使用美國 Lindberg 公司製造之 51442 型，搭配 Eurotherm 818P 型程式溫控器的管狀爐，其溫度上限為 1,000°C。

(3) X 光繞射儀（X-ray Diffractometer）

使用 BrukerX 光繞射儀，X 光源產生之原理為利用 40kV 的操作電

壓，加速電子撞擊銅靶以激發銅原子，經單光晶體分光，使之產生波長為 1.5405 Å ，$K\alpha_1$ 的 X 射線，量測時之操作電流為 20 mA。掃瞄範圍之 2θ 值為 5 至 80 度，掃瞄模式為 $2\theta/\theta$，掃瞄速率為每分鐘 10 度。量測前先將樣品研磨成均勻細粉，固定在 holder 上進行量測；必要時以矽粉做內標，以校正繞射峰之 2θ 值。

(4)螢光光譜儀 (Spectrofluorometer)

使用美國 Jobin Yvon-Spex Instruments S. A. Inc.公司所製 Spex Fluorolog-3 螢光光譜儀，搭備 450W 氙燈與 Hamamatsu Photonics 所製造 R928 型光電倍增管為偵測器，掃瞄波長範圍為 200nm 至 1000 nm。

(5) 色度座標測定 (Determination of CIE Chromaticity Coordinates)

使用日本LAIKO公司所產製DT-100 Color Analyzer，搭配螢光光譜儀即可測得輝度、 對比度、 閃爍以及色度。

(6) 場發射掃瞄式電子顯微鏡 (Field Emission SEM, FESEM)

採用國家奈米元件實驗室（NDL）的Hitachi S-4000型的FESEM，其加速電壓為0.5-30 kV，放大倍率為20-30萬倍。

3.3 下轉換與上轉換螢光粉之製備

3.3.1 下轉換 $Na_2CaPO_4F:Eu^{2+}$ 螢光粉之製備

本研究使用高溫固態法合成$Na_2CaPO_4F:Eu^{2+}$綠色螢光粉，依照化學計量(如圖21)將所有起始物Na_2CO_3、$CaCO_3$、$(NH_4)_2HPO_4$與Eu_2O_3均勻混合，置於瑪瑙研缽中，同時加入了反應物總重量20%的NaF作為助熔劑，研磨並且均勻混合後，然後置入氧化鋁坩堝中，在40% H_2/60%Ar還原氣氛下，於800-1000℃高溫燒結8小時。

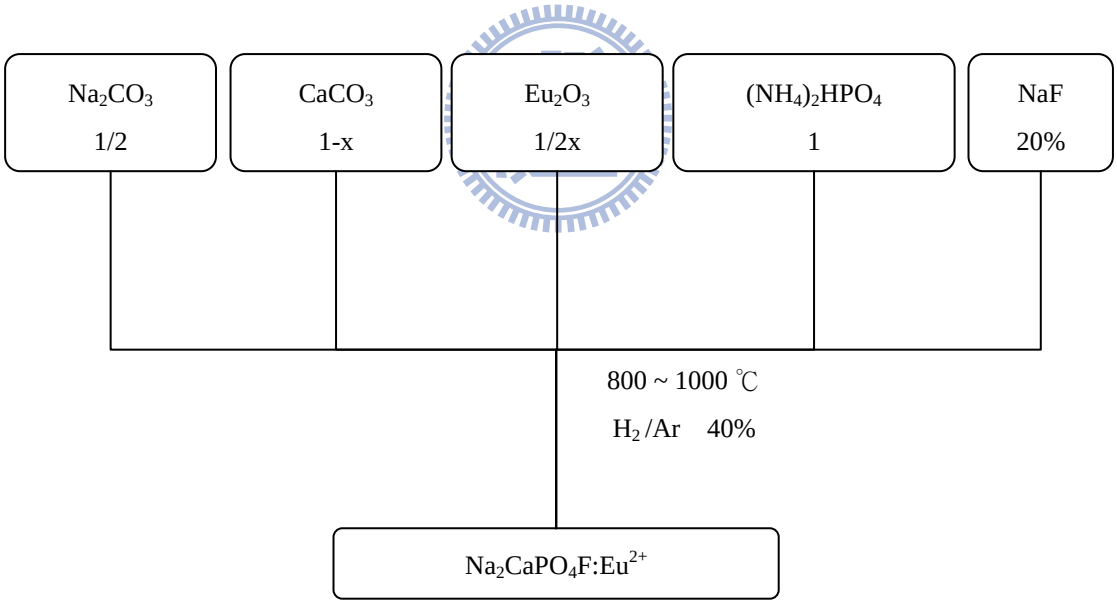

圖 21 $Na_2CaPO_4F:Eu^{2+}$螢光粉高溫固態法合成流程

3.3.2 下轉換 $KMGd(PO_4)_2:Eu^{3+}$ (M= Ca、Sr)螢光粉之製備 [16, 17]

紅光 $KMGd(PO_4)_2:Eu^{3+}$螢光粉係使用固態法進行合成，依照化學計量(如圖 22)將所有起始物$(NH_4)_2HPO_4$、K_2CO_3、Eu_2O_3、$SrCO_3$、$CaCO_3$與 Gd_2O_3均勻混合，置於瑪瑙研缽中，同時加入了反應物總重量 5%的 NH_4Cl 作為助熔劑，研磨並且均勻混合後，然後置入氧化鋁坩堝中，於 900-1200℃燒結時間 6 小時。詳細流程如圖 22 所示：

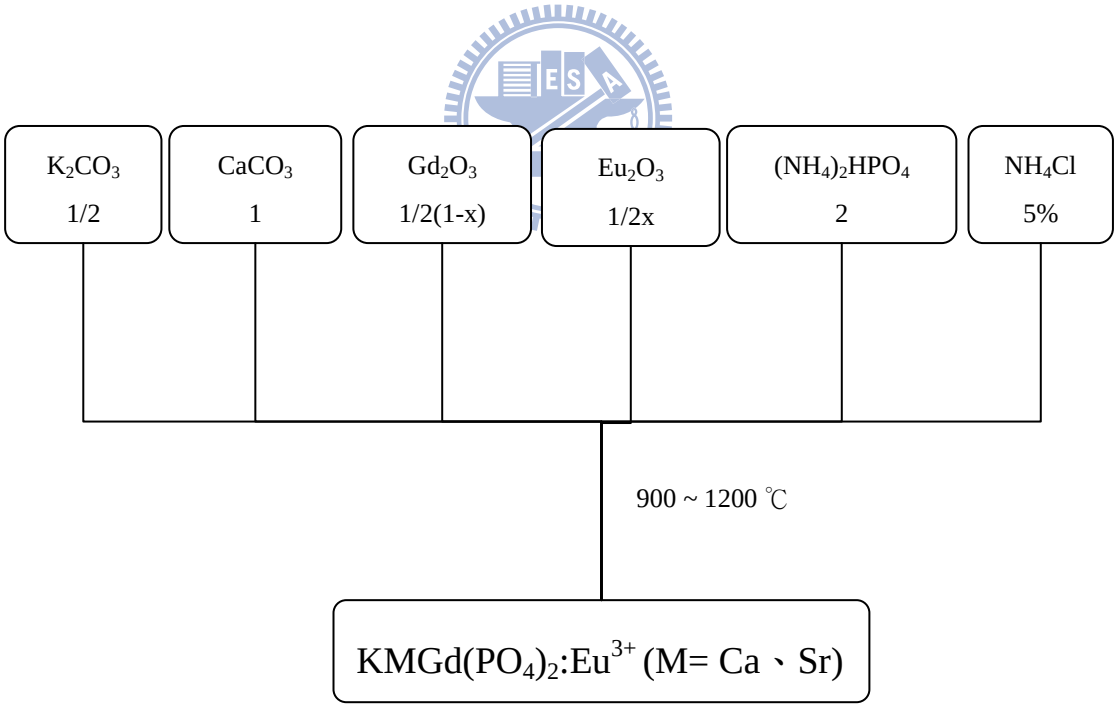

圖 22 $KMGd(PO_4)_2:Eu^{3+}$螢光粉固態法製備流程

3.3.3 上轉換 $La_2Mo_2O_9:Yb^{3+}, R^{3+}$ (R = Er, Ho)螢光粉之製備

[18]

上轉換$La_2Mo_2O_9:Yb^{3+}$, R^{3+} (R = Er, Ho) 螢光粉的合成係以兩步驟進行，以$La_2Mo_2O_9:Yb^{3+},Er^{3+}$為例，首先秤取化學計量之$La_2O_3$ MoO_3 Yb_2O_3 與Er_2O_3 ，其中Er^{3+}或Yb^{3+}為同時取代La^{3+}格位之活化劑，因此當改變Er^{3+}或Yb^{3+}比例時，La^{3+}計量也隨之改變，接著將秤好的起始物置入5% HCl溶液中使其溶解，並將溶液放入烘箱乾燥，可得亮黃色粉末，使用瑪腦研缽將粉末研磨均勻，再置入氧化鋁乾堝中以進行第二步高溫燒結，於900℃、經8小時熱處理，再經研磨均勻後後，可得白色$La_2Mo_2O_9:Yb^{3+}, Er^{3+}$粉末，詳細流程如下圖23所示：

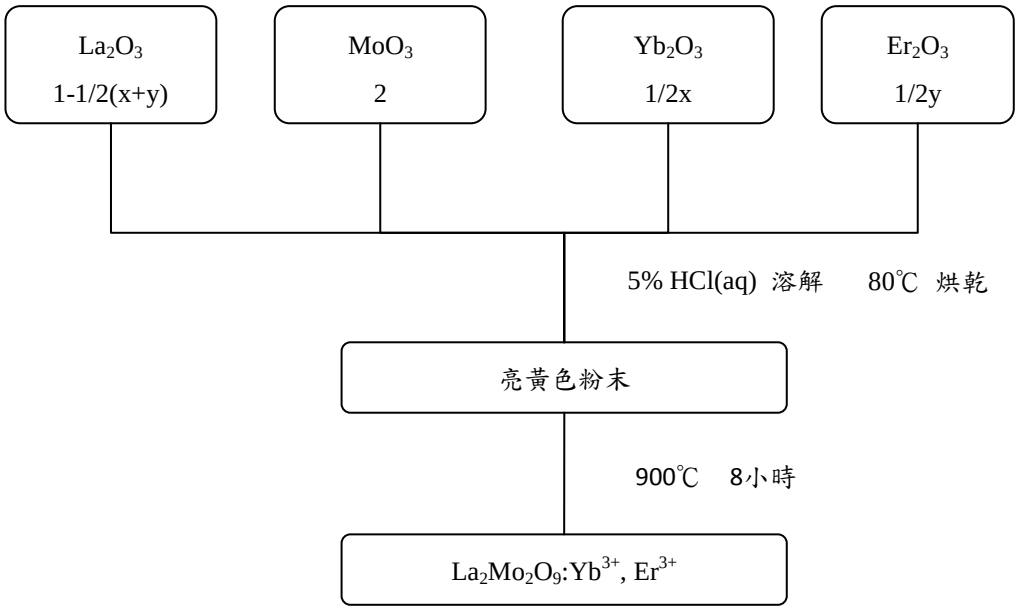

圖 23 $La_2Mo_2O_9:Yb^{3+}, R^{3+}$ (R = Er, Ho)螢光粉之製備流程

3.3.4 上轉換 $KCaGd(PO_4)_2:Yb^{3+},M$ (M= Er, Ho) 螢光粉之製備

紅光$KMGd(PO_4)_2:Eu^{3+}$螢光粉之製備，主要使用固態燒結法進行，起始物使用$(NH_4)_2HPO_4$、K_2CO_3、Yb_2O_3、Er_2O_3、Ho_2O_3、$SrCO_3$、$CaCO_3$與Gd_2O_3，將起始物依照化學計量比例量秤，以瑪瑙研缽研磨混合均勻後置入氧化鋁坩堝中，所使用的燒結溫度為1000-1200℃，時間8小時。詳細流程如圖24所示：

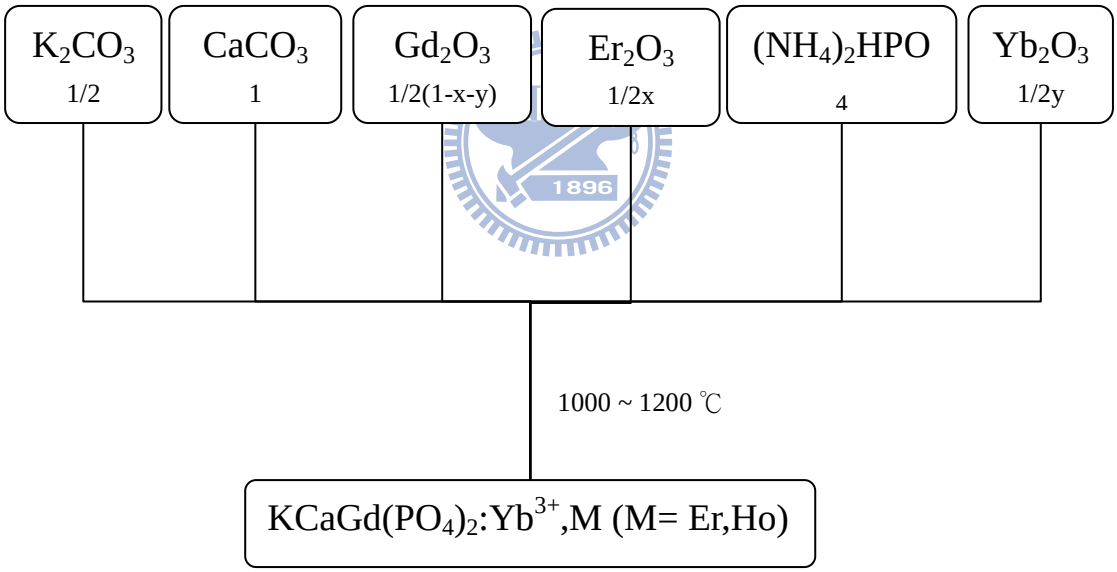

圖 24 $KMGd(PO_4)_2:Eu^{3+}$螢光粉之固態燒結法製備流程

3.3.5 螢光粉塗佈光譜轉換型太陽能電池製程

對上述所合成的上轉換與下轉換螢光粉，我們利用具有良好光學穿透特性的聚甲基丙烯酸甲酯（Poly(methyl methacrylate, PMMA)）

高分子作為媒介，將螢光粉與PMMA的比例1：10取出後，相互攪拌均勻混合後，利用網印的方式，將螢光粉塗佈在太陽能電池的受光正面(front side)，塗佈完成後，於130℃高溫爐中烘烤10分鐘，即可完成。圖25所示為螢光粉塗佈光譜轉換型太陽能電池製作流程：

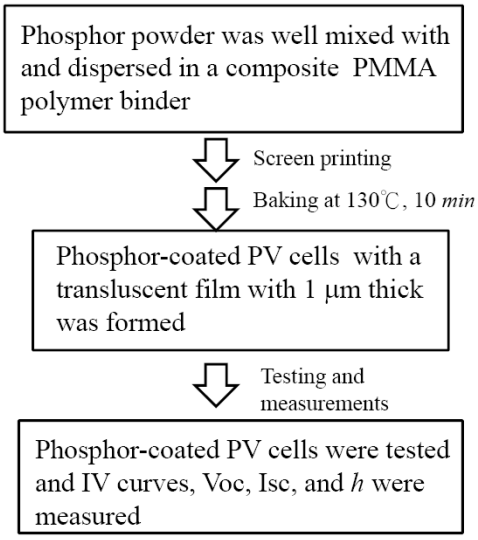

圖 25 螢光粉塗佈光譜轉換型太陽能電池製作流程

3.3.6 太陽電池測試

圖26所示為太陽電池元件測試電路示意圖，所使用者為四端點(four probe)的量測方法，藉由可調變電源負載提供，來量測元件在照光清況下的電流值與電壓值，圖27所示則為較常見的太陽電池元件的電性量測結果。從所測得I-V 曲線圖中，可分別萃取出元件的開路電壓(Voc)、短路電流(Isc)、填充因子(FF)、轉換效率(η)等物理參數。

其個別定義如下所述：(1)開路電壓(Voc)：當太陽電池元件電流等於零時，所得之電壓值。(2)短路電流(Jsc)：當太陽電池元件電壓等於零時所得之電流值。(3)轉換效率(Efficiency)：η%＝（元件的最大功率輸出值/（入射光譜能量* 元件面積））*100（4）填充因子(Fill Factor)：FF ＝（元件的最大功率輸出值/(Voc * Jsc)）*100，圖中Pmp 所代表的是最大功率輸出，Imp 為最大功率輸出時太陽電池元件所貢獻的最大電流值， Vmp 為最大功率輸出時太陽電池元件所貢獻的最大電壓值。

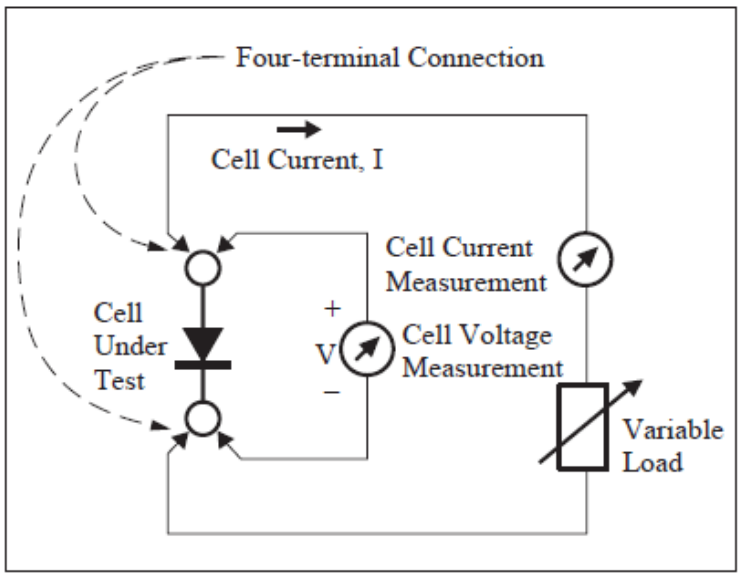

圖 26 太陽電池元件測試的電路示意圖

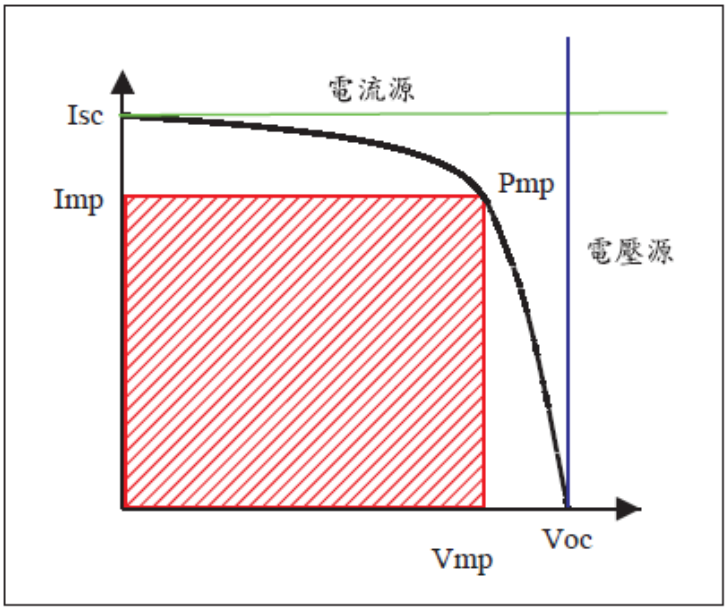

圖 27 太陽電池元件 I-V 電性量測結果示意圖

3.3.7 太陽電池模組封裝測試

封裝測試流程為先檢查電池的外觀，接著使用電激發光原理以觀察矽晶圓內部是否有內裂缺陷，進而利用太陽能光譜儀量測光電特性與相關參數，之後封裝成單片模組後，再檢查外觀和光電特性，最後可移至室外，直接曝曬陽光並量測Voc、Isc、Vpm、Ipm與FF等參數，並進一步與利用太陽能光譜儀量測之結果相互比較。其流程歸納如圖28所示：

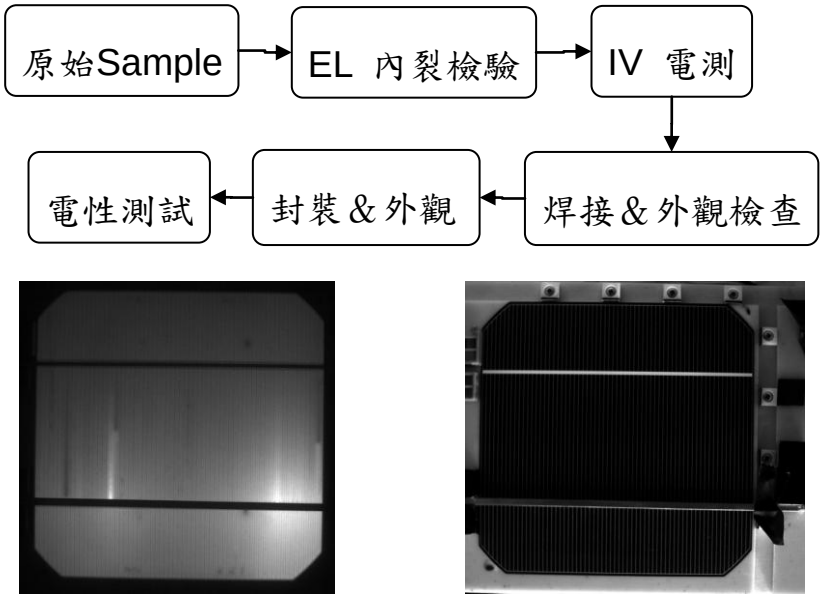

圖 28 太陽電池模組封裝測試流程示意圖

第四章 結果與討論

4.1 下轉換螢光粉晶相分析、微結構與發光特性之研究

4.1.1 $Na_2CaPO_4F:Eu^{2+}$螢光粉 X 光繞射圖譜、晶相分析、微結構與發光光譜之研究

由 3.3.1 節固態燒結反應所得的產物，經由 X 光粉末繞射進行鑑定分析，再與 ICSD 資料庫編號 56962 化合物作為比對之參考(圖 29)，分析結果顯示合乎 Na_2CaPO_4F 的晶體結構，在摻雜 Eu^{2+}離子之後，其結構依然是 Na_2CaPO_4F 的主體結構。

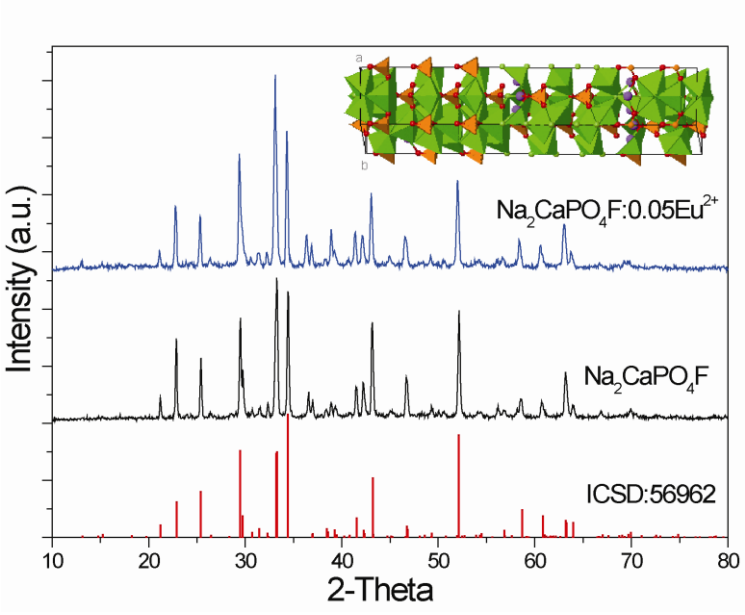

圖 29 未摻雜與摻雜 $Eu^{2+}Na_2CaPO_4F$XRD 圖譜之比較

將反應所得的 $Na_2CaPO_4F:Eu^{2+}$產物進行 SEM 鑑定，以了解螢光

粉之微結構與形貌，圖 30 為 $Na_2CaPO_4F:Eu^{2+}$之 SEM 影像，我們發現其形貌為珊瑚狀均勻，顆粒大小約在 5μm。

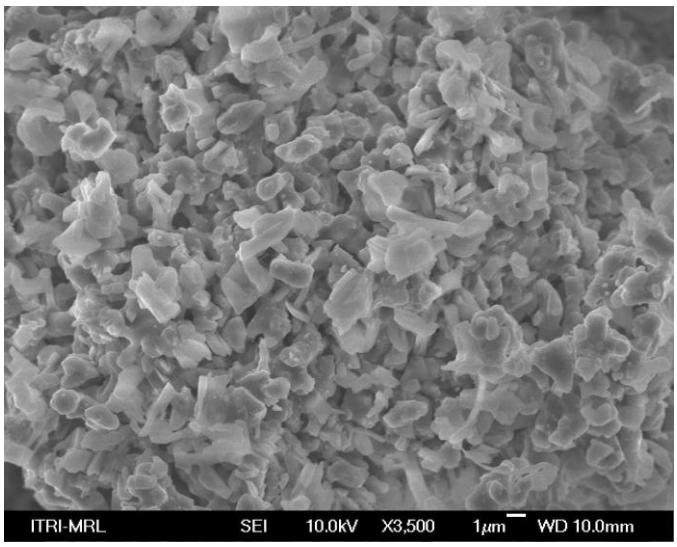

圖 30 $Na_2CaPO_4F:Eu^{2+}$螢光粉之 SEM 影像

利用高溫燒結所合成綠光$Na_2CaPO_4F:Eu^{2+}$螢光粉，先利用螢光光譜儀量測其光學特性，首先利用螢光光譜儀將不同濃度Eu^{2+}摻雜的$Na_2CaPO_4F:Eu^{2+}$找出可激發的波長為寬譜帶的激發，從250-450 nm的範圍，最佳激發波長約為355nm。其放射光譜為一寬帶發光，放光的範圍在450nm-650nm，最佳的放光波長為506 nm。該主體為摻雜Eu^{2+}探討其放光波長為506 nm，主要源自於Eu^{2+}離子$4f^6 5d^1 \rightarrow 4f^7$的躍遷所致，其發光光譜如圖31所示。

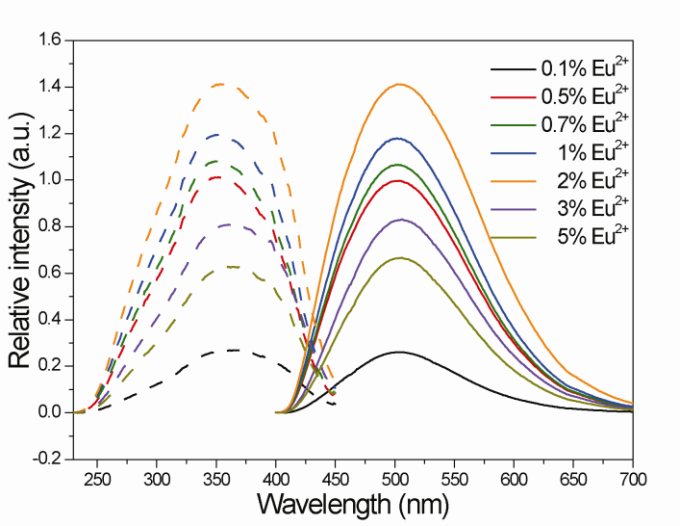

圖 31 $Na_2CaPO_4F:xEu^{2+}$ (x = 0.001－0.05)激發與發射光譜之比較

此外，圖32為$Na_2CaPO_4F:Eu^{2+}$鹵磷酸鹽發光光譜對溫度之依存性，因其熱消光特性影響螢光粉在太陽能電池之應用穩定性，本研究將$Na_2CaPO_4F:Eu^{2+}$與$Ba_2SiO_4:Eu^{2+}$(BOS)商品螢光粉相互比較，發現前者之熱穩定性較差，在溫度150℃時，其發光強度僅為室溫時之50%。

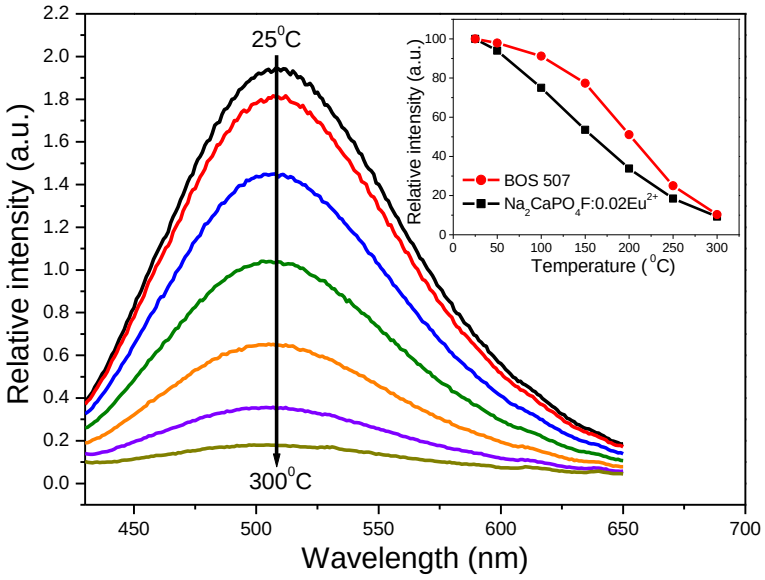

圖 32 $Na_2CaPO_4F:Eu^{2+}$與 BOS 熱消光特性與發光光譜之比較

4.1.2 $KMGd(PO_4)_2:Eu^{3+}$(M = Ca, Sr) X 光繞射圖譜、晶相分析、微結構與發光光譜之研究

反應所得產物經由 X 光粉末繞射儀鑑定，經由 X 光粉末繞射進行鑑定分析，再與 JCPDS 資料庫編號 34-0125 與 34-0118 化合物作為比對之參考，分析結果如圖 33 可顯示其吻合。

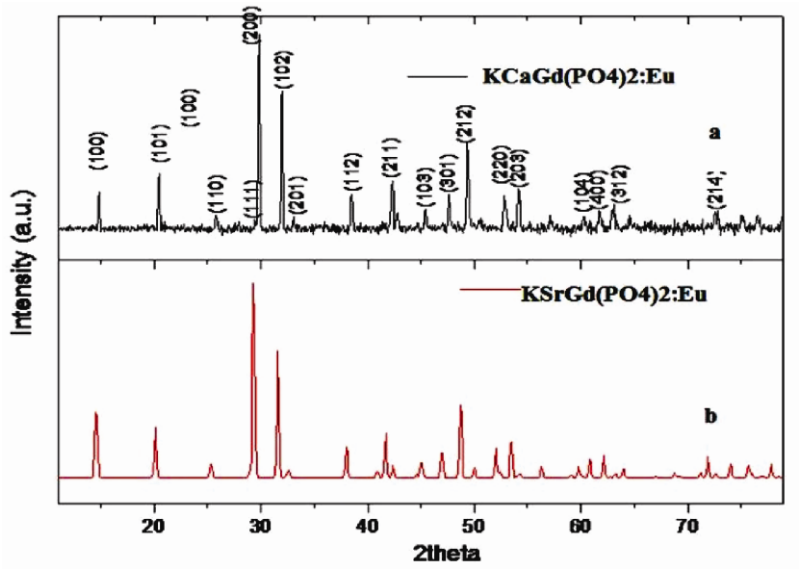

圖 33 $KMGd(PO_4)_2:Eu^{3+}$(M = Ca, Sr)XRD 圖譜之比較

本研究將反應所製備 $KCaGd(PO_4)_2:Eu^{3+}$和 $KSrGd(PO_4)_2:Eu^{3+}$產物分別進行 SEM 微結構鑑定，以了解螢光粉之晶粒粒徑之分布與形貌，圖 34 (a)與(b)分別為 $KCaGd(PO_4)_2:Eu^{3+}$和 $KSrGd(PO_4)_2:Eu^{3+}$螢光粉之 SEM 影像，由圖片中可以觀察其粉體顆粒較為細且形狀不規則。

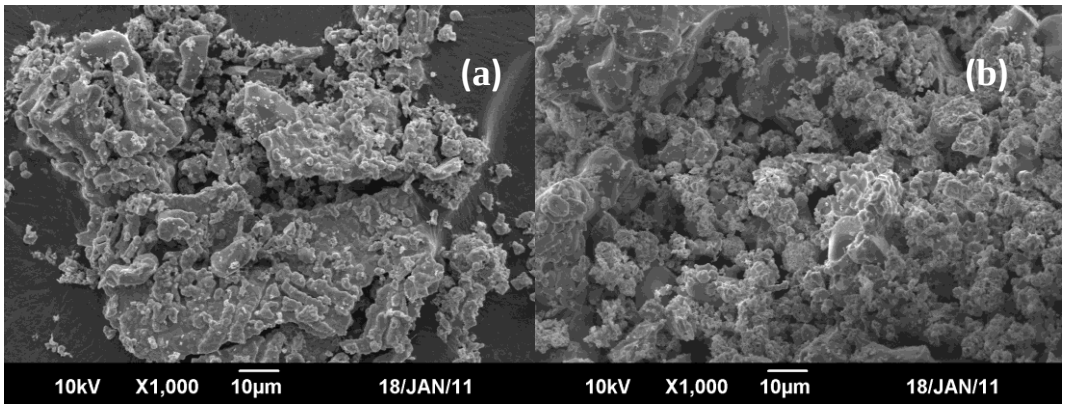

圖 34 (a) $KCaGd(PO_4)_2:Eu^{3+}$與(b) $KSrGd(PO_4)_2:Eu^{3+}$SEM 影像之比較

本研究選擇使用雙磷酸鹽為主體的螢光粉$KCaGd(PO_4)_2:Eu^{3+}$和$KSrGd(PO_4)_2:Eu^{3+}$，為何選擇磷酸鹽為主體呢？其主因為太陽能電池為一種P-N型元件，在抗反射層之下為p型摻雜的Si，若螢光粉可形成另一種P-N模式，則將有助於提升更高的轉換效率。為量測其光電特性，首先我們利用螢光光譜儀找出不同Eu^{3+}濃度摻雜的$KCaGd(PO_4)_2:Eu^{3+}$和$KSrGd(PO_4)_2:Eu^{3+}$的激發波形為寬譜帶激發，在波長為250-450 nm的範圍中，其最佳激發波長約為393 nm。其放射光譜位置亦為一寬譜帶的發光，放光的範圍在584-700 nm之間，其最佳的發光波長為585 nm。

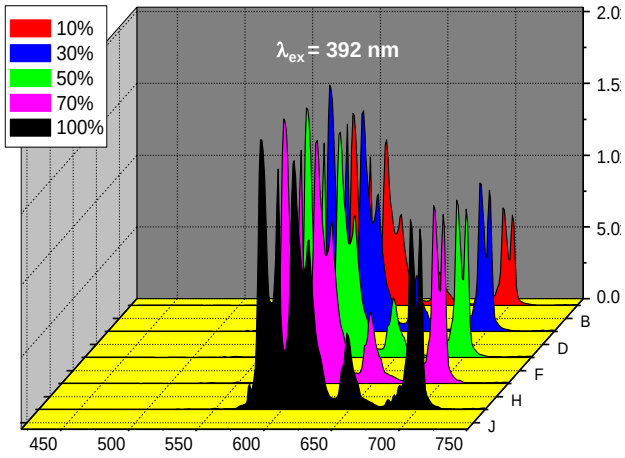

Comparison of PL spectra of $KCaGd(PO_4)_2$:x%Eu^{3+}

圖 35 不同 Eu^{3+}濃度摻雜 $KCaGd(PO_4)_2$:Eu^{3+}的發射光譜

圖 36 與圖 37 分別為 $KCaGd(PO_4)_2$:50%Eu^{3+}與 $KSrGd(PO_4)_2$50%Eu^{3+}之激發與發射光譜，激發光譜中 250-400 nm 間主要為源自 Eu^{3+} 4f-4f 之線型吸收；而激發光譜中 575-710 nm 間主要為源自 Eu^{3+} 4f-4f 之線型放射峰。

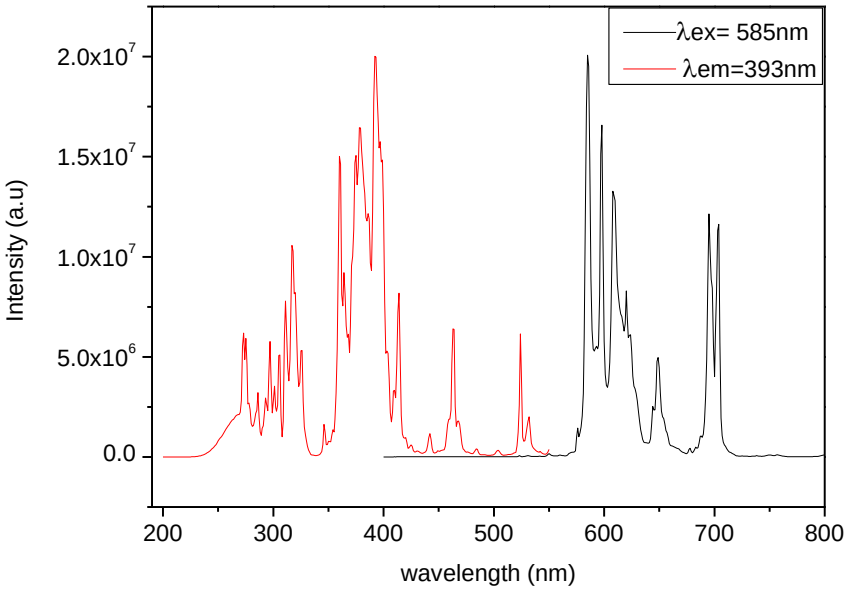

圖 36　$KCaGd(PO_4)_2$:50%Eu^{3+}的激發與發射光譜

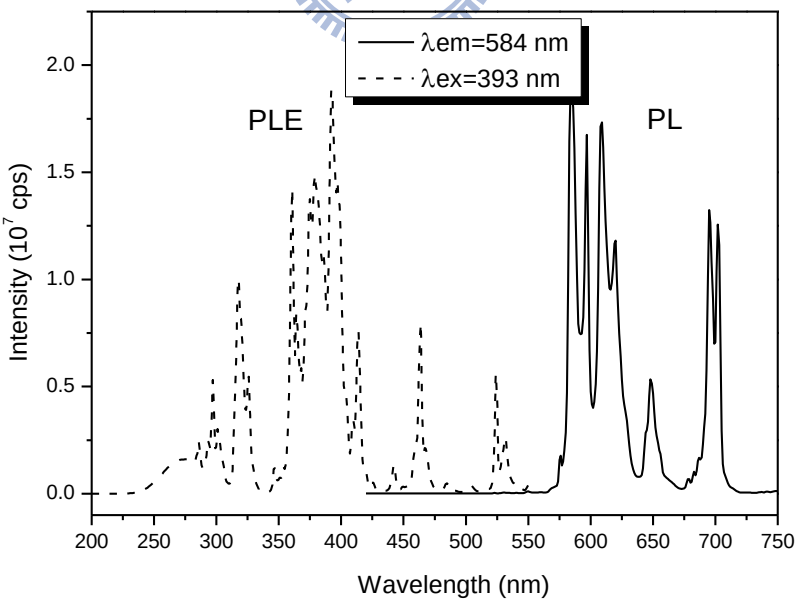

圖 37 $KSrGd(PO_4)_2$: 50%Eu^{3+}的激發與發射光譜

4.2 上轉換螢光粉之製備、微結構與發光特性之研究

4.2.1 $KCaGd(PO_4)_2:Yb^{3+},R^{3+}$ (R = Er,Ho)螢光粉之晶相分析、微結構與發光特性之研究

反應結果經由 X 光粉末繞射鑑定，並以 JCPDS: 34-0125 和 34-0118 資料庫化合物作為比對，結果可由圖 38 與圖 39 判斷，發現其結構 XRD 圖譜是互相吻合。

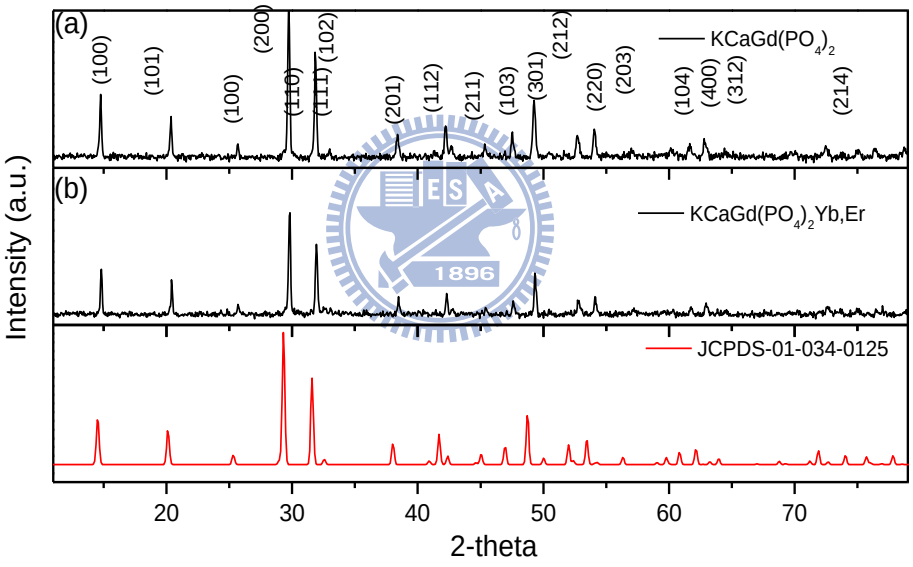

圖 38 $KCaGd(PO_4)_2$ 與 $KCaGd(PO_4)_2:Yb^{3+},Er^{3+}$ XRD 圖譜之比較

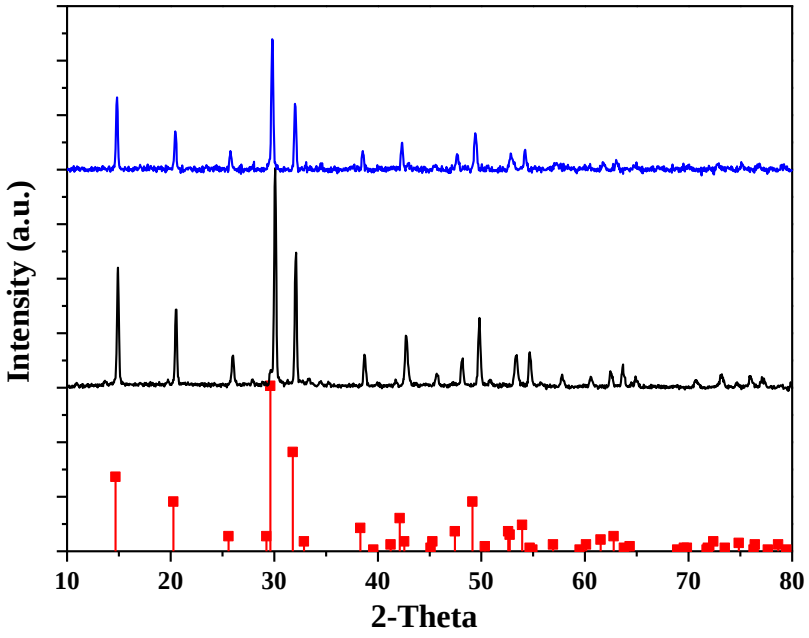

圖 39 $KCaGd(PO_4)_2$ 與 $KCaGd(PO_4)_2:Yb^{3+},Ho^{3+}$XRD 圖譜之比較

我們將上述兩雙磷酸鹽化合物進行SEM影像鑑定以了解化合物之微結構，圖 40 與圖 41 分別為 $KCaGd(PO_4)_2:Yb^{3+},Ho^{3+}$ 和 $KCaGd(PO_4)_2:Yb^{3+},Er^{3+}$之SEM影像，其晶粒呈不規則形狀，粒徑為數十微米。

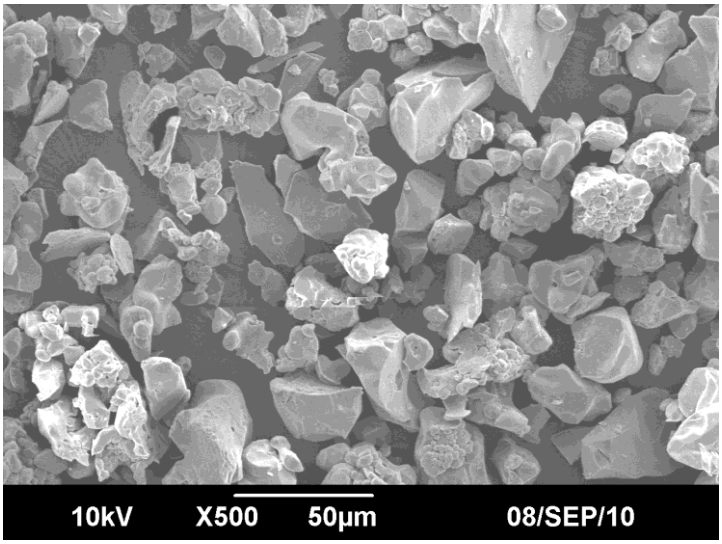

圖 40 $KCaGd(PO_4)_2:Yb^{3+},Ho^{3+}$之 SEM 影像

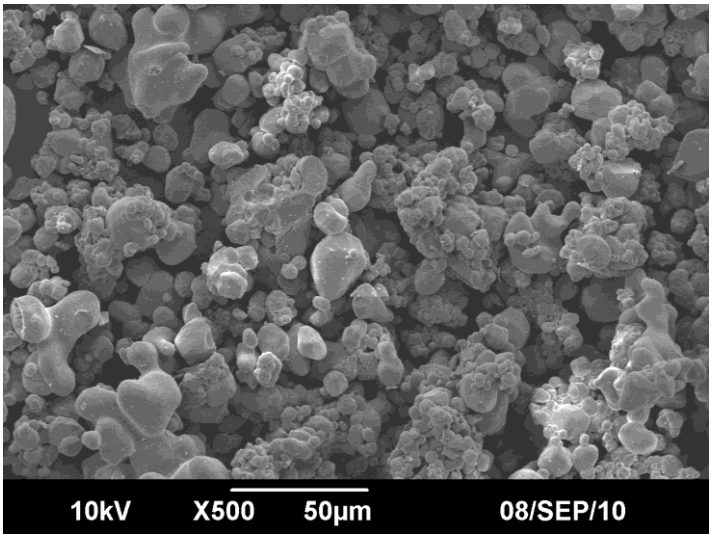

圖 41 $KCaGd(PO_4)_2:Yb^{3+},Er^{3+}$之 SEM 影像

因前述$KCaGd(PO_4)_2:Eu^{3+}$具有提升太陽能電池效率之潛力，因此我們也嘗試利用相同主體摻雜上轉換的稀土離子對，以探討如此組合是否具有相同效果。圖42與圖43為利用980 nm波長雷射激發$KCaGd(PO_4)_2:Yb^{3+}$,1%R (R = Er或Ho)兩螢光體所測得上轉換光譜，圖42與圖43分別顯示：隨Yb^{3+}離子濃度由10%增至80%，$KCaGd(PO_4)_2:Yb^{3+}$,1%R之發光強度也隨之增強。

發射光譜分析顯示，當Yb^{3+}摻雜濃度為80%時，$KCaGd(PO_4)_2$:80%Yb,R (R = Er或Ho)呈現最佳的發光強度。

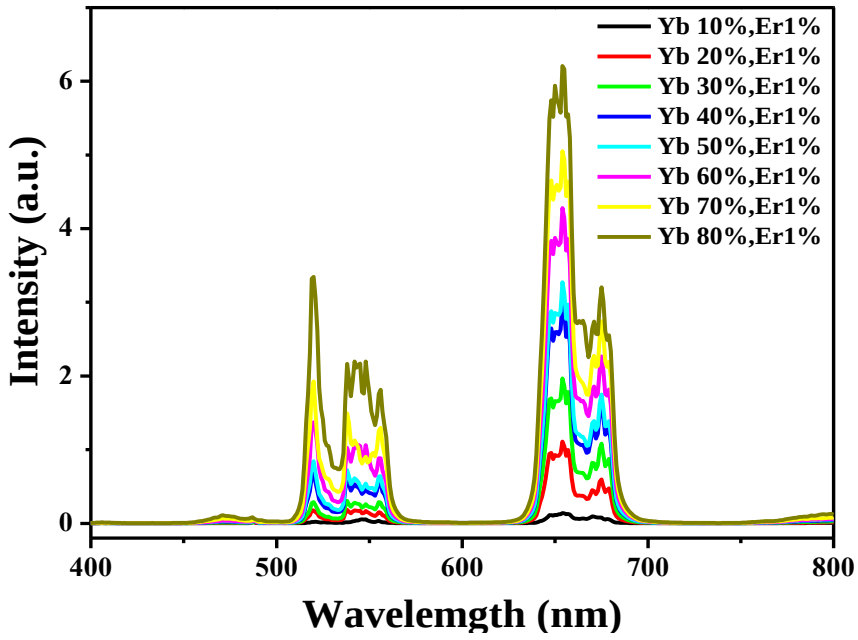

圖 42 以 980 nm 波長紅外光激發 $KCaGd(PO_4)_2$:Yb,Er 所得上轉換光譜

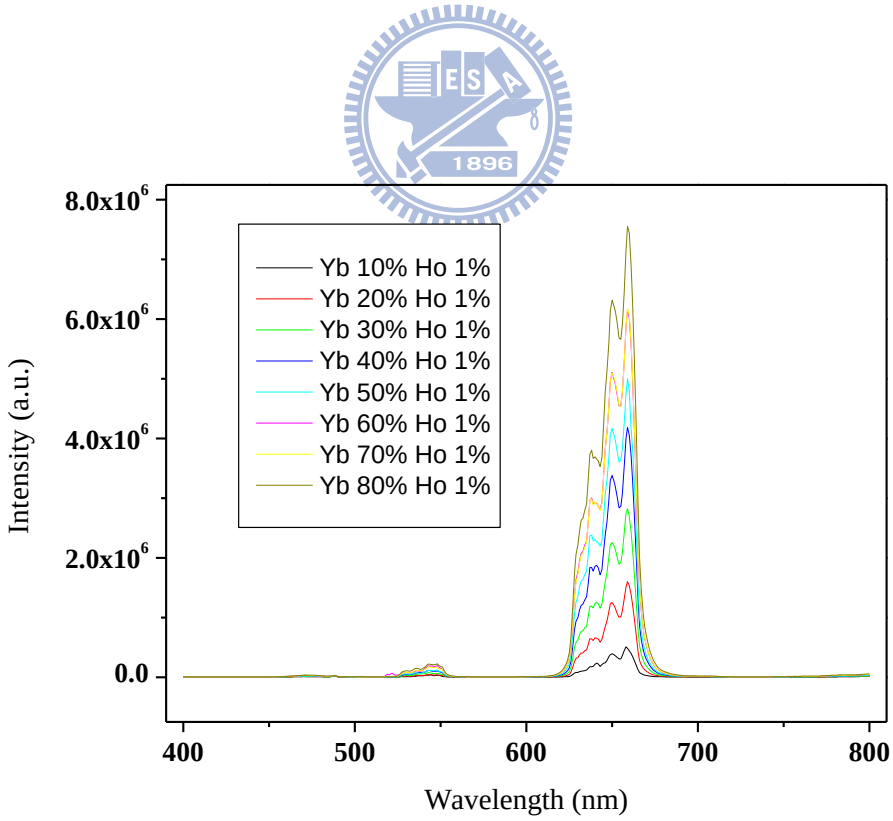

圖 43 以 980 nm 紅外光激發 $KCaGd(PO_4)_2$:Yb,Ho 所得之上轉換光譜

4.2.2 $LaMo_2O_9:Yb^{3+},R^{3+}$ (R = Er,Ho)螢光粉之晶相、微結構與發光特性之研究

將反應所製備產物進行x光粉末繞射晶相鑑定分析，其結果再與ICDS資料庫編號98459檔案進行比對，可以得知是否形成$La_2Mo_2O_9$:Yb^{3+}, Er^{3+}與其晶相純度。由XRD圖譜(圖44)可發現$La_2Mo_2O_9:Yb^{3+},Er^{3+}$與$La_2Mo_2O_9:Yb^{3+},Ho^{3+}$兩上轉換螢光粉均為純相。

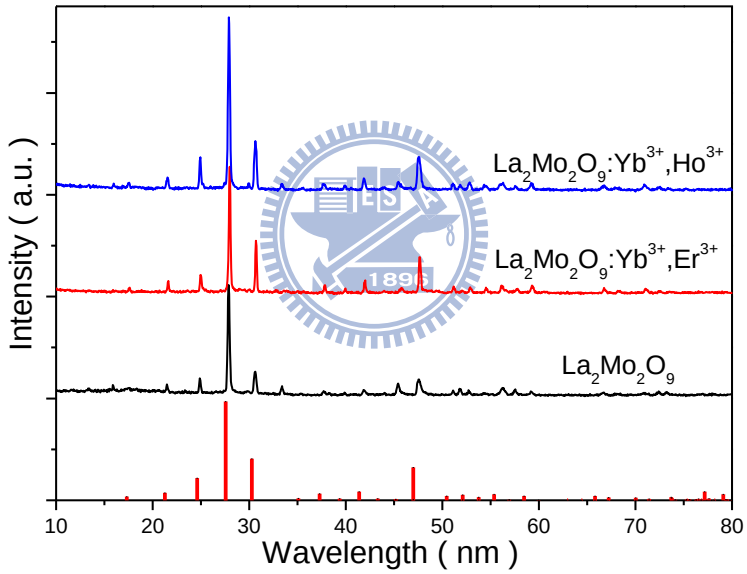

圖 44 $La_2Mo_2O_9:Yb^{3+},R^{3+}$ (R= Ho, Er)XRD 圖譜之比較

將反應所得產物進行SEM微結構鑑定分析，圖45為$La_2Mo_2O_9:Yb^{3+}$, Er^{3+}螢光粉之SEM影像，圖45顯示$La_2Mo_2O_9$顆粒大小分布在10 μm以下且大多數小於5 μm，但是由於我們的合成方式為高溫燒結，因此會有部分的聚集且有熔融現象產生。圖46(a)與(b)分別為$La_2Mo_2O_9$: 9%Yb^{3+}, 1%Ho^{3+}之SEM影像。

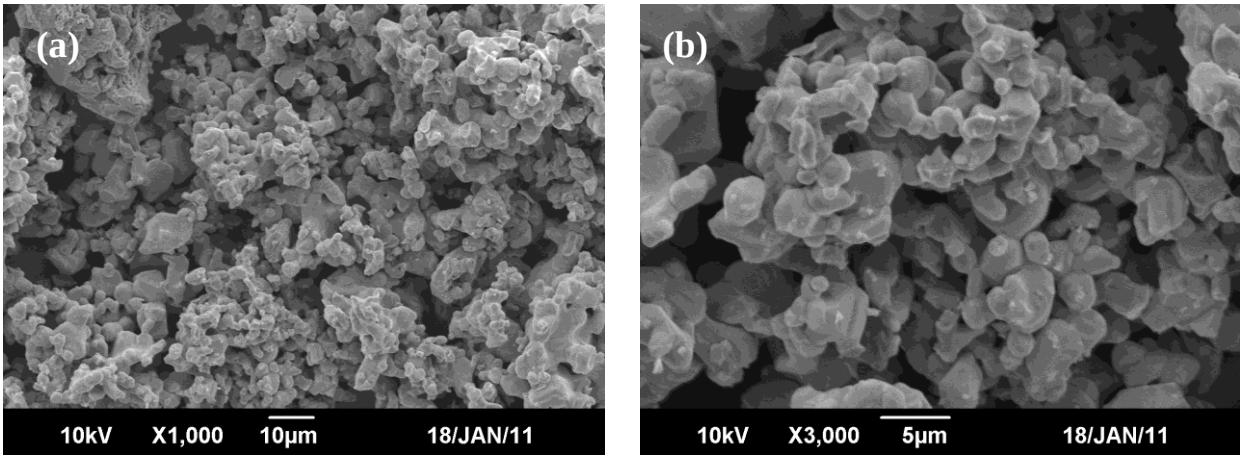

圖 45 (a)與(b) $La_2Mo_2O_9:Yb^{3+},Er^{3+}$上轉換螢光粉之 SEM 影像

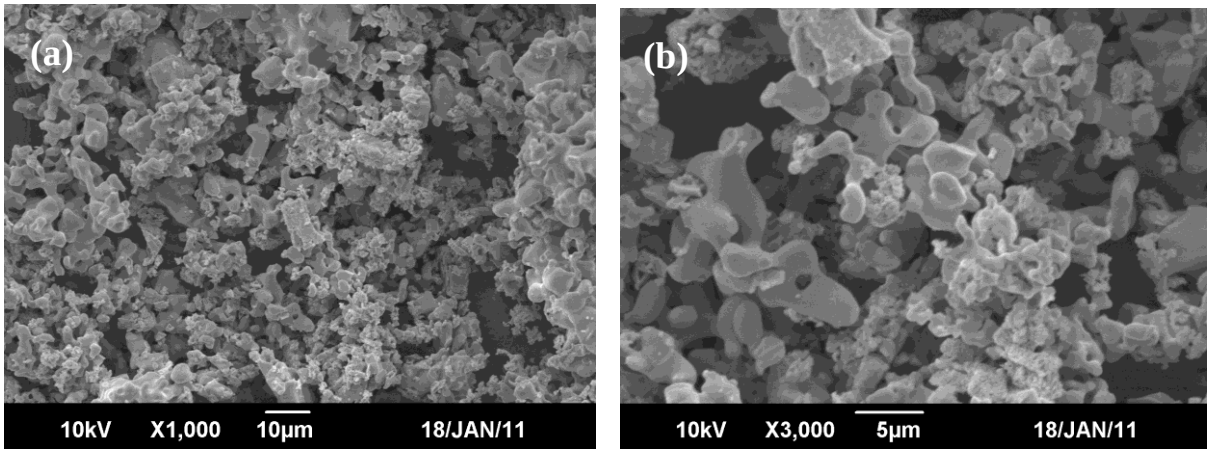

圖 46 (a)與(b) $La_2Mo_2O_9:Yb^{3+},Ho^{3+}$上轉換螢光粉之 SEM 影像

4.3 下轉換螢光粉修飾矽太陽能電池

4.3.1 $Na_2CaPO_4F:Eu^{2+}$螢光粉塗佈矽太陽能電池之製作與光電特性量測

本研究利用網印塗佈製程製作螢光粉修飾矽太陽能電池，以探討螢光粉之塗佈對效率提升之效應，首先將 $Na_2CaPO_4F:Eu^{2+}$螢光粉與高

分子膠材聚甲基丙烯酸甲酯(PMMA)依照 1:10 的比例混合均勻，然後使用網目大小為 400 mesh 之網版，刮刀的壓力為 0.25 Pa 之條件下進行網印。太陽能電池網印前，先量測其效率；網印完成後，使用烘箱於 150℃烘烤 5 分鐘後，靜置回到室溫，再利用太陽能光譜儀測量其轉換效率。實際的量測發現其提升效率為 0.2%。

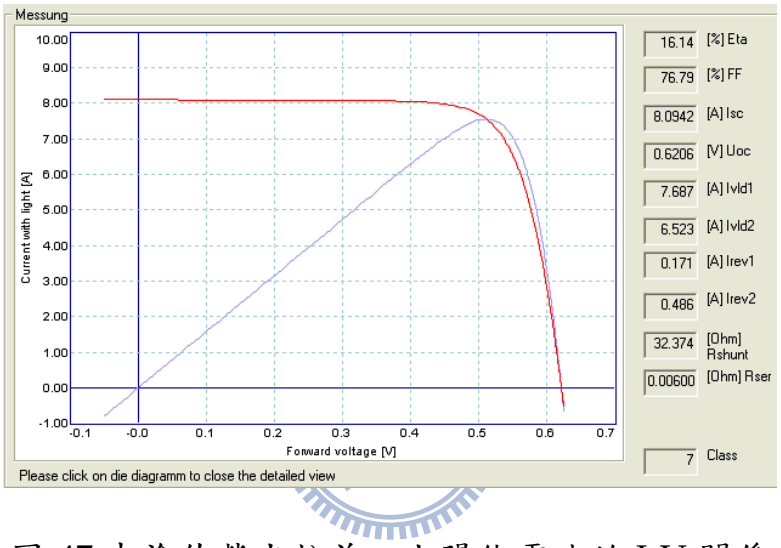

圖 47 未塗佈螢光粉前之太陽能電池的 I-V 關係

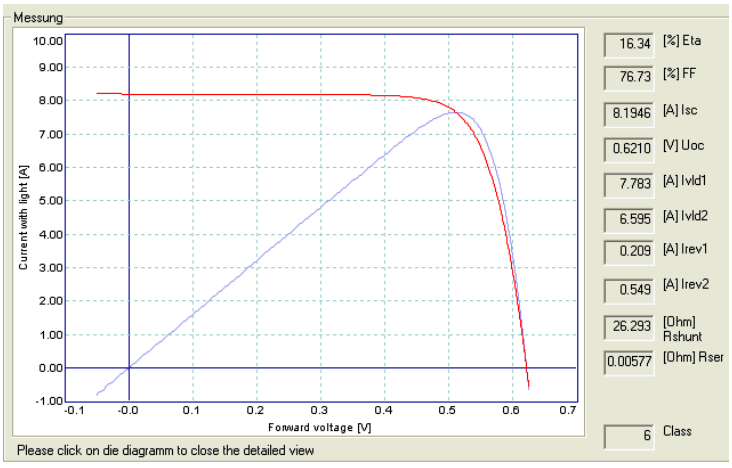

圖 48 塗佈 $Na_2CaPO_4F:Eu^{2+}$太陽能電池的 I-V 關係

4.3.2 $KMGd(PO_4)_2:Eu^{3+}$ (M = Ca, Sr)塗佈太陽能電池之製作與光電特性量測

此外，我們將一種下轉換雙磷酸鹽螢光粉$KMGd(PO_4)_2:Eu^{3+}$ (M = Ca, Sr)，依照我們所使用的網印方式將其塗佈在太陽能電池片的正面(front side)，其電池結構示意圖如圖49：

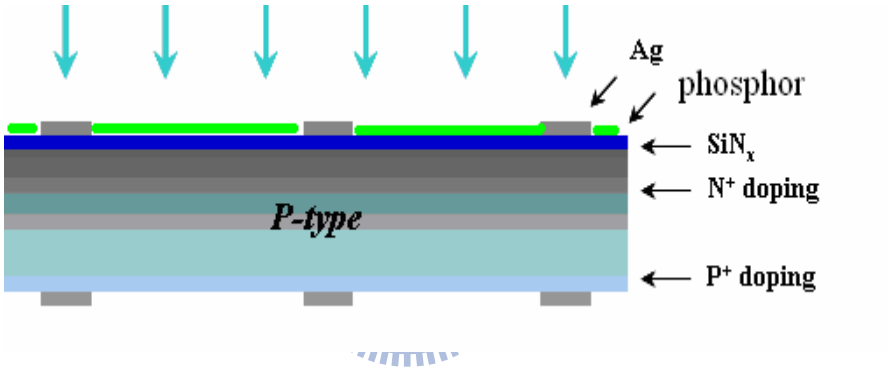

圖 49 $KMGd(PO_4)_2:Eu^{3+}$螢光粉塗佈太陽電池元件結構示意圖

圖 50 與圖 51 分別為未塗佈螢光粉與利用網印法塗佈$KCaGd(PO_4)_2:10\%Eu^{3+}$於太陽能電池表面後所測得之 I-V 關係圖。經比較塗佈螢光粉前後電池之效率與光電性差異，我們發現當未塗佈螢光粉之前，其光電轉換效率只有15.93%，然而，以$KCaGd(PO_4)_2:10\%Eu^{3+}$塗佈之後，發現其電轉換效率大幅提升至16.59%。換言之，整體效率提升了0.66%$\pm$0.01%，此為一項令人驚訝的發現!

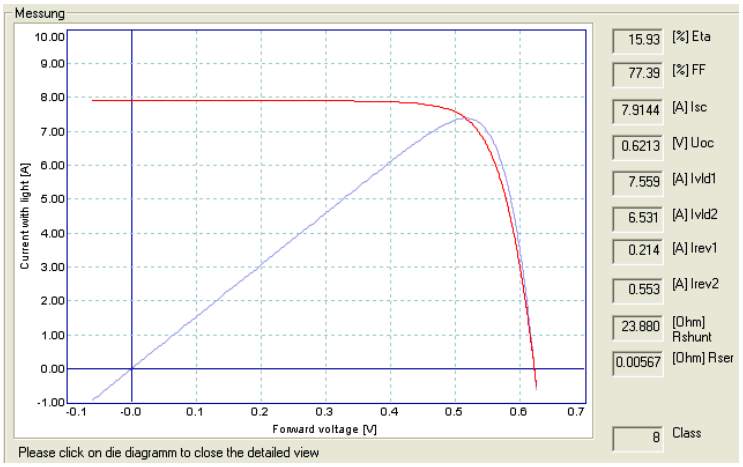

圖 50 尚未塗佈螢光粉前的 6 吋太陽能電池的 I-V 關係

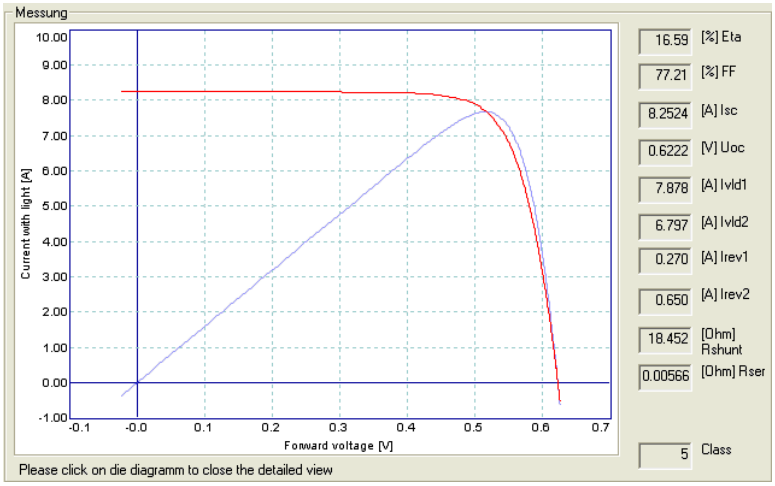

圖 51 以 $KCaGd(PO_4)_2$:10%Eu^{3+}塗佈 6 吋太陽能電池的 I-V 關係

當發現在太陽能電池表面塗佈 $KCaGd(PO_4)_2$:10%Eu^{3+}可提升轉換效率之後，我們更進一步探討具 $KCaGd(PO_4)_2$:x%Eu^{3+}組成且 x 值為 50 與 100 兩種螢光粉樣品。圖 52 與圖 53 分別為未經螢光粉塗佈與以 $KCaGd(PO_4)_2$:50%Eu^{3+}螢光粉塗佈，在分別進行網印塗佈之後，光電特性量測顯示：當 Eu^{3+}濃度提高到 50%時，其光電轉換效率由 15.91%增至 16.62%，其提升值高達 0.71%±0.01%。

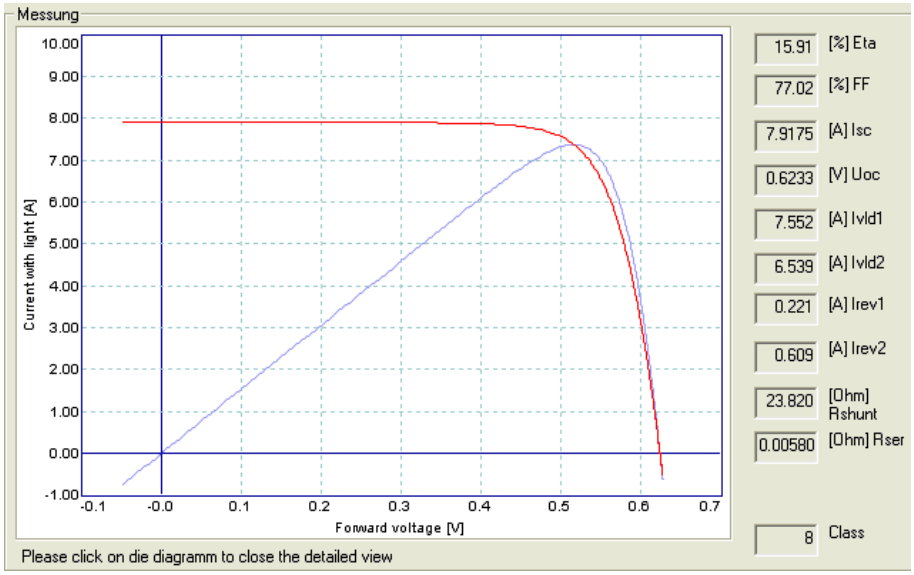

圖 52 尚未塗佈螢光粉前太陽能電池的 I-V 關係

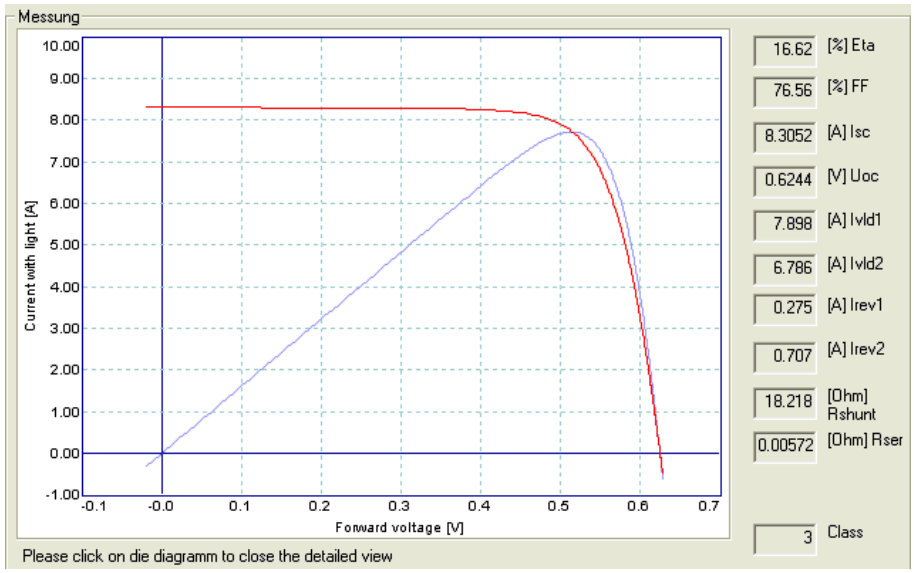

圖 53 塗佈 K CaGd$(PO_4)_2$:50%Eu^{3+}之 6 吋太陽能電池的 I-V 關係

圖54與圖55分別為未經螢光粉塗佈與以KCaEu$(PO_4)_2$螢光粉塗佈之太陽能電池，在分別進行網印塗佈之後，測量其I-V關係曲線，光電特性量測顯示：但當Eu^{3+}取代濃度提高至100%時，其光電轉換效率僅由15.89%提升至16.41%，其增加值下降為0.52%±0.01%。其原因應

為當Eu^{3+}摻雜濃度過高，致取代全部Gd^{3+}格位時，可能產生濃度淬滅與消光效應，以至於塗佈在太陽能電池表面時，其轉換效率呈現下降。

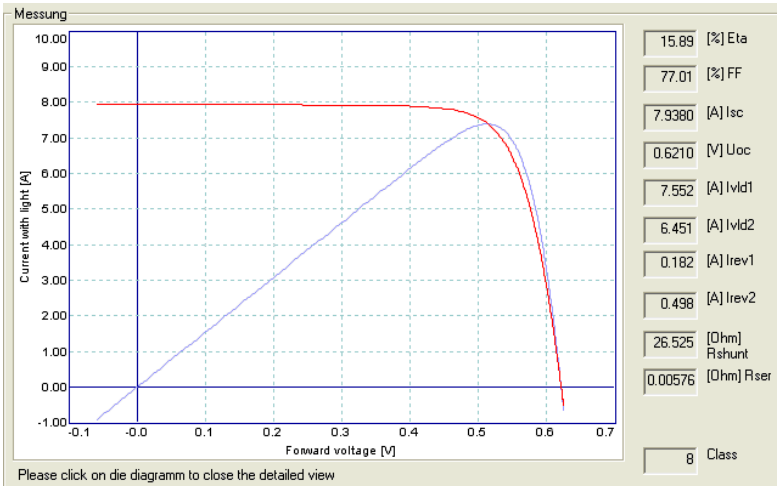

圖 54 尚未塗佈 $KCaEu(PO_4)_2$ 螢光粉 6 吋太陽能電池的 I-V 關係

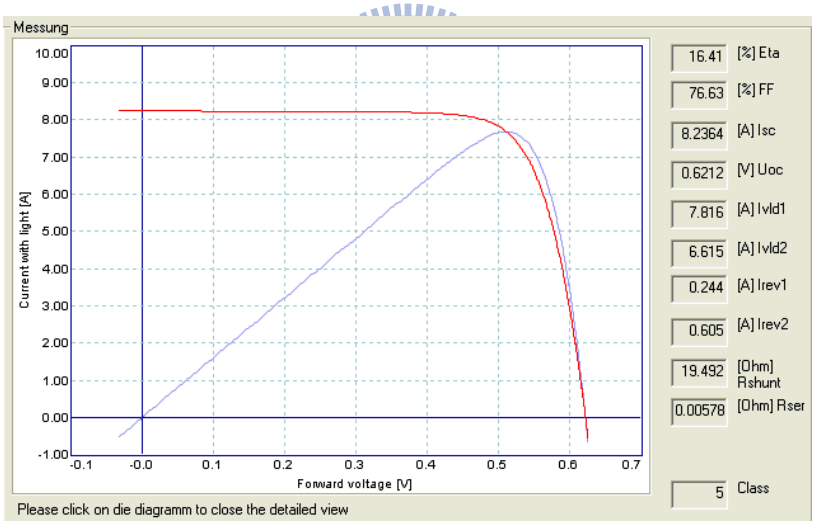

圖 55 $KCaEu(PO_4)_2$ 塗佈 6 吋太陽能電池的 I-V 關係

為何轉換效率會呈現明顯提升?我們可以從反射光譜上看得出端倪，圖56為分別以$KCaGd(PO_4)_2:Eu^{3+}$與$KSrGd(PO_4)_2:Eu^{3+}$塗佈太陽能電池所測得反射光譜之比較，藍色曲線表示太陽能電池表面只有SiN當作抗反射層，黃色和粉紅曲線分別代表著是在太陽能電池上分別塗

佈$KCaGd(PO_4)_2:Eu^{3+}$(KGP)和$KSrGd(PO_4)_2:Eu^{3+}$(KSP)。當將螢光粉塗佈在太陽能電池後，在200-400 nm的紫外光範圍顯示其反射率明顯下降，此間接說明了螢光粉能吸收紫外光，進而可以提升轉換效率。由圖56跟圖36-37來比較發現，反射率下降的位置恰巧與其UV吸收位置相符，也證明了反射率下降是來自於螢光粉的吸收。

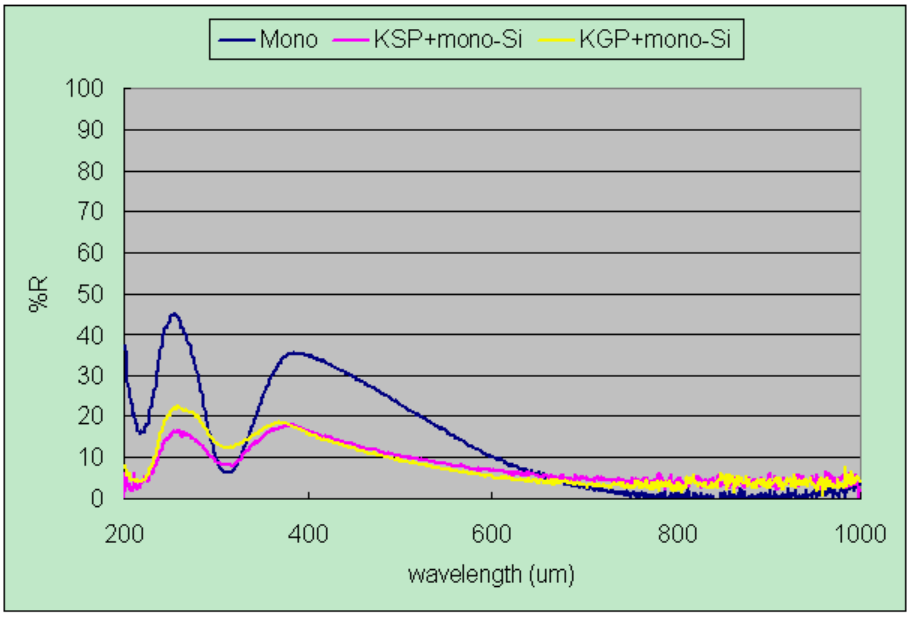

圖 56 分別以 $KCaGd(PO_4)_2:Eu^{3+}$與 $KSrGd(PO_4)_2:Eu^{3+}$塗佈太陽能電池反射光譜之比較

此外，圖57-59分別為利用SEM所測得太陽能電池表面影像，圖57僅有抗反射層於太陽能電池表面，螢光粉塗佈之前為整齊氮化矽結構，而圖58顯示在塗佈螢光粉後比較粗糙的表面，圖59由側面觀察，得知其厚度大約在3-4 μm之間。

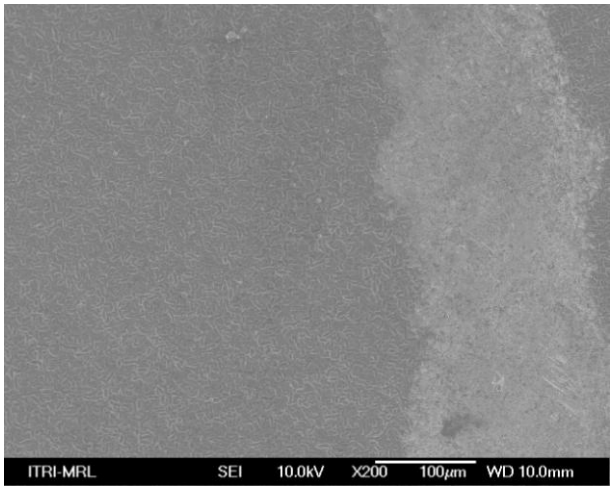

圖 57 只有氮化矽抗反射層太陽能電池之正面 SEM 影像

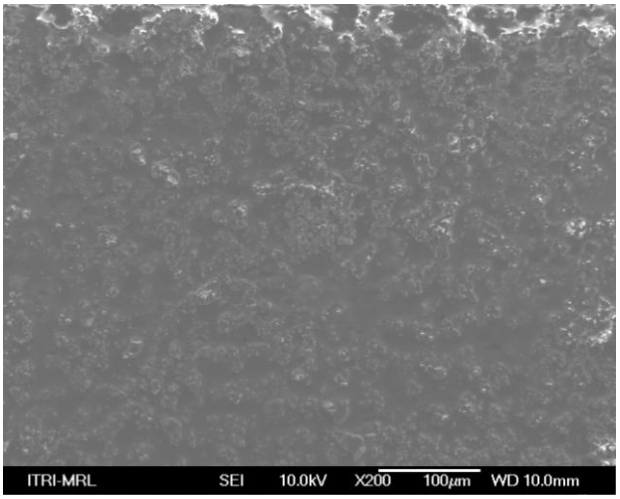

圖 58 太陽能電池塗佈螢光粉之正面 SEM 影像

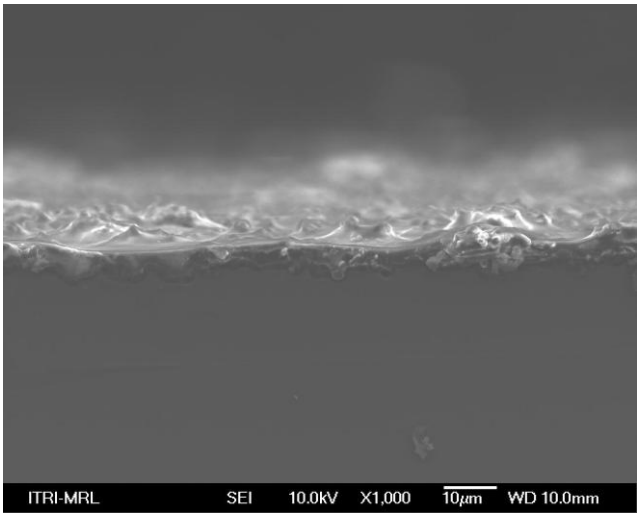

圖 59 螢光粉塗佈太陽能電池之側面 SEM 影像

4.4 上轉換螢光粉修飾矽太陽能電池之製備、微結構與光電特性之研究

4.4.1 $La_2Mo_2O_9:Yb^{3+}, R^{3+}$ (R = Er, Ho)螢光粉塗佈矽太陽能電池之製備

上轉換螢光粉是有別於一般的螢光粉概念，因為此類螢光粉乃是利用紅外線甚至遠紅外線的的光源轉換成可見光，這類轉換通常牽涉到2個到2個以上的紅外光子才能轉換一個可見光子。今天我們所要用到鉬酸類主體原本是一個具有導體功能的粉體，如果摻雜一些常見的上轉換稀土離子對，應該可以滿足在太陽能需求的上轉換螢光粉。這主體我們利用到兩個系統$La_2Mo_2O_9:Yb^{3+}, R^{3+}$ (R = Er, Ho)，因為這兩個系統轉換出的光子分別是黃綠光和橘紅光，而這兩種可見光對於太陽能電池的效率影響也是我們所要探討的。

首先我們利用螢光光譜儀測定其放光波長與能階，圖60所示為利用980 nm波長雷射為光源所測定之上轉換光譜。本研究發現$La_2Mo_2O_9$:Yb,Er在980 nm波長激發下，呈現三種波長分別為525 nm、550 nm與655 nm之可見光光子放射，由圖61能階示意圖發現此放射峰的發光源自於Er^{3+}能階之間的$^4H_{11/2} \rightarrow {}^4I_{15/2}$、$^4S_{3/2} \rightarrow {}^4I_{15/2}$與$^4F_{9/2} \rightarrow {}^4I_{15/2}$電子遷移，

另外，$La_2Mo_2O_9$:Yb,Ho在980 nm雷射的激發下，產生548 nm和657 nm發光，此兩放射峰分別源自於Ho^{3+} $^5F_4$,$^5S_2 \rightarrow {}^5I_8$ 與$^5F_5 \rightarrow {}^5I_8$電子遷移。

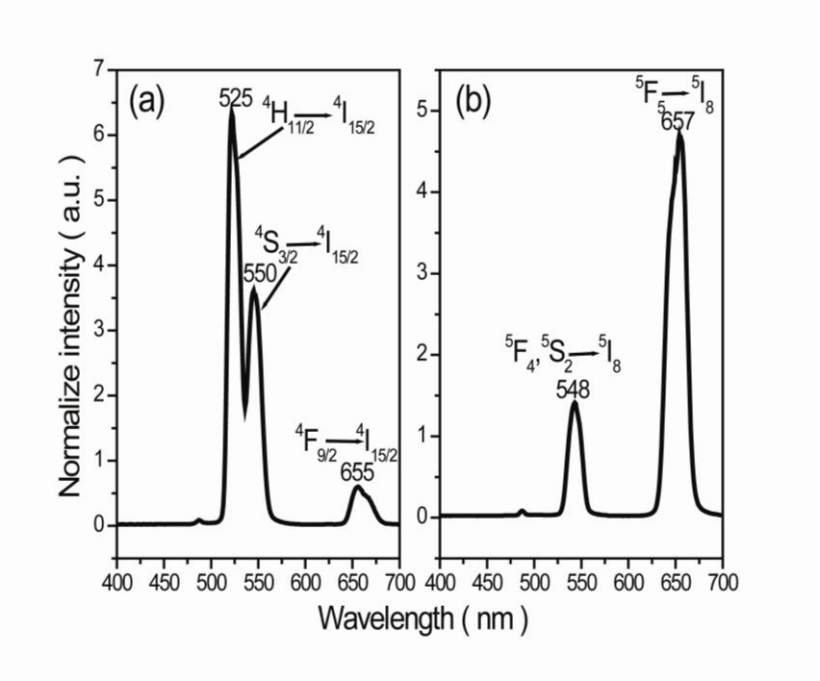

圖 60 $La_2Mo_2O_9$:Yb,R 螢光粉之上轉換光譜：R= (a) Er 與(b) Ho

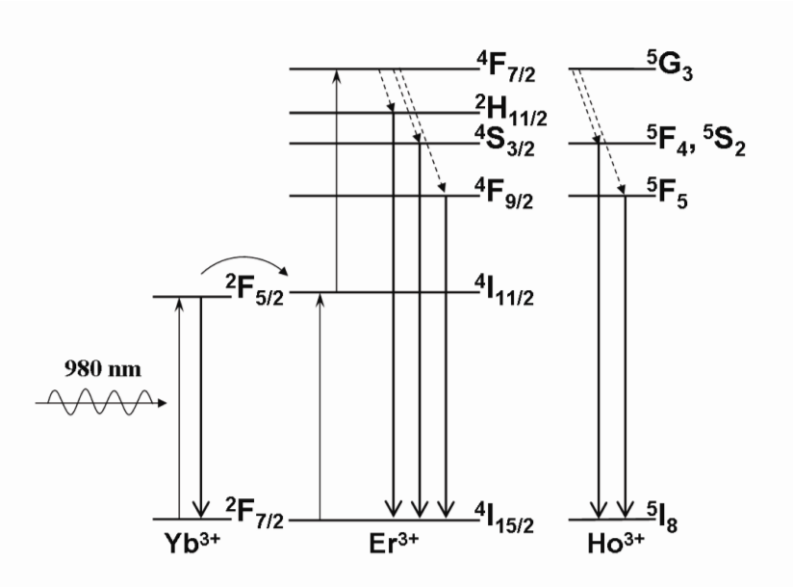

圖 61 $La_2Mo_2O_9$:Yb,Er,Ho 能階圖

在量測效率之前，我們先量測太陽能電池之反射光譜，期盼觀察其反射率是否下降？圖62顯示分別為有與無$La_2Mo_2O_9$:Yb,Er螢光粉塗佈之太陽能電池反射光譜之比較，我們發現$La_2Mo_2O_9$:Yb,Er螢光粉塗佈太陽能電池反射率呈現明顯下降，其下降幅度約為10%-15%。

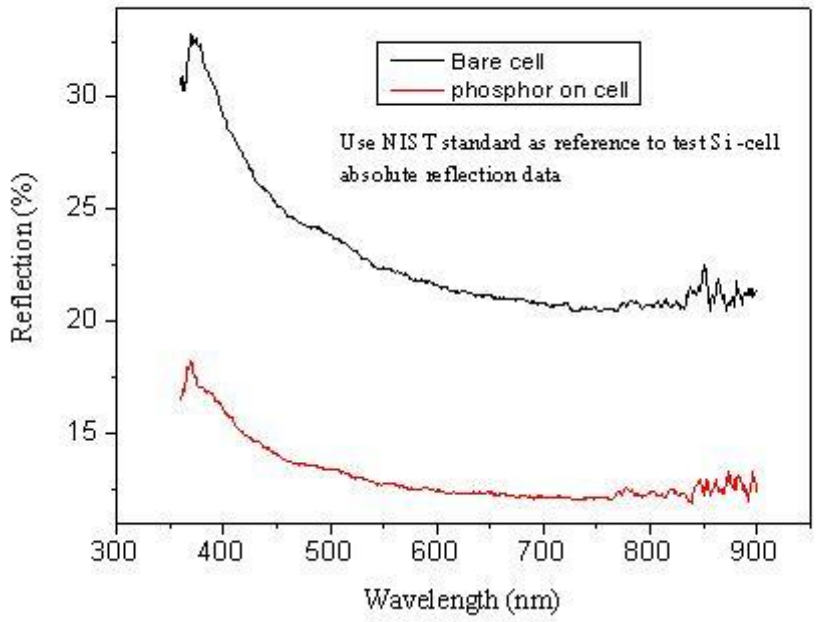

圖 62 有與無 $La_2Mo_2O_9$:Yb,Er 螢光粉塗佈太陽能電池反射光譜之比較

表3為$La_2Mo_2O_9$:Yb^{3+},R^{3+} (R = Er, Ho)塗佈在太陽能的光電參數值之比較，其中樣品No.1-2皆為$La_2Mo_2O_9$:Yb, Ho；而樣品No.3為$La_2Mo_2O_9$:Yb,Er塗佈之太陽電池；而No.4為將$La_2Mo_2O_9$:Yb, Er螢光粉塗佈在太陽能電池的背面之樣品。由表3中可以得知：樣品No.1-3之間，其ΔIsc與Δη值差異不大，但是樣品No.4的轉換效率提升卻是全部最高者，上述實驗結果源自元件結構之差異。圖63 (a)與(b)顯示兩種

上轉換螢光粉塗佈太陽電池結構之差異，如圖63 (b)所示，上轉換螢光粉應塗佈於太陽電池背面，方能獲得較高之轉換效率(Δη = 0.44%)。

表 3 $La_2Mo_2O_9:Yb^{3+},R^{3+}$ (R = Er, Ho)塗佈太陽電池光電特性之比較

Sample	Isc (bare)	Isc (coated)	ΔIsc	η (before)	η (after)	Δη (% increase)
No.1	8.05	8.18	0.13	16.53	16.78	0.25(+1.50%)
No.2	8.04	8.19	0.15	16.52	16.81	0.29(+1.76%)
No.3	8.06	8.21	0.15	16.53	16.80	0.27(+1.63%)
No.4	8.13	8.31	0.18	16.23	16.67	0.44(+2.71%)

No.1-3塗佈在cell前面，No.4是塗佈在cell後面

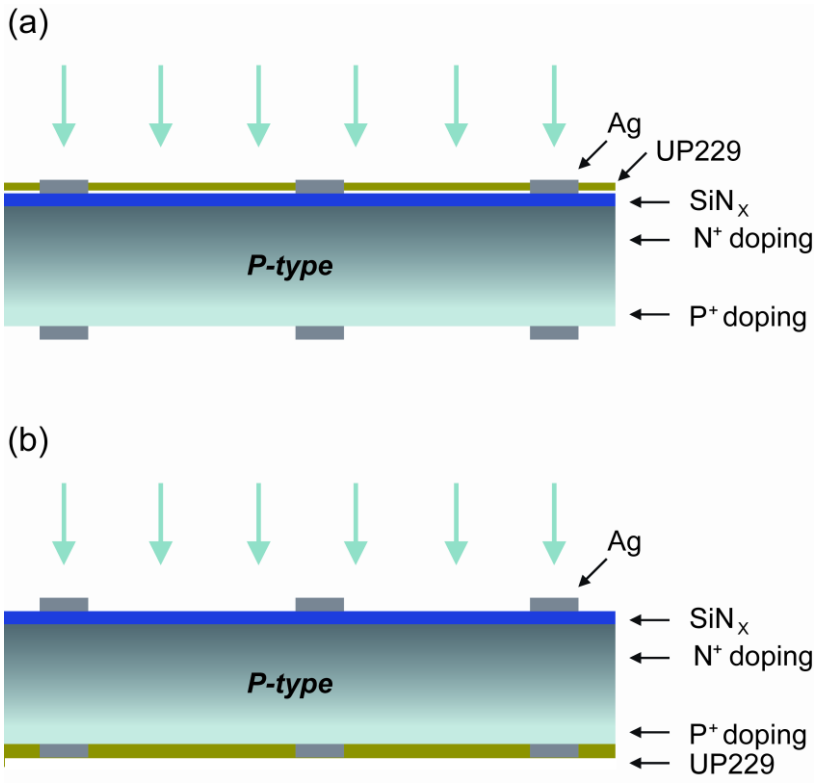

圖 63 上轉換螢光粉塗佈架構示意圖：(a)電池正面與(b)電池背面

由樣品No 3和樣品No 4之間Δη值的差異可以證實紅外線確實能穿透太陽能電池，如果將上轉換螢光粉塗佈於背鋁層之上，而背鋁層就能

扮演反射鏡面，將螢光粉上轉換所得到的可見光反射回P-N接面處。此項結構改變，由於需要改變太陽電池製程，需要特別處理，一般廠商比較少意願協助開發，故實驗數據相對較少。

4.4.1 $KCaGd(PO_4)_2:Yb^{3+}$,M (M= Er, Ho)螢光粉修飾矽太陽能電池之製備

因前述4.3.1節中$KCaGd(PO_4)_2:Eu^{3+}$螢光粉被塗佈於太陽能電池表面，已證實能提升轉換效率，因此本研究也嘗試利用相同的$KCaGd(PO_4)_2$主體，並摻雜具有上轉換功能的稀土離子對，以探討如此組合是否亦能提升轉換效率。圖64係利用980 nm波長雷射激發$KCaGd(PO_4)_2$:*x*Yb,1%Er所得之上轉換光譜，實驗結果顯示：當固定Er濃度為1%時，隨著Yb^{3+}離子濃度增高，其放射峰強度也隨之增強。

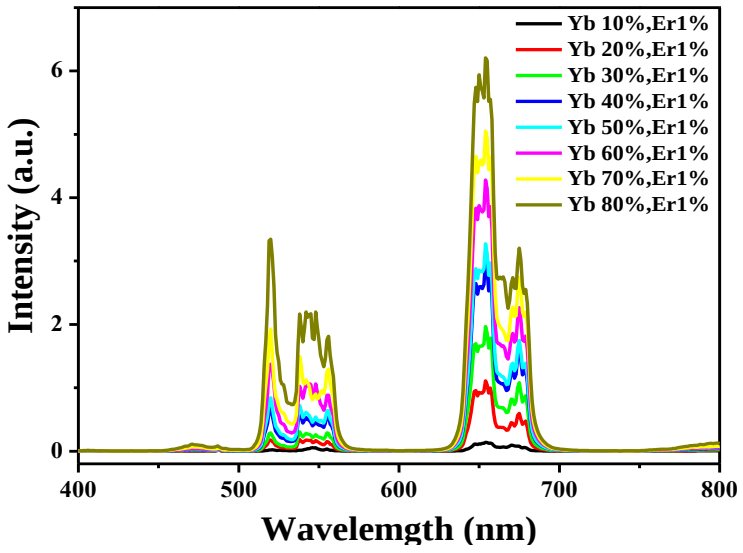

圖 64 以 980 nm 紅外光激發 $KCaGd(PO_4)_2$:*x*Yb,Er 所得上轉換光譜

分析圖64光譜顯示：當Yb^{3+}濃度為80%時，有最強的發光強度，因此我們將$KCaGd(PO_4)_2$:80%Yb,1%Er螢光粉與高分子膠材聚甲基丙烯酸甲酯(PMMA)，依照1:10的比例混合均勻後，使用網版網目尺寸為400 mesh，刮刀的壓力為0.25 Pa條件，將螢光粉塗佈於太陽電池的正面。網印前，先量測同一太陽電池轉換效率，其結果如圖65所示。網印完成後使用烘箱烘烤，在150℃烘烤5分鐘後，靜置回到室溫，再利用太陽能光譜儀測量其I-V關係曲線，其結果如圖66所示。

分析比較圖65與圖66結果顯示，在太陽能電池塗佈$KCaGd(PO_4)_2$:80%Yb,1%Er之後，其轉換效率由16.23%躍升至16.67%，其Isc值由8.1392 A躍升至8.3164 A，$\Delta\eta$值約為0.44±0.01%。

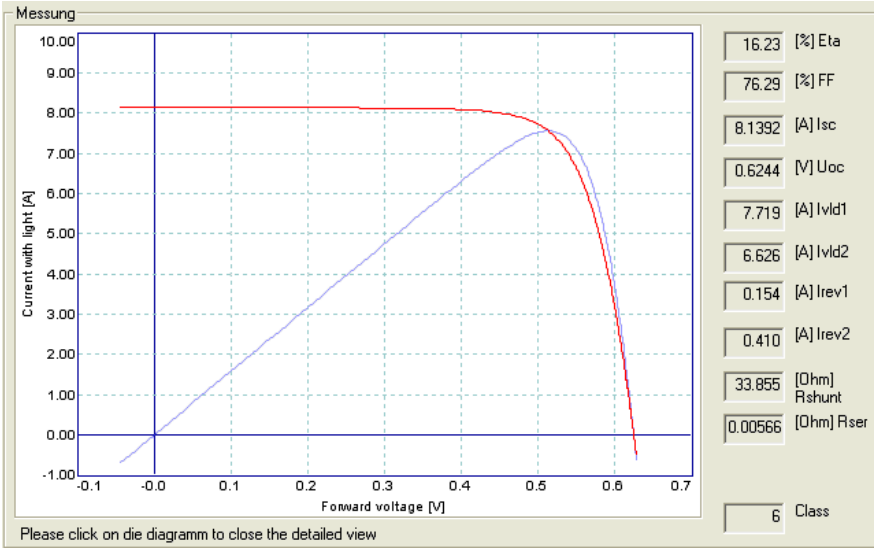

圖 65 未塗佈螢光粉之前太陽電池的 I-V 關係

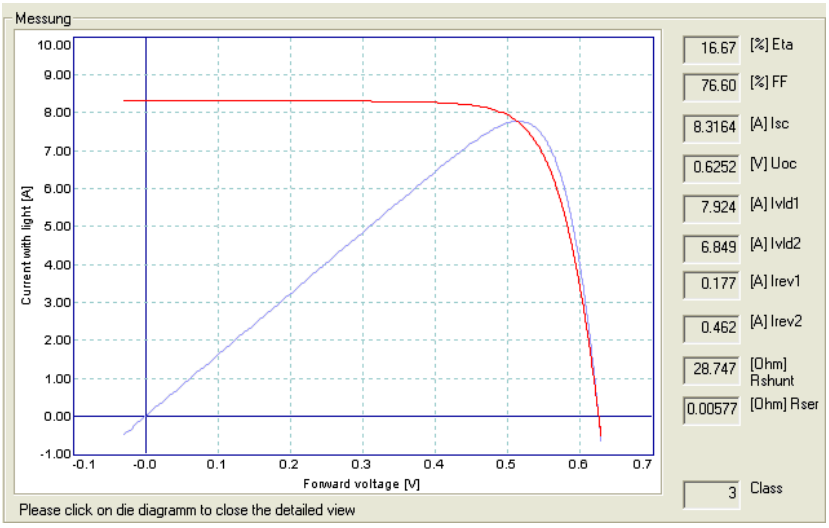

圖 66 已塗佈 $KCaGd(PO_4)_2$:80%Yb,1%Er 之後太陽電池的 I-V 關係

圖67係利用980 nm波長雷射激發$KCaGd(PO_4)_2$:*x*Yb,1%Ho所得之上轉換光譜，實驗結果顯示：當固定Ho濃度為1%時，隨著Yb^{3+}離子濃度增高，其放射峰強度也隨之增強。當Yb^{3+}濃度為80%時，有最強的發光強度。

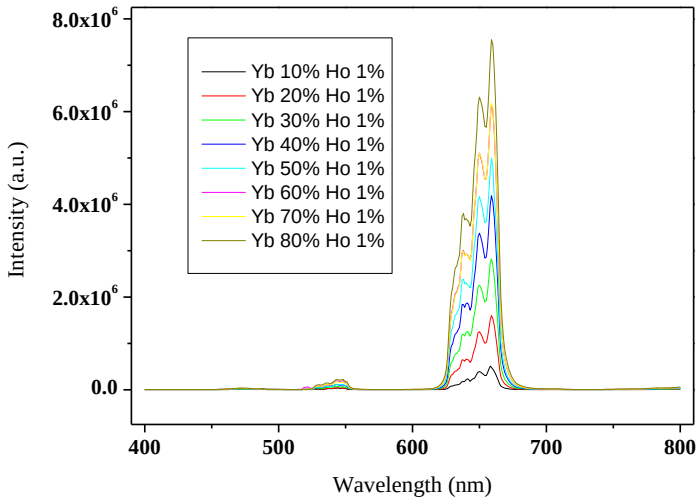

圖 67 以 980 nm 紅外光激發 $KCaGd(PO_4)_2$:*y*Yb,1%Ho 所得上轉換光譜

因此，我們將$KCaGd(PO_4)_2$:80%Yb,1%Ho螢光粉塗佈於太陽電池的正面。網印前，先量測同一太陽電池轉換效率，其結果如圖68所示。網印完成後使用烘箱烘烤，在150℃烘烤5分鐘後，靜置回到室溫，再利用太陽能光譜儀測量其I-V關係曲線，其結果如圖69所示。

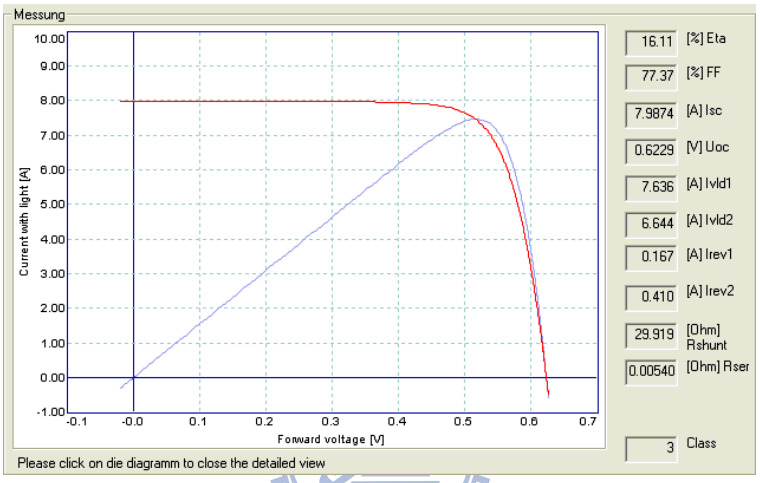

圖 68 未塗佈螢光粉之前太陽能電池的 I-V 關係

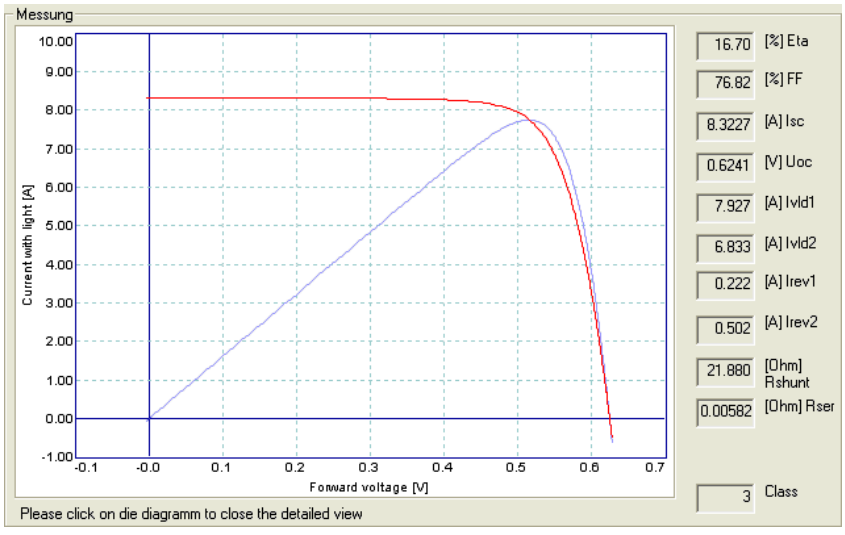

圖 69 已塗佈 $KCaGd(PO_4)_2$:80%Yb,1%Ho 後太陽能電池的 I-V 關係

分析比較圖68與圖69結果顯示，在太陽能電池塗佈$KCaGd(PO_4)_2$:80%Yb,1%Ho之後，其轉換效率由16.11%躍升至16.70%，其Isc值由7.9874A躍升至8.3227 A，Δη值約為0.59±0.01%。

結果發現其轉換效率也有明顯提升，其效果甚至較另一$La_2Mo_2O_9$:Yb^{3+},R^{3+} (R = Er, Ho)螢光粉(參閱4.4.1節)為強。整體的轉換效率提升幅度在3.7%以上。歸納其可能原因有二： 其一，原本$KCaGd(PO_4)_2$磷酸鹽主體較鉬酸鹽$La_2Mo_2O_9$主體具有較低的聲子振動能，所以上轉換的效率較高；其二，磷酸鹽類主體較適合塗佈在太陽電池，所以無論下轉換或上轉換螢光粉，在太陽能電池轉換效率之提升都呈現較佳之表現。

4.5 螢光粉塗佈矽太陽能電池轉換效率提升與元件參數之分析

以上實驗數據顯示，本論文所探討的四系列螢光粉中，似以$KCaGd(PO_4)_2$:50%Eu^{3+}提升太陽能電池轉換效率效果最佳，因此本研究選擇以$KCaGd(PO_4)_2$:50%Eu^{3+}來比較平均值，我們挑選同樣效率等級的太陽能cell，用$KCaGd(PO_4)_2$:50%Eu^{3+} 放大量產網印實驗片數後，再測量其光電性，表4為本實驗所製作40片太陽能電池的Isc與η之平均值與標準誤差之一覽。

表4 40片以$KCaGd(PO_4)_2$:50%Eu^{3+}塗佈太陽電池所測得Isc與η之平均值與標準誤差

#	Isc (A) (before)	Isc (A) (after)	Eff. (%) (Before)	Eff. (%) (After)
1	8.14	8.36	16.52	16.91
2	8.12	8.36	16.49	17.02
3	8.10	8.35	16.58	17.02
4	8.12	8.35	16.59	16.96
5	8.12	8.36	16.51	16.97
6	8.09	8.34	16.51	16.94
7	8.11	8.36	16.56	17.04
8	8.12	8.36	16.51	16.96
9	8.10	8.40	16.52	16.91
10	8.13	8.36	16.60	17.00
11	8.13	8.37	16.47	16.89
12	8.13	8.39	16.56	16.87
13	8.11	8.35	16.57	17.00
14	8.07	8.36	16.44	16.96
15	8.10	8.36	16.49	17.03
16	8.11	8.34	16.52	17.07
17	8.09	8.34	16.49	17.09
18	8.11	8.31	16.47	17.02
19	8.14	8.32	16.54	17.00
20	8.09	8.32	16.54	16.99
21	8.10	8.32	16.58	16.96
22	8.06	8.31	16.50	17.01
23	8.08	8.36	16.50	17.06
24	8.13	8.35	16.57	16.96
25	8.05	8.34	16.47	17.01
26	8.04	8.35	16.51	17.04
27	8.06	8.36	16.57	17.03
28	8.07	8.34	16.42	17.07
29	8.10	8.36	16.54	17.08
30	8.12	8.33	16.56	17.07
31	8.09	8.31	16.40	17.00
32	8.11	8.32	16.46	17.01
33	8.11	8.34	16.44	17.04
34	8.12	8.35	16.58	17.08
35	8.10	8.34	16.52	17.01
36	8.10	8.34	16.46	16.96
37	8.03	8.36	16.51	17.04
38	8.04	8.35	16.56	16.97
39	8.06	8.36	16.57	17.03
40	8.10	8.34	16.53	16.98
Average	8.10	8.35	16.52 %	17.00 %
standard deviation	0.0277	0.0194	0.0495 %	0.0517 %

由此系列實驗數據發現，以一定的參考數量來看，可以穩定增加約0.5%的轉換效率。這意味不考量每片太陽能電池存在的個別缺陷，依然可以提升其轉換效率，故此磷酸鹽為主體的螢光粉具有相當應用

潛力。

本研究後期，我們嘗試將上述40片電池進行封裝測試，以探討封裝後元件的效率，結果發現其操作效率呈現十分穩定，圖70與圖71為封裝元件的圖示與結果。

圖 70 由 36 小片電池所封裝而成之太陽能電池模組

Panel :		S636 by-S654-KRA-1
Type :		6x10
Panel no :		5
Serial no :		#03
Date :		090827
Ref. cell type :		Mono+th
Id. number :		MTP 2012-2
Sensitivity		104.4 mV
Act. temp.:		26.7 C
Result :		00 - Class A
Temp. =	25.0	C
Irrad.=	0.994	kW
Isc =	8.47	A
Voc =	22.47	V
Eff. =	16.12	%
FF =	72.08	%
MPP =	137.143	W
V@mpp =	17.46	V
I@mpp =	7.85	A
I@vref=	7.85	A
P@vref=	137.143	W
Rser. =	0.390	Ohm
Rsht =	131.569	Ohm

圖 71 由 36 小片電池所封裝之太陽能電池模組光電參數資料

我們也嘗試將塗佈$La_2Mo_2O_9$:Yb,Er單片的太陽能電池片進行封裝(如圖72所示)，隨後量測其封裝後的單片轉換效率與光電參數。

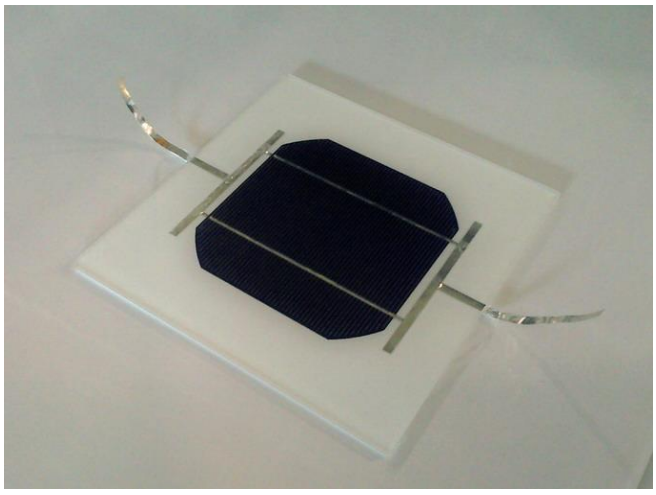

圖 72 已封裝之單片 $La_2Mo_2O_9$:Yb,Er 塗佈太陽能電池片及光電轉換數據

4.6 螢光粉修飾矽太陽能電池轉換效率提升之展望與未來工作重點

就目前的實驗結果而言，上轉換螢光粉和下轉換螢光粉對於太陽能電池轉換效率的提升都具有一定的效果，本論文確立下轉換螢光粉須塗佈於太陽能電池片的正面，其效果優於上轉換螢光粉，其原因為上轉換螢光粉需要光子的累積，其本身的發光效率較下轉換螢光粉差。上轉換螢光粉塗佈於電池背面，其提升轉換效率的效益較大。未來螢光粉對於太陽能電池效率的提升，仍有許多工作尚待完成，如：正確規則之建立、粉體粒徑大小之最佳化，均為未來須探討的工作。

本研究迄今已經獲致初步的成果，未來仍須以下列工作為重點：

1.網印時，最佳化並建立網板規格，以製作光波頻譜轉換型太陽電池。

2.製作光波頻譜轉換型太陽電池，所需各種粒徑上/下轉換螢光粉之製備與適當漿料之篩選。

3.光譜轉換型太陽電池結構(back-side/front-side contacted, bifacial)與螢光粉層厚度之最佳化研究。

4.塗佈用無機螢光粉粒徑之最佳化之研究 ，如：利用水熱化學反應製備奈米螢光粉以製作光頻譜轉換型太陽電池，再與其他粒徑螢光粉之效果做比較。

5. 有與無轉換材料時，太陽電池表面折射係數之量測與評估。

6.太陽電池表面反射(或穿透)光譜之光譜轉換法，以下轉換與上轉換螢光體提升多晶矽太陽電池光電轉換效率。

第五章 結論

本論文的研究目標主要利用太陽光譜轉換原理，藉由網印塗佈技術結合上/下轉換螢光粉與各型元件結構之太陽電池，期望有效改善矽太陽能電池之轉換效率。

本研究利用 X-光繞射進行螢光粉晶相鑑定，以激發、發射與反射光譜探討上/下轉換螢光粉發光特性，同時以掃描式電子顯微鏡術分析螢光粉微結構，此外我們使用太陽光譜模擬機進行光電轉換參數與電流-電壓曲線之量測。

本研究證實成本低廉、簡易可行的網印技術可被使用於將下轉換螢光粉 $Na_2CaPO_4F:Eu^{2+}$ 與 $KMGd(PO_4)_2:Eu^{3+}$ (M =Ca, Sr)塗佈於太陽能電池正面，利用螢光粉將太陽光譜紫外波段轉換成可見光，藉以增加矽基板轉換效率。實驗證實：經 $Na_2CaPO_4F:Eu^{2+}$ 塗佈後，太陽電池之效率由 15.93%增至 16.59%；而經三種 $KCaGd(PO_4)_2:x\%Eu^{3+}$ 螢光粉分別塗佈太陽電池後，其轉換效率增加值分別為 $0.66\pm0.01\%$ (x = 10)、$0.71\pm0.01\%$ (x = 50)與 $0.52\pm0.01\%$(x = 100)，其中 0.01%為標準誤差。

此外，本研究亦將上轉換螢光粉 $La_2Mo_2O_9:Yb, R$ 與 $KCaGd(PO_4)_2:Yb,R$ (R = Er, Ho)分別網印塗佈於太陽能電池之背層，實驗證實，不同化學組成的螢光粉可以提高太陽能電池轉換效率不等，結果顯示：上轉換螢光粉塗佈太陽能電池中，以 $La_2Mo_2O_9:Yb,R$

塗佈者，其效率分別增加 0.25-0.29± 0.01% (R = Er)與 0.44± 0.01% (R = Ho)。另一方面，以 $KCaGd(PO_4)_2$:Yb,R 塗佈者，其轉換效率分別增加 0.44± 0.01% (R = Er)與 0.59± 0.01% (R = Ho)。

實驗結果顯示，下轉換螢光粉應塗佈於太陽能電池的正面，亦即在氮化矽抗反射層之表面，如此即可提高光電轉換效率；而上轉換螢光粉應塗佈於太陽能電池的背面，亦即鋁背底層之上，因紅外線可穿透電池達到鋁背底層，除不影響原本的抗反射層外觀，亦可達成光電轉換效率之提升。

本研究已掌握具有高效率頻譜轉換螢光材料、穩定而可靠的漿料與不同元件結構太陽電池之供應來源，經初步試驗證實太陽電池轉換效率之增幅最高可達 5%，預期可望縮減矽太陽電池轉換效率提升之成本。實驗數據證實，利用螢光粉以提升太陽電池光電轉換效率是可行的，且所提升的效果顯著，本項技術成本低廉、簡易可行極具商業化之潛力。

參考文獻

1. 中國大百科全書－化學篇II P.1126.
2. G..Blasse and B. C. Grabmaier, *"Luminescent Materials"*, Springer, Berlin (1994).
3. R. C. Ropp , *"Luminescence and the Solid State"*, Amsterdam Elsevier (1991).
4. 蘇勉曾、吳世康,發光材料, Vol.4, p.9.
5. 顧鴻濤:「太陽能電池元件導論」(全威圖書出版公司 2008/6 初版).
6. 高逢時 科學發展 2003 367期 64-69.
7. 陳頤承、郭昭顯「太陽能電池量測」工業材料雜誌 258 期，2008.
8. B.S. Richards, *Solar Energy Materials & Solar Cells*, 90 (2006) 2329–2337.
9. C. Strumpel, M. McCann, *Solar Energy Materials & Solar Cells*, 91 (2007) 238–249.
10. A. Shalav, B. S. Richards, and T. Trupke, *Applied Physics Letters*, 86, (2005) 013505.
11. A. Shalav, B. S. Richards, M. A. Green, *Solar Energy Materials & Solar Cells*, 91 (2007) 829–842.
12. P. Chung, H.H. Chung, and P. H. Holloway, *J. Vac. Sci. Technol"* A,

25 (2007) 61-66.

13. H. Shpaisman, O. Niitsoo, I. Lubomirsky and D. Cahen, *Solar Energy Materials & Solar Cells*, 92, (2008), 1541-1546.
14. Y. Li, W. Shan, S. Cheng, M. Ko. (Intematix Corp. USA), Wavelength-converting phosphors for enhancing the efficiency of a photovoltaic device, WO 2007/133344.
15. 張守進：「先進網印技術及螢光粉在進太陽能電池製程之應用」國家科學委員會專題研究計畫成果報告 NSC92-2622-E006-119-CC3 (2004/8/31).
16. Y. C. Chen, W. Y. Huang and T. M. Chen, Journal of Rare Earths 2011 accepted.
17. Z. J. Zhang, J. L .Yuan, C. J. Duan, D. B. Xiong, H. H. Chen, J. T. Zhao, G. B. Zhang, C. S. Shi, *J. Appl. Phys.*2007, 102, 093514.
18. Y. C. Chen, T. M. Chen, Journal of Rare Earths 2011 accepted.

附錄一

Enhancing the Performance of Photovoltaic Cells by Using Down-Converting $KCaGd(PO_4)_2:Eu^{3+}$ Phosphors

Yen-Chi Chen, Woan-Yu Huang and Teng-Ming Chen*

Phosphors Research Laboratory and Department of Applied Chemistry, National Chiao Tung University, Hsinchu 30010, Taiwan

Abstract：The goal of this work is aimed to improve the power conversion efficiency of single crystalline silicon-based photovoltaic (PV) cells by using the solar spectral conversion principle, which employs a down-converting phosphor to convert a high-energy ultraviolet photon to the less energetic red-emitting photons to improve the spectral response of Si solar cells. In this study, the surface of silicon solar cells was coated with a red-emitting $KCaGd(PO_4)_2:Eu^{3+}$ phosphor by using the screen-printing technique. In addition to the investigation on the microstructure using SEM, we have measured the short circuit current (Isc), open circuit voltage (Voc), and power conversion efficiency (η) of spectral-conversion cells and compared with those of bare solar cells as a reference. Preliminary experimental results revealed that in an optimized PV cell, an enhancement of $0.64\pm0.01\%$ (from 16.03% to 16.67%) in $\Delta\eta$ of a Si-based PV cell has been achieved.

Keywords: Solar cells; Down-converting phosphor; $KCaGd(PO_4)_2:Eu^{3+}$; Screen-printing

To face the challenge of global warming, the development of green energy materials has been an important issue in materials research. The photovoltaic (PV) cell is one of the devices that can be used to generate sustainable energy; therefore, many research attempts have been made to explore materials that are able to enhance the power conversion efficiency (η) of solar cells. The conversion efficiency from light to electricity in a PV cell is highly dependent on the wavelength (λ) of incident light, and the η-λ relationship is characterized by the spectral response.[1] In general, the PV cells are able to convert only a small portion (*i.e.*, longer wavelength domain) of solar spectrum into electricity, with ultraviolet (UV) and infrared (IR) spectral domains wasted. Attempts to improve the conversion efficiency of PV cells using spectral conversion technique by employing up- or down-conversion phosphors have been well documented in the literature [1–7].

In recent years, a series of double phosphates, represented as $ABM(PO_4)_2$ (where A = alkali metal, B = alkaline earth, M = Gd, Y or La) and isotypic with $LaPO_4$, have been reported[8–14]. With appropriate doping, the $ABM(PO_4)_2$ phosphates were reported to show wide applications in plasma displays and mercury-free lamps; mainly, because the host of $ABM(PO_4)_2$ exhibits low phonon energy and potential quantum-cutting property.[14].

In this research, the effect of coating a down-conversion phosphor that is expected to form a radiation-sensitive surface on the silicon-based PV cells in attempt to increase the power conversion efficiency was investigated. Essentially, this deposited phosphor layer is suitable for absorption and emission in the portion of solar spectrum and further benefits utilization of sun light, thus improving the η value of the PV cells. Furthermore, the coated phosphor layer exhibits lower refractive index, which may serve as an antireflection layer in addition to solar spectral conversion.

We have screened and selected phosphors such as $KCaGd(PO_4)_2:Eu^{3+}$ ($KCGP:Eu^{3+}$), with low phonon energy and lower refractive index than Si or Si_3N_4 that may be capable of converting more UV photons into photons with longer wavelengths to induce a greater spectral response for a Si-based PV cell. This work is attempted to evaluate and examine the potential applications of the down-converting $KCaGd(PO_4)_2:Eu^{3+}$ in an attempt to improve

Foundation item: Supported by National Science Council of Taiwan under contract No NSC98-2113-M-009-005-MY3. Corresponding author: Teng-Ming Chen (E-mail: tmchen@mail.nctu.edu.tw; Tel: +886-3-5731695)

the efficiency of silicon-based PV cells. We have utilized a screen-printing technique to form a phosphor layers directly onto a commercial Si PV cell to convert the UV photons into those with wavelengths longer than 500 nm. The dependence of photovoltaic efficiency on the phosphor compositions, photoluminescence (PL) and PL excitation (PLE) spectra, and microstructure of the phosphor layer were investigated and discussed.

1 Experimental

Stoichiometric starting materials of $(NH_4)_2HPO_4$, K_2CO_3, Eu_2O_3, $SrCO_3$, $CaCO_3$ (all analytic grade), and Gd_2O_3 (99.99% pure) were mixed together with NH_4Cl as a flux and transferred to an alumina crucible; the materials were then heat treated at 800°C for 6 h and at 1200°C for 6 h. In comparison with the process described by Zhang *et al.*[7], our synthesis process takes only one-third of the time needed to prepare $KMGd(PO_4)_2$ (M = Ca, Sr). The phase purity of $KMGd(PO_4)_2:Eu^{3+}$ phosphors was checked by powder X-ray diffraction with a Bruker AXS D8 advanced automatic diffractometer with Cu Kα radiation and all of reflections between 2θ = 10° and 80° were collected at room temperature. Photoluminescence (PL) and PL excitation (PLE) spectra were obtained using a Jobin Yvon-Spex FluoroLog-3 fluorophotometer equipped with a 450 W Xe lamp as a light source.

The fabrication of $KCaGd(PO_4)_2:Eu^{3+}$ ($KGP:Eu^{3+}$)-coated solar cells is summarized in the flow diagram shown in Figure 1. Briefly, the $KCaGd(PO_4)_2:Eu^{3+}$ phosphor was well-mixed with and dispersed in a composite polymethylmethacrylate (PMMA) polymer binder and the phosphor/binder mixture was then screen-printed on top of the prestructured Si_3N_4 reflective layer of a 6"x6" Si solar cell to form a transluscent film with 3-4 μm in thickness. The phosphor-coated solar cell was then baked at about 130℃ in the air for 10 minutes. The device structure of down-converting $KCaGd(PO_4)_2:Eu^{3+}$ phosphor-coated solar cells is schematically shown in Figure 2.

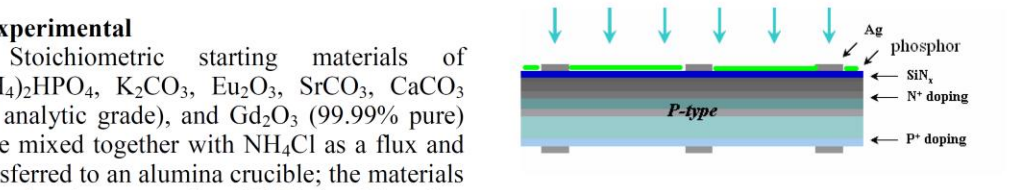

Figure 1 Flow diagram for fabrication of phosphor-coated Si solar cells.

Figure 2 The device structure of down-converting $KCaGd(PO_4)_2:Eu^{3+}$ phosphor-coated solar cells.

Furthermore, the open-circuit voltage (Voc), short-circuit current (I_{sc}), and power conversion efficiency (η) of the phosphor-coated solar cells were then measured using an h.a.l.m IV curve tracer (cetisPV-CTL1) and a Sun simulator (Xenon-Flasher cetisPV-XF2).

2 Results and discussion

The XRD patterns of $KCaGd(PO_4)_2:Eu^{3+}$ and $KSrGd(PO_4)_2:Eu^{3+}$ samples shown in Figures 3a and 3b, respectively, were found to match well with those reported in JCPDS cards 34-0125 and 34-0118, respectively. Except for slight differences in the cell parameters of the unit cell, $KCaGd(PO_4)_2$ and $KSrGd(PO_4)_2$ have the same crystal structure similar to $KCaNd(PO_4)_2$, which is isostructural with hexagonal $LaPO_4$.

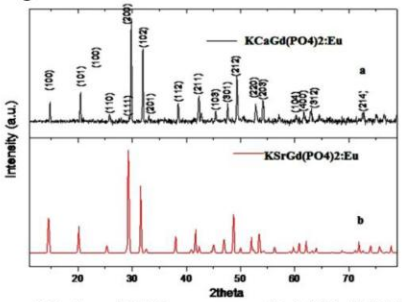

Figure 3 Indexed XRD patterns of (a) $KCaGd(PO_4)_2:Eu^{3+}$ and (b) $KSrGd(PO_4)_2:Eu^{3+}$.

The $KCaGd(PO_4)_2$ host was found not to absorb in the ultraviolet region. The $KGP:Eu^{3+}$ phosphor can be excited with 393 nm UV light

and produces orange-red emission peaking at 585 nm. The PLE spectrum of KGP:Eu^{3+} phosphor shows absorption in the wavelength domain of 260 to 530 nm and a maximal emission in the wavelength domain of 580 to 700 nm, as indicated in Figure 4. Since the silicon wafer shows poor absorption in the UV spectral range, applying the KGP:Eu^{3+} or KSP:Eu^{3+} phosphor as a radiation-sensitive layer on the surface a PV cell would be expected to increase the UV absorption and thus enhance the efficiency of power conversion.

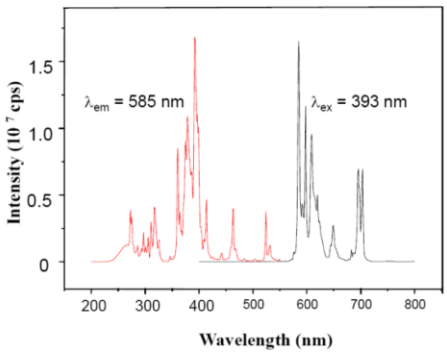

Figure 4 PLE and PL spectra of $KCaGd(PO_4)_2$ at room temperature.

Figure 5 shows and compares the reflectance spectra for bare, soley binder-coated, and KGP:xEu^{3+} (x = 5%, 10%, 30%, 50%, and 100%)-coated solar cells.

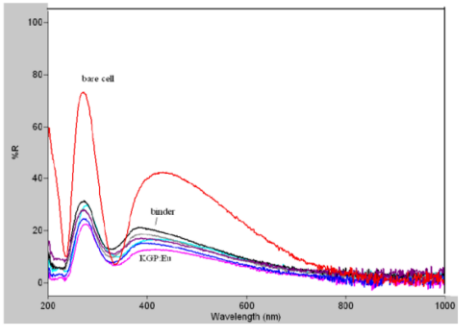

Figure 5 Comparison of reflectance spectra for bare and KGP:Eu^{3+}-coated solar cells. From top: bare cell, binder+cell, and cells with 5%-, 10%-, 30%-, 50%, and 100% KGP:Eu^{3+}-coating.

Comparison of the reflectance spectra for the bare, binder-coated, and phosphor-coated cells indicates that the phosphor coating on the surface of the Si wafer can effectively reduce reflection and increase light absorption. A drastic reduction in the reflectance was observed for the phosphor KCGP:100%Eu^{3+}-coated cell. In addition to the decrease in reflectance, the observed Isc obtained from KCGP:Eu^{3+}-coated solar cells was simultaneously found to increase with phosphor coating. Figure 6 presents the current-voltage data for an optimized Si solar cells with and without coating of KCGP:Eu^{3+}, respectively. Data analysis indicates that KCGP:Eu^{3+}-coated solar cell has greater I_{sc} due to the efficient light conversion. That is, the I_{sc} value was found to increase from 7.9664 to 8.3058 A, Voc increases from 0.6231 to 0.6247 V, and η was found to increase from 16.03% to 16.67%. These data revealed that I_{sc} increases significantly with Voc unchanged upon phosphor coating.

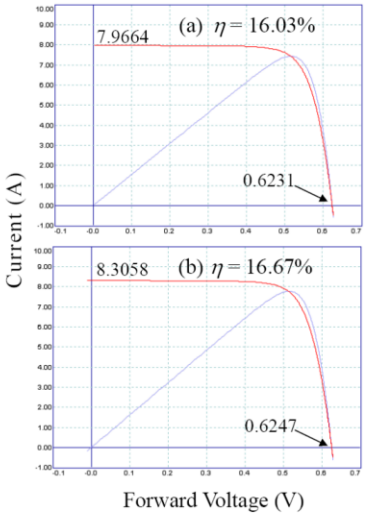

Figure 6 Experimental current–voltage curves for a representative Si solar cells: (a) without and (b) with KGP:Eu^{3+} phosphor coating.

To further verify the experimental results that coating of KCGP:Eu^{3+} phosphor increases the power conversion efficiency, we measured the Isc, Voc, η, ΔIsc, ΔVoc and Δη for forty solar cells coated with and without KCGP:Eu^{3+} phosphor. Table 1 summarizes the comparison on the average values and standard deviations of I_{sc}, Voc, η, ΔIsc, ΔVoc, and Δη.

On the average, we have observed that short-circuit current increases appreciably from 8.10 to 8.35A and the open-circuit voltage varies from 0.63115 to 0.63200V insignificantly, respectively.

Table 1. Comparison of averaged Isc, Voc, η, ΔIsc , ΔVoc, and $\Delta\eta$ obtained for forty solar cells with and without coating of $KCaGd(PO_4)_2:Eu^{3+}$ investigated in this work.

	$I_{sc}(1)$	$I_{sc}(2)$	ΔI_{sc}	$V_{oc}(1)$	$V_{oc}(2)$	ΔV_{oc}	η_1	η_2	$\Delta\eta\ (\eta_2-\eta_1)$
Average	8.10	8.35	0.25	0.63115	0.63200	0.0085	16.52%	17.00%	0.48 %
Standard deviation	0.02	0.02		0.0010	0.0010		0.0495	0.0517	

We have also observed that η increase for 0.48% from an average value 16.52% to 17.00%. To investigate the microstructure of the phosphor-coated solar cell, we have investigated the SEM micrographs of a screen-printed $KGP:Eu^{3+}$-coated solar cell after baking. Figures 7(a) and (b) show the top- and side-view of the cell and the surface exhibits granular feature inherited from phosphor particles, whereas the radiation-sensitive layer is estimated to be 3.4 μm in thickness, as revealed in the side-view SEM micrograph.

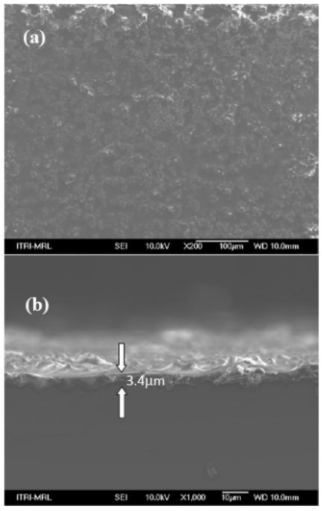

Figure 7 SEM micrographs of a $KGP:Eu^{3+}$-coated Si solar cell: (a) top view and (b) side view.

3 Conclusions

We have prepared a double phosphate phosphor $KCaGd(PO_4)_2:Eu^{3+}$ and demonstrated that the down-converting $KCaGd(PO_4)_2:Eu^{3+}$ phosphor coated on the surface of a polycrystalline silicon solar cell can effectively increase the values of Isc, Voc, and η of the cell. The increase in η is about 0.48% on the average, which corresponds to an increment of from 16.52% to 17.00%. However, in an optimized case, we have observed an increase in η from 16.03% to 16.67%, which corresponds to an increase of 0.64%. Coating orange red-emitting down-converting phosphors by screen printing technique on the surface of conventional solar devices is effective in enhancing the η value and has been demonstrated in this research. The coated phosphor forms not only a spectral conversion layer for one part of the solar spectrum but also serves a low reflective layer for a different part of the solar spectrum. The PMMA may provide a transparent matrix for phosphor coating. Further work to improve the power conversion efficiency and select more efficient phosphors for solar application is currently in progress.

Acknowledgments

This research was supported by National Science Council of Taiwan under contract No. NSC98-2113-M-009-005-MY3.

References

[1] Trupke T, Green M A, Würfel P. Improving solar cell efficiencies by down-conversion of high-energy photons. *J. Appl. Phys.* 2002, **92**: 1668.

[2] Shalav A, Richards B S, Trupke T. An Application of $NaYF_4:Er^{3+}$ up-converting phosphors for enhanced near-infrared silicon solar cell response. *Appl. Phys. Lett.* 2005, **86**: 013505.

[3] Trupke T, Shalav A, Richards B S, Würfel P, Green M A. Efficiency enhancement of solar cells by luminescent up-conversion of sunlight. *Solar Energy Materials and Solar Cells*, 2006, **90**:3327.

[4] Chung P, Chung H, Holloway P H. Phosphor coatings to enhance Si photovoltaic cell performance. *J. Vacuum Scien. Tech. A* 2007,**25**: 61.
[5] Shalav A, Richards B S, Green M A. Luminescent layers for enhanced silicon solar cell performance: Up-conversion. *Solar Energy Materials and Solar Cells* 2007, **91**: 829.
[6] Shpaisman H, Niitsoo O, Lubomirsky I, Cahen D. Can up- and down-conversion and multi-exciton generation improve photovoltaics? *Solar Energy Materials and Solar Cells* 2008, **92**:1541.
[7] Li Y, Shan W, Cheng S, Ko M. (Intematix Corp. USA). "Wavelength-converting phosphors for enhancing the efficiency of a photovoltaic device" Patent: WO 2007/133344.
[8] Devriesh A J, Kiliaan S, Blase G. An investigation of energy migration in luminescent diluted Gd^{3+} systems. *J. Solid StateChem.*1986,**65**:190.
[9] Blase G. New luminescent materials . *Chem. Mater.*1989,**1**:294.
[10] Tabirou M E, Daoudi A, Une nouvelle famille de phosphates triples d'éléments alcalins, alcalinoterreux et de terres rares. *C.R. Acad. Sci. Série C* 1980, **291**: 93.
[11] Srivastavma A M, Sobierasj T, Ruan K, Banks E. Sensitization of the Gd^{3+} lattice by Pr^{3+} in $GdBO_3$ and energy transfer to Ln^{3+} (Ln^{3+} = Dy^{3+}, Sm^{3+}, and Tb^{3+}). *Mater. Res. Bull.* 1986,**21**:1455.
[12] Srivastava A M, Gieger T S, Banks E. Luminescence and energy transfer in $BaGdB_9O_{16}$. *Mater. Chem. Phys.* 1989, **21**: 327.
[13] Hiran H, Blasse G. Energy transfer phenomena in luminescent materials based on GdB_3O_6. *Mater. Chem. Phys.* 1985, **12**: 257.
[14] Zhang Z J, Yuan J L, Duan C J, Xiong D B, Chen H H, Zhao J T, Zhang G B, Shi C S. Vacuum ultraviolet spectroscopic properties of rare earth (RE = Ce,Tb,Eu,Tm,Sm)-doped hexagonal $KCaGd(PO_4)_2$ phosphate. *J. Appl. Phys.*2007,**102**:093514.

附錄二

Improvement of Conversion Efficiency of Silicon Solar Cells using Up-conversion Molybdate $La_2Mo_2O_9$:Yb,R (R = Er, Ho) Phosphors

Yen-Chi Chen and Teng-Ming Chen*

Phosphors Research Laboratory and Department of Applied Chemistry, National Chiao Tung University, Hsinchu 30010, Taiwan

Abstract：The goal of this work is aimed to integrate the solar spectral up-conversion principles and predesigned device structures to enhance the conversion efficiency. The performance of up-conversion phosphors is influenced by the host structure and the active ion concentration. In this study, the surface of multicrystalline silicon solar cells was coated with an up-conversion molybdate phosphor to improve the responsitivity of the solar cell in the near-infrared spectral range. The short circuit current (Isc), open circuit voltage (Voc), and conversion efficiency (η) of spectral conversion cells were measured. Preliminary experimental results revealed that the light conversion efficiency of a 1.5-2.7% increase in Si-based cell has been achieved.

Keywords: up-conversion phosphors; $La_2Mo_2O_9$:Yb^{3+},Er^{3+} (Ho^{3+}); solar cell

Over the past decade, it has been well known that up-conversion (UC) phosphors emit photons with a higher energy than that of photons excited via a two- or more-photon system. This process is based on the presence of at least two metastable excited states that are used to add up the energy of excitation photons, which convert infrared (IR) or near-IR (NIR) excitation into visible (VIS) luminescence. The materials used for upconversion typically include trivalent rare-earth sensitizer (e.g., Yb^{3+} and Er^{3+}) and activator (e.g., Er^{3+}, Ho^{3+}, Pr^{3+}, and Tm^{3+}) ions, which act together in a multi-photon process [1]. UC phosphors have been extensively studied due to their applicability in various areas [2,3]. UC is also one of the approaches in the framework of the so-called third generation photovoltaics, first proposed by Green in 2002 [4]. Detailed balance calculations have shown that application of an up-converter increases the efficiency limit of silicon solar cells from 31% to 37.4% [4,5]. Because low-energy photons are transmitted through silicon solar cells, the up-converter should be placed on the rear of spectral conversion solar cells. If the conversion of two incident infrared photons into one visible photon is realized, then the energy loss due to thermalization of the electron-hole pairs could be effectively minimized.

Because the relationship between the conversion efficiency and wavelength is often characterized by the spectral response [6], our research evaluates and examines the potential applications of two up-converters $La_2Mo_2O_9$:Yb,R (R = Er, Ho) in improving the conversion efficiency of polycrystalline solar cells. The crystal structure of $La_2Mo_2O_9$, reported to be a new fast ion-conductor, was studied by Goutenoire et al. [7] and found that La and Mo cations alternate to form a lattice of distorted parallelepipeds and define buckled La-Mo-O planes perpendicular to the three axes.

From the first claims of their performance as a solid electrolyte [7,8], spectral conversion photovoltaic cells consisting of $La_2Mo_2O_9$:Yb,R phosphor-coated silicon wafers, which convert photons into electricity with an efficiency dependent on the wavelength, were fabricated by using the screen-printing technique. In this study, UC phosphor layers were deposited directly onto Si photovoltaic cells to convert the photons with 980 nm in wavelength to those with wavelengths longer than 500 nm. The dependence of photovoltaic efficiency on the phosphor quantum efficiency, photoluminescence (PL) and PL excitation (PLE) spectra were then demonstrated and discussed

Foundation item: Supported by National Science Council of Taiwan under contract No NSC98-2113-M-009-005-MY3.
Corresponding author: Teng-Ming Chen (E-mail: tmchen@mail.nctu.edu.tw; Tel: +886-3-5731695)

1 Experimental

The two molybdate up-converters $La_2Mo_2O_9$:Yb,R (R = Er, Ho) were prepared by a two step method. A mixture of La_2O_3, MoO_3, Yb_2O_3, and R_2O_3 in the stoichiometric composition of (1-x-y):2:x:y with x = 0.09 and y =0.01 was dissolved in aqueous solution of 5% HCl and a light yellow powder precursor was obtained after drying. The obtained yellowish powder was then ground and well mixed with an agate mortar and then placed in an alumina crucible, which was heated at 900 °C for 8 h, and then cooled slowly. Several regrindings and heatings were necessary to obtain a white compound with high purity. $La_2Mo_2O_9$:Yb,Ho was labeled sample No. 1 and $La_2Mo_2O_9$:Yb,Er samples were labeled as samples No. 2-4. Each of the four samples was mixed with PMMA polymer binder in a ration of 1:10 in weight % and then coated on a 6"x6" polycrystalline Si solar cell for measurements .

The phase purity of the $La_2Mo_2O_9$:Yb,R phosphors was then checked by X-ray powder diffraction (XRD) analysis using a Bruker AXS D8 advanced automatic diffractometer with Cu Kα radiation. PL spectra were obtained by using a Jobin Yvon-Spex Fluolog-3 fluorophotometer equipped with light coming from a 450 W Xe lamp. We also used a 1 Watt 980-nm laser diode to characterize the molybdate phosphors and the measurements of short circuit current (Isc), open circuit voltage (Voc), and conversion efficiency (η) were obtained using an h.a.l.m IV curve tracer (cetisPV-CTL1) and a Sun simulator (Xenon-Flasher cetisPV-XF2). The fabrication of $La_2Mo_2O_9$:Yb,R (R = Er, Ho)-coated solar cells is represented the flow diagram shown in Fig. 1.

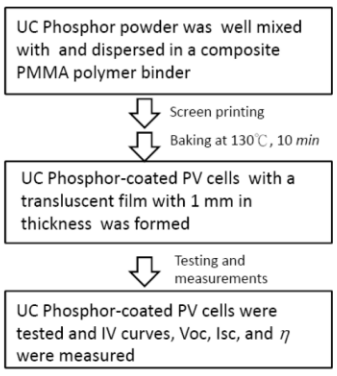

Figure 1 Flow diagram for fabrication of phosphor-coated polycrystalline Si solar cells.

To investigate the effect of photovoltaic device structure on the conversion efficiency, we have fabricated two types of phosphor-coated solar cells, namely, the one with phosphor coated on front-side (samples No.1-3) and the one with $La_2Mo_2O_9$:Yb,Er coated on the rear surface of the Si cell (sample No.4). The phosphor used in sample No. 1 is $La_2Mo_2O_9$:Yb,Ho and that used for samples Nos. 2 and 3 is $La_2Mo_2O_9$: Yb,Er. Briefly, the $La_2Mo_2O_9$:Yb,R phosphors were well-mixed with and dispersed in a composite polymethyl methacrylate (PMMA) polymer binder and the following baking temperature was about 130℃ for 10 minutes. A translucent phosphor film with a thickness of about few μm was then formed on the surface. The structure of the devices that we used is shown in Fig. 2.

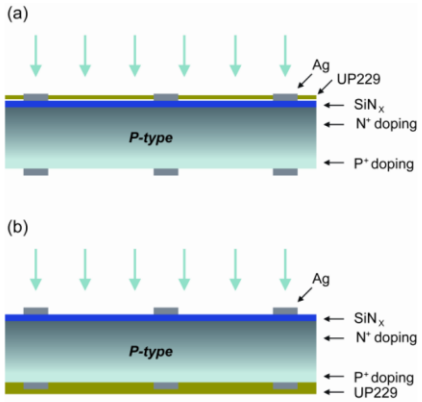

Figure 2 Solar cell with up-converter coated on (a) front side (samples No 1-No 3) and (b) rear side (sample No. 4) of a polycrystalline Si solar cell

2 Results and discussion

Figure 3 shows the XRD patterns for as-prepared $La_2Mo_2O_9$:Yb,R (R = Er or Ho) UC phosphors, and both the diffraction angle (2θ) and peak intensity are consistent with that reported in ICDS file No. 98459. The XRD analysis indicates that the structure of $La_2Mo_2O_9$ host lattice was retained upon codoping of Yb^{3+} and Er^{3+} or Yb^{3+} and Ho^{3+}, respectively, and no X-ray detectable impurity was found in the UC phosphor samples.

The processes of near-IR pumping and UC emission were represented in the energy level diagrams of Yb^{3+}, Er^{3+} and Ho^{3+} ions, as shown in Fig. 4, for explaining the green and orange emissions obtained through up-conversion,

respectively, from $La_2Mo_2O_9$:Yb,Er and $La_2Mo_2O_9$:Yb,Ho phosphors prepared in the solid state system under infrared excitation (λ_{ex} = 980 nm).

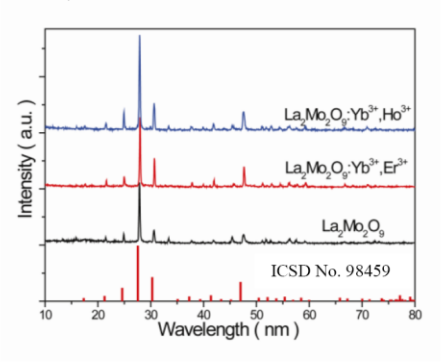

Figure 3 X-ray diffraction patterns for $La_2Mo_2O_9$, $La_2Mo_2O_9$:Yb,Er, and $La_2Mo_2O_9$:Yb,Ho phosphors

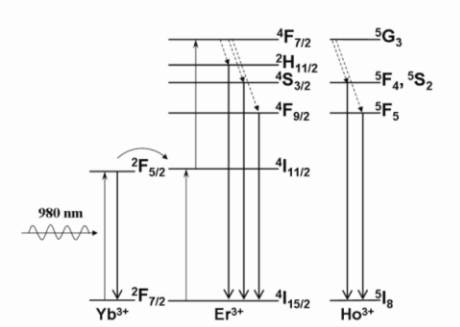

Figure 4 Upconversion processes of Yb^{3+}-sensitized Er^{3+} (or Ho^{3+}) in $La_2Mo_2O_9$:Yb,R and a schematic illustration of excitation and emission.

By codoping the system with Yb^{3+} ions, the intensity of Ho^{3+} and Er^{3+} emission was found to increase, as shown in Fig. 5. The structure consisting of $La_2Mo_2O_9$:Yb,Er with 980-nm laser excitation could emit a yellow-green light, as we observed emissions peaking at 525, 550, and 655 nm, respectively. However, when we co-dope the $La_2Mo_2O_9$ structure with the ion pair of Yb and Ho, we found a series of emissions peaking at 548 and 657 nm (red). The energy level structure shown in Fig. 4 matches these observed energy levels. Therefore, the emitted light could be used by a silicon-based solar cell.

Following this process, we obtained useful data to corroborate our conceptualization. UC Phosphors coated on solar cells were found to enhance electric current and efficiency. Upconversion from near-IR to visible occurs when materials are photoexcited at a long wavelength but produce photoemission at a short wavelength. We investigated the feasibility and application of rare earth-doped up-converting phosphors as potential materials for increasing the sub-bandgap NIR spectral response of silicon solar devices.

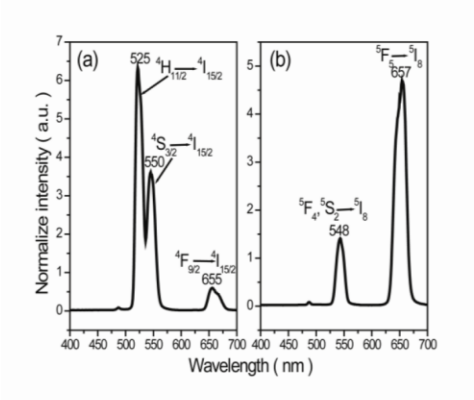

Figure 5 Up-conversion PL spectra for (a) green emission of $La_2Mo_2O_9$:Yb,Er and (b) orange emission of $La_2Mo_2O_9$:Yb,Ho under infrared excitation at 980 nm

Fig. 6 shows reflectance spectra for a bare cell and a cell coated with $La_2Mo_2O_9$:Yb,Er UC phosphor. A comparison of the spectra indicates that the phosphor-coated silicon surface can reduce reflection and enhance light absorption. A drastic reduction of reflectance was observed in the cell coated with $La_2Mo_2O_9$:Yb,Er phosphor. The reflectance spectra show that the bare cell has a higher %reflectance than UC phosphor-coated cells,

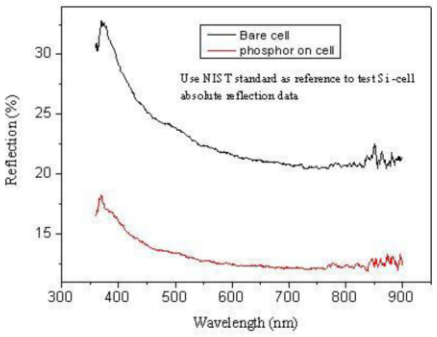

Figure 6 Comparison between the reflectance spectra of bare cell and cell coated with UC phosphor ($La_2Mo_2O_9$:Yb,Er).

especially for the wavelength between 200 *nm* to 600 *nm*. Therefore, the UC phosphor could reduce light scattering and increase light input. The UC phosphor coating on a Si cell device

could increase Isc and efficiency (η) by increasing the visible light input.

Table 1 summarizes and compares the Isc, Voc and η for bare and UC phosphor-coated solar cells investigated in this research. The values of Isc, Voc, and η (with accuracy of ± 0.01%) were found to increase by coating the UC phosphor $La_2Mo_2O_9$:Yb,R (R = Er or Ho) on the surface of the Si wafer. The increase in efficiency for the three samples with $La_2Mo_2O_9$:Yb,R (R = Er or Ho) coated on the Si wafer are the same. The fourth sample showed an even higher efficiency only because it was coated with the up-conversion phosphor on the backside of the cells. These results may indicate that the UC phosphor transforms IR to visible green or red no differently, but when phosphor is coated on the backside, the sample exhibits higher increment in conversion efficiency.

Table 1. Comparison of Isc, Voc, and η (±0.01%) for bare and UC $La_2Mo_2O_9$:Yb,R (R = Er or Ho) phosphor-coated solar cells. (No. 1: $La_2Mo_2O_9$:Yb,Ho and No.2 and 3: $La_2Mo_2O_9$:Yb,Er. No.4: $La_2Mo_2O_9$:Yb,Er coated on the rear surface of the Si cell)

	Isc (bare)	Isc (coated)	ΔIsc	η (bare)	η (coated)	Δη (increase)
1	8.05	8.18	0.13	16.53	16.78	0.25(+1.50%)
2	8.04	8.19	0.15	16.52	16.81	0.29(+1.76%)
3	8.06	8.21	0.15	16.53	16.80	0.27(+1.63%)
4	8.13	8.31	0.18	16.23	16.67	0.44(+2.71%)

[a]Phosphor coated on front-side (No.1-3) and back-side (No.4) of cells.

3 Conclusions

We have demonstrated that up-conversion (UC) phosphors coated on the surface of a polycrystalline silicon solar cell can effectively increase the photovoltaic Isc, Voc, and conversion efficiency (η). The increase in conversion efficiency is about <3%, which was mainly attributed to the low upconversion efficiency of existing up-converters whose performance is limited by both the absorption range and conversion efficiency. However, coating UC phosphors by screen printing technique on the surface of conventional solar devices is a feasible method and has been proven to enhance the efficiency for 1.50-2.71% in this research, depending on solar cells with different structures. Further work to improve the conversion efficiency and optimizing the appropriate phosphors are currently in progress.

Acknowledgments

This research was supported by National Science Council of Taiwan under contract No. NSC98-2113-M-009-005-MY3.

References

[1] F. E. Auzel, Materials and devices using double-pumped-phosphors with energy transfer. *Proc. IEEE,* 61 (1973) 758-786.

[2] J. Silver, M. I. Martinez-Rubio, T. G. Ireland, G. R. Fern, R. J. Withnall, The effect of particle morphology and crystalline size on the upconversion lumenescence properties of erbium and ytterbium co-doped yttrium oxide. *J. Phys. Chem. B*, 105 (2002) 948-953.

[3] J. A. Capobianco, F. C. Vetrone, J. Boyer, A. Speghini, M. Bettinelli, Enhancement of Red Emission ($^4F_{9/2} \rightarrow {}^4I_{15/2}$) via Upconversion in Bulk and Nanocrystalline Cubic $Y_2O_3:Er^{3+}$. *J. Phys. Chem. B*, 106,6 (2002) 1181-1187.

[4] M. A. Green in 29th IEEE PVSC 29th IEEE PVSC, Third Generation Photovoltaics, Third Generation Photovoltaics. May 20-24, 2002, New Orleans, LA., USA.

[5] T. Trupke, M.A. Green, P. Würfel, Improving solar cell efficiencies by up-conversion of sub-band-gap light. *J. Appl. Phys.* 92 (2002) 4117-4122.

[6] P. Chung, H. H. Chung, P. H. Holloway, Phosphor coatings to enhance Si photovoltaic cell performance. *J. Vac. Sci. Technol. A*, 25 (2007) 61-66.

[7] F. Goutenoire, O. Isnard, R. Retoux, P. Lacorre, On the crystal structure of $La_2Mo_2O_9$, a new fast oxide-ion conductor. *Chem. Mater.* 12 (2000) 2575-2580.

[8] P. Lacorre, F. Goutenoire, O. Bohnke, R. Retoux, Y. Laligant, Designing fast oxide-ion conductors based on $La_2Mo_2O_9$. *Nature*, 404 (2000) 856-858.

附錄三

Journal of Materials Chemistry

Dynamic Article Links

Cite this: *J. Mater. Chem.*, 2011, **21**, 5645

www.rsc.org/materials

PAPER

Near UV-pumped yellow-emitting $Sr_8MgSc(PO_4)_7:Eu^{2+}$ phosphor for white-light LEDs with excellent color rendering index

Chien-Hao Huang,[a] Yen-Chi Chen,[a] Teng-Ming Chen,*[a] Ting-Shan Chan[b] and Hwo-Shuenn Sheu[b]

Received 25th December 2010, Accepted 7th February 2011
DOI: 10.1039/c0jm04524a

An Eu^{2+}-activated $Sr_8MgSc(PO_4)_7:Eu^{2+}$ yellow-emitting phosphor with strong luminescence was synthesized and its crystal structure has been refined and determined from the XRD profiles using synchrotron light source by Rietveld refinement method. Non-radiative transitions between Eu^{2+} ions in the $Sr_8MgSc(PO_4)_7$ host have also been demonstrated to be attributable to dipole–dipole interactions, and the critical distance was estimated to be 24.83 Å by using spectral overlap methods. In addition, white-light near-UV LEDs were fabricated by using a phosphor blend of composition-optimized yellow-emitting $Sr_8MgSc(PO_4)_7:0.01Eu^{2+}$ and blue-emitting $BaMgAl_{10}O_{17}:Eu^{2+}$ commodity pumped with a 400 nm near-UV chip and the *Ra* value and reduced color temperature of were found to be 96.7 and 5,614 K, respectively. These results indicate that yellow-emitting $Sr_8MgSc(PO_4)_7:xEu^{2+}$ can serve as a promising candidate for application in white-light LEDs.

1 Introduction

Nowadays, the majority of white light emitting diodes (white-LEDs) uses a combination of a blue InGaN chip and yellow-emitting $Y_3Al_5O_{12}:Ce^{3+}$ (YAG : Ce^{3+}) phosphor.[1] They are also characterized by cool white color temperatures, *e.g.*, correlated color temperature (CCT) = 7756 K, and poor color rendering indices (CRI, *Ra*), *e.g.*, *Ra* = 75,[2] and the lack of red-light contribution also obstructs its extension for more vivid application.[3] In recent years, trichromatic ultraviolet LEDs (UV-LEDs, 360–380 nm) or near ultraviolet LEDs (near-UV LEDs, 380–420 nm) have elicited interest since they can potentially provide improved color temperatures and *Ra's* in comparison with white-LEDs. This is because of their high color-rendering properties[4,5] and also because their color temperatures can be tuned by changing the R/G/B or Y/B ratios. The trichromatic phosphors of UV-excitable or near-UV excitable have been elucidated and investigated for many hosts. According to Chiu *et al.*,[6] a near-UV LED chip combining trichromatic red-emitting $CaAlSiN_3:Eu^{2+}$, green-emitting $(Ba,Sr)_2SiO_4:Eu^{2+}$, and blue-emitting $Ca_2PO_4Cl:Eu^{2+}$ phosphors provides a relatively high CRI of *Ra* = 93.4 and low CCT of 4590 K. Kim *et al.*[7] reported that $Ba_3MgSi_2O_8:Eu^{2+},Mn^{2+}$ can be used as a phosphor for fabrication of a warm white-LED. They concluded that with optimal excitation wavelength at 375 nm $Ba_3MgSi_2O_8:Eu^{2+},Mn^{2+}$ was observed to show three emission bands centered at 440 nm, 505 nm (the emission bands are attributed to 4*f*–5*d* transition of Eu^{2+} ion substituted by Ba^{2+} (I) site and Ba^{2+} (II, III) sites), and 620 nm (this emission band originates from the ^4T–^6A transition of Mn^{2+} ion). Tuning the relative composition of Eu^{2+}/Mn^{2+} ions in $Ba_3MgSi_2O_8$ host lattice, various shades of white light can be generated. Similar type of white light was also observed by Guo *et al.*[8] in the $Ba_2Ca(BO_3)_2:Ce^{3+},Mn^{2+}$ phosphor. The $Ba_2Ca(BO_3)_2:Ce^{3+},Mn^{2+}$ phosphor shows three emission bands centered at 420 nm and 480 nm (attributed to the Ce^{3+} ions occupying two different Ba^{2+} ion sites) and 625 nm was assigned to the emission of Mn^{2+}. The emission color-tunable white light can be realized by coupling the emission bands centered at 420, 480 and 625 nm ascribed to the contribution from Ce^{3+}(1), Ce^{3+}(2) and Mn^{2+} with CIE chromaticity coordinates of (0.23, 0.33)∼(0.40, 0.29), CCT of 13,588–1,991 K and *Ra* of 55–95.

To the best of our knowledge, the crystal structure and luminescence properties of $Sr_8MgSc(PO_4)_7:xEu^{2+}$ have not been reported in the literature. In this study, we have firstly demonstrated the crystal structure of a yellow-emitting $Sr_8MgSc(PO_4)_7:xEu^{2+}$ phosphor. In addition, white-light near-UV LEDs possessing an excellent *Ra* value have been fabricated using the $Sr_8MgSc(PO_4)_7:0.01Eu^{2+}$ phosphor and their optical properties have been investigated.

2 Experimental

2.1 Materials and synthesis

Polycrystalline phosphors with compositions of $(Sr_{1-x}Eu_x)_8MgSc(PO_4)_7:xEu^{2+}$ (SMSP:xEu^{2+}) were prepared from a mixture of $SrCO_3$ (A. R., 99.9%), MgO (A. R., 99%), Sc_2O_3 (A. R., 99.99%), $(NH_4)_2HPO_4$ (Merck ≥ 99%), and Eu_2O_3 (A. R., 99.99%) in a stoichiometric composition of (8–8*x*):1 : 1/2 : 7:4*x* by

[a]*Phosphors Research Laboratory and Department of Applied Chemistry, National Chiao Tung University, Hsinchu, 30010, Taiwan, R.O.C. E-mail: tmchen@mail.nctu.edu.tw; Tel: +886-35731695*
[b]*National Synchrotron Radiation Research Center, Hsinchu Science Park, Hsinchu, 30076, Taiwan, R.O.C.*

high-temperature solid-state reaction method. The starting materials were thoroughly ground in an agate mortar, and the homogeneous mixture was transferred to an alumina crucible and calcined in a furnace at 1473–1573 K for 8 h under a reducing atmosphere of 15% H_2/85% N_2.

2.2 Materials characterization

The crystal structure of the as-synthesized samples was refined and determined by using synchrotron XRD profiles with λ = 0.774908 Å, recorded with a large Debye-Scherrer camera installed at beam line 01C2 of National Synchrotron Radiation Research Center (NSRRC) in Hsinchu, Taiwan; the GSAS program[9] was used for the structural refinements. The diffuse reflectance (DR) spectra were measured with a Hitachi 3010 double-beam UV-Vis spectrometer (Hitachi Co., Tokyo, Japan). The photoluminescence (PL) and PL excitation (PLE) spectra of the samples were analyzed by using a Spex Fluorolog-3 Spectrofluorometer equipped with a 450-W Xe light source. The Commission International de l'Eclairage (CIE) chromaticity coordinates for all samples were measured by a Laiko DT-101 color analyzer equipped with a CCD detector (Laiko Co., Tokyo, Japan).

3 Results and discussion

3.1 Crystal structure of $Sr_8MgSc(PO_4)_7$:0.05Eu^{2+}

Fig. 1 shows the observed (crosses), calculated (solid line), and difference (bottom) synchrotron XRD profiles for the Rietveld refinement of $Sr_{7.6}MgSc(PO_4)_7$:0.05Eu^{2+} (SMSP:0.05Eu^{2+}) phosphor at T = 295 K and with λ = 0.774908 Å. These results indicate that when doped with 0.05 mol Eu^{2+}per mol Sr^{2+}, the SMSP host almost a single-phase structure. There are a negligible amount of impurities at 2-theta = 14.25 and 22.04 site, *i.e.*, $Sr_3(PO_4)_2$. SMSP:0.05Eu^{2+} crystallizes in a monoclinic unit cell with space group I2/a and lattice constants a = 18.0115(25) Å, b = 10.6006(18) Å, c = 18.3659(34) Å, β = 132.976(5)^0, and cell volume = 2565.6(8) Å^3. The refinement finally converged to R_p = 3.94%, R_{wp} = 7.86% and χ^2 = 5.15 is shown in Table 1. The Sr^{2+} ions have five different coordination numbers. Sr(1) is defined as being eight-coordinated; Sr(2), Sr(3), and Sr(4) are defined as being nine-coordinated; and Sr(5) is defined as being ten-coordinated. The ionic radii for eight-, nine-, and ten-coordinated Sr^{2+} are 1.26, 1.31, and 1.36 Å, respectively. However, the ionic radii for eight-, nine-, and ten-coordinated Eu^{2+} are 1.25, 1.3, and 1.35 Å, respectively. On account of the matching of ionic radii, the Eu^{2+} ions are expected to randomly occupy the Sr^{2+} ions sites in the $Sr_8MgSc(PO_4)_7$ host.

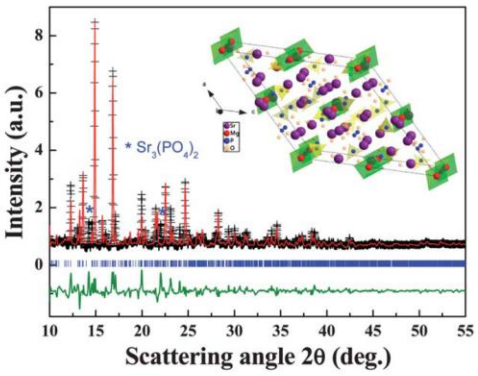

Fig. 1 Observed (crosses), calculated (solid line), and difference (bottom) synchrotron XRD profiles for the Rietveld refinement of $Sr_8MgSc(PO_4)_7$:0.05Eu^{2+} at 295 K with λ = 0.774908 Å. Bragg reflections are indicated with tick marks.

3.2 Photoluminescence properties of $Sr_8MgSc(PO_4)_7$:Eu^{2+}

Fig. 2 shows the concentration dependence of the relative PLE and PL intensity of SMSP:$x$$Eu^{2+}$ (x = 0.003–0.05) phosphors. Under 400 nm excitation, the SMSP:$x$$Eu^{2+}$ phosphors emit yellow light in the form of two broad emission bands centered at 518 and 600 nm, respectively; these bands can be attributed to the typical $4f^7 5d^1 \rightarrow 4f^7$ transition of Eu^{2+} ions. By Gaussian deconvolution, the PL spectra of SMSP:0.05Eu^{2+} phosphors can be decomposed into five Gaussian profiles with peaks centered at 501, 529, 568, 606 and 665 nm (Fig. 2(b), wine dashed lines), respectively, that can be ascribed to five different emission sites and it can also be identified by the refinement results that five Sr^{2+} sites are occupied by Eu^{2+} ions.[10,11] The emission intensity increases with the Eu^{2+} content x, when x < 0.01. For SMSP:$x$$Eu^{2+}$ phosphors, the emission intensity was the optimized composition at x = 0.01; since the Eu^{2+} doping concentration was >0.01 mol, concentration quenching was observed and the emission intensity was found to decrease. The PLE spectrum shows a broad absorption from 240 to 480 nm, which corresponds to the $4f^7 \rightarrow 4f^7 5d^1$ transition of Eu^{2+} ions. The excitation edge shifts toward a longer wavelength as the Eu^{2+} doping concentration increases. Therefore, the broad absorption band matches well with the emission of near-UV chips; thus, SMSP:$x$$Eu^{2+}$ phosphors can be combined with near-UV chips for white-light near-UV LED applications.

Upon excitation at a wavelength of 400 nm, the internal quantum efficiencies of composition-optimized SMSP:0.01Eu^{2+}

Table 1 Rietveld refinement and crystal data of $Sr_8MgSc(PO_4)_7$:0.05Eu^{2+} phosphors

Formula	$(Sr_{0.95}Eu_{0.05})_8MgSc(PO_4)_7$
Radiation type	0.774908
2θ range (deg.)	10–55
T/K	295
Formula weight	1460.855
Symmetry	Monoclinic
Space group	I2/a
a/Å	18.0115(25)
b/Å	10.6006(18)
c/Å	18.3659(34)
β (deg.)	132.976(5)
γ (deg.)	90
Volume/Å^3	2565.6(8)
Z	4
R_p	3.94%
R_{wp}	7.86%
χ^2	5.15

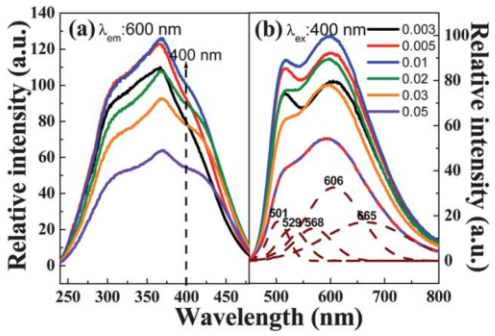

Fig. 2 Concentration dependence of relative PLE and PL intensity of $Sr_8MgSc(PO_4)_7$:xEu^{2+} (x = 0.003–0.05) under 400 nm excitation.

and commercial $(Sr,Ba)_2SiO_4$:Eu^{2+} (570 nm) phosphor were found to be 30.5% and 91.2%, and absorption are 68.2% and 80.2%. The external quantum efficiency of SMSP:0.01Eu^{2+} and $(Sr,Ba)_2SiO_4$:Eu^{2+} (570 nm) phosphor are determined to be 20.8% and 73.1%, respectively. However, quantum efficiencies of SMSP:0.01Eu^{2+} is 28.5% of that of $(Sr,Ba)_2SiO_4$:Eu^{2+} (570 nm) phosphor. The lower quantum efficiencies of SMSP:0.01Eu^{2+} could be further enhanced by process optimization.

The decay curves of SMSP:0.01Eu^{2+} phosphors were measured and represented as shown in Fig. 3. The corresponding luminescence decay times can be best fitted with a second-order exponential equation: $I = A_1\exp(-t/\tau_1) + A_2\exp(-t/\tau_2)$, where I is the luminescence intensity, A_1 and A_2 are constants, t is the time, τ_1 and τ_2 are rapid and slow lifetimes for exponential components, respectively. The decay lifetime values of τ_1 and τ_2 were calculated to be 146.6 and 637.7 ns [monitored at 518 nm, Fig.3(a)], and 165.2 and 656.5 ns [monitored at 600 nm, Fig.3(b)]. The average decay times (τ^*) can be determined by the formula given in the following:[12]

$$\langle\tau^*\rangle = (A_1\tau_1^2 + A_2\tau_2^2)/(A_1\tau_1 + A_2\tau_2) \quad (1)$$

The average decay times (τ^*) were calculated to be 598 ns (monitored at 518 nm) and 615 ns (monitored at 600 nm). This results indicates that the Eu^{2+} ions are occupy the two different Sr^{2+} ions coordination environment in the $Sr_8MgSc(PO_4)_7$ host.[13]

Fig. 4 shows the PL and PLE spectra as functions of the Eu^{2+} concentration (x) for SMSP:xEu^{2+} (x = 0.003–0.05) phosphors. The optimal doping concentration was observed to be x = 0.01 mol. However, according to the Dexter theory, the non-radiative transitions between Eu^{2+} ions took place *via* electric multipolar interactions.[14] The mechanism of interaction between Eu^{2+} ions can be expressed by the following equation:[15]

$$\frac{I}{\chi} = \frac{k}{1+\beta(x)^{\theta/3}} \quad (2)$$

where χ is the activator concentration; k and β are constants for each interaction for a given host lattice; and θ = 6, 8, and 10 corresponds to dipole–dipole, dipole–quadrupole, and quadrupole–quadrupole interactions, respectively. The relationships of $\log(x\text{Eu}^{2+})$ *versus* $\log(I/x\text{Eu}^{2+})$ are shown in the inset of Fig. 4; in this plot, the slope of the straight line equals $-\theta/3$. The value of θ was found to be ~6. The result indicates that non-radiative transitions between Eu^{2+} ions occur *via* dipole–dipole interactions for the concentration quenching of Eu^{2+} ions in the SMSP: $x$$Eu^{2+}$ host; The result was similar to those previously investigated and observed in our group.[16]

The critical distance R_c between the Eu^{2+} ions was calculated using the concentration quenching method. R_c can be calculated using the relation given by Blasse[17]

$$R_c \approx 2\left[\frac{3V}{4\pi x_c N}\right]^{1/3} \quad (3)$$

where V is the volume of the unit cell, x_c is the critical concentration of the Eu^{2+} ion, and N is the number of Z ions in the unit cell. For the SMSP crystal structure, the analytical and

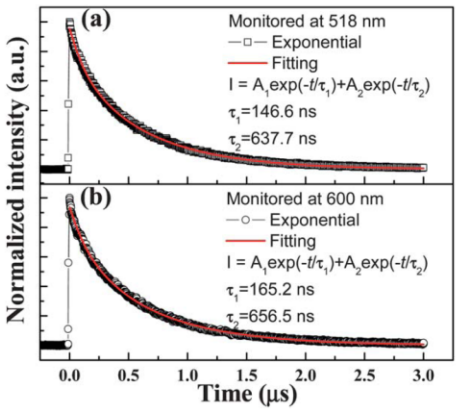

Fig. 3 Decay curves of Eu^{2+} emission in $Sr_8MgSc(PO_4)_7$:0.01Eu^{2+} phosphor monitored at (a) 518 nm and (b) 600 nm.

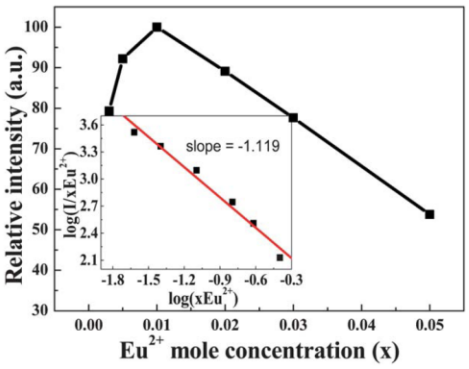

Fig. 4 PL intensity of $Sr_8MgSc(PO_4)_7$:xEu^{2+} as a function of Eu^{2+} content. The inset shows the relationships of $\log(x\text{Eu}^{2+})$ *versus* $\log(I/x\text{Eu}^{2+})$.

experimental values were $V = 2565.6$ Å^3, $Z = 4$, and $x_c = 0.08$. Therefore, R_c was calculated to be 24.83 Å.

3.3 Optical spectra of $Sr_8MgSc(PO_4)_7$:xEu^{2+}

Fig. 5 shows the diffuse reflection (DR) spectra of the SMSP host and SMSP:xEu^{2+} phosphors. The SMSP host material shows energy absorption in the ≦340 nm region. As Eu^{2+} ions were doped into SMSP host, a strong absorption in the range of 240–480 nm assigned to the $4f^7 \rightarrow 4f^65d^1$ absorption of Eu^{2+} ions was observed. The absorption range from 240 to 480 nm was observed to be matched in the excitation spectrum. The absorption edge gradually extends to longer wavelengths, and the absorption is enhanced for higher Eu^{2+} ion concentrations, which results in a red shift of the excitation wavelength to 480 nm.

3.4 Thermal quenching of $Sr_8MgSc(PO_4)_7$:$0.01Eu^{2+}$

For the application of high power LEDs, the thermal stability of phosphor is one of important issues. Temperature dependence of relative emission intensities for SMSP:$0.01Eu^{2+}$ and commercial $(Sr,Ba)_2SiO_4$:Eu^{2+} (570 nm) phosphors under 400 nm excitation are compared in Fig. 6.

The relative emission intensity decreases with an increase in temperature. We observed decays of 45.7% and 85.2% at 150 and 300 °C, respectively, for SMSP:$0.01Eu^{2+}$, and decays of 49% and 95% for commercial $(Sr,Ba)_2SiO_4$:Eu^{2+} (570 nm) phosphors. The inset displayed the activation energy (E_a) of SMSP:$0.01Eu^{2+}$ and $(Sr,Ba)_2SiO_4$:Eu^{2+} (570 nm) phosphors. The activation energy (E_a) can be expressed by:[18]

$$\ln\left(\frac{I_o}{I}\right) = \ln A - \frac{E_a}{k_B T} \quad (4)$$

where I_o and I are luminescence intensity of phosphor at room temperature and testing temperature (25–300 °C), respectively; A is constant; k_B is Boltzmann constant, 8.617×10^{-5} eV K^{-1}. The E_a were obtained to be 0.1586 and 0.2687 eV for SMSP:$0.01Eu^{2+}$ and $(Sr,Ba)_2SiO_4$:Eu^{2+} (570 nm) phosphors. Thus, the SMSP:$0.01Eu^{2+}$ phosphor shows higher thermal stability than that of (Sr, Ba)$_2$SiO$_4$:Eu^{2+} (570 nm) commodity. The results demonstrated that SMSP:$0.01Eu^{2+}$ phosphor could be a promising phosphor for high power LED application.

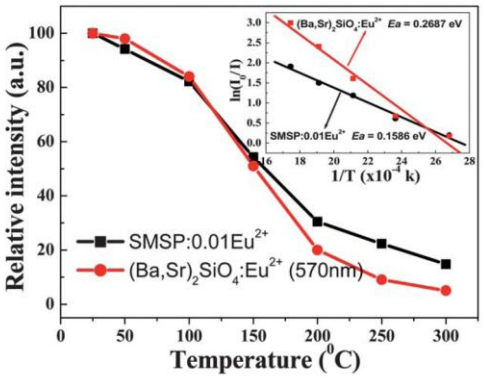

Fig. 6 Temperature dependence of relative emission intensity for $Sr_8MgSc(PO_4)_7$:$0.01Eu^{2+}$ and commercial $(Sr,Ba)_2SiO_4$:Eu^{2+} phosphors under 400 nm excitation. The inset shows the activation energy (E_a) of $Sr_8MgSc(PO_4)_7$:$0.01Eu^{2+}$ and $(Sr,Ba)_2SiO_4$:Eu^{2+} phosphors.

3.5 LED lamp fabrication and EL spectrum

Fig. 7 shows the *Ra* of the electroluminescent (EL) spectrum of a white-LED lamp driven by a current of 350 *m*A. White-light near-UV LED lamps were fabricated as follows. A mixture of transparent silicon resin and phosphors (yellow-emitting SMSP:$0.01Eu^{2+}$ and blue-emitting $BaMgAl_{10}O_{17}$:Eu^{2+} (BAM:Eu^{2+}) commodity) was dropped onto a 400-nm near-UV chip and roast at 120 °C/10 h afterwards. The EL spectrum clearly shows a near-UV band at around 400 nm, a blue-emitting band corresponding to BAM:Eu^{2+} phosphor at around 454 nm, and yellow-emitting bands corresponding to the SMSP:$0.01Eu^{2+}$ phosphors at around 510 and 597 nm.

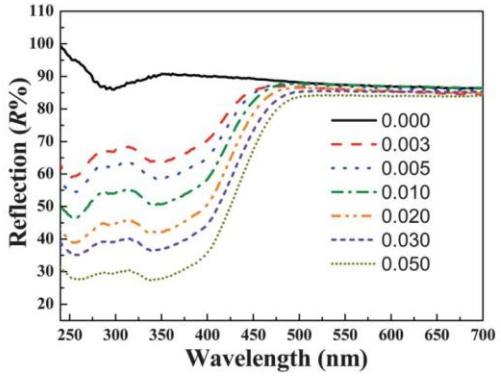

Fig. 5 Diffuse reflectance spectra of $Sr_8MgSc(PO_4)_7$ and $Sr_8MgSc(PO_4)_7$:xEu^{2+} ($x = 0.003$–0.05).

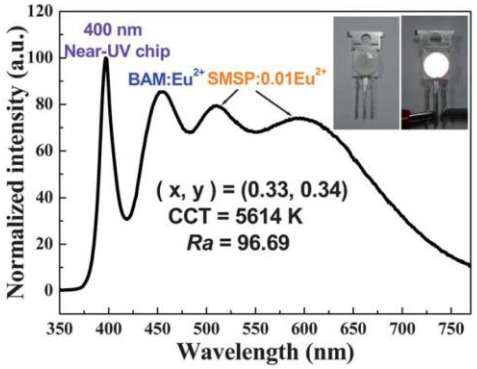

Fig. 7 EL spectrum of a white-LED lamp driven by a current of 350 *m*A. The inset shows a photograph of an LED lamp package.

Table 2 Full set of 14 CRIs and Ra of a 400 nm near-UV chip pumped with SMSP:0.01Eu^{2+} and BAM:Eu^{2+} phosphors

R1	R2	R3	R4	R5	R6	R7	R8	R9	R10	R11	R12	R13	R14	*Ra*
97.6	97.8	96.4	98.3	97.8	95.6	95.9	94.1	86.7	93.9	95.5	95.1	97.5	97.8	96.7

These results reveal that the CIE color coordinates are $x = 0.33$ and $y = 0.34$ at a warm white light CCT of 5614 K. The full set of 14 CRIs with the color rendering index $Ra = 96.7$ is listed in Table 2. The inset shows a photograph of the LED lamp package under a forward bias of 350 *m*A and off. In comparison with the blue InGaN chip pumped with YAG:Ce^{3+} phosphor ($Ra = 75$, CCT = 7756 K),[2] the white-light near-UV LEDs fabricated in this study show $Ra = 96.69$ and CCT = 5614 K. Therefore, the SMSP:0.01Eu^{2+} phosphors show promise for application tin white-light near-UV LEDs.

4 Conclusions

In summary, we have synthesized yellow-emitting $Sr_8MgSc(PO_4)_7$:xEu^{2+} phosphors by a solid-state reaction method and investigated their luminescence properties as a function of the activator (Eu^{2+}) concentration. We have successfully demonstrated that $Sr_8MgSc(PO_4)_7$:0.05Eu^{2+} crystallized in a monoclinic unit cell with space group I2/a. The non-radiative transitions between Eu^{2+} ions in the $Sr_8MgSc(PO_4)_7$ host have been demonstrated as being attributable to dipole–dipole interactions, and the critical distance was estimated to be 24.83 Å by using spectral overlap methods. A warm white light LED with CCT = 5614 K, $Ra = 96.7$, and CIE = (0.33, 0.34) was fabricated using yellow-emitting $Sr_8MgSc(PO_4)_7$:0.01Eu^{2+} and blue-emitting $BaMgAl_{10}O_{17}$:Eu^{2+} phosphors pumped by a 400 nm near-UV chip. These results demonstrate that $Sr_8MgSc(PO_4)_7$:xEu^{2+} phosphors have considerable potential for use in near-UV chips, as compared to that [CCT = 7756 K, $Ra = 75$, CIE = (0.292, 0.325)] incorporating YAG:Ce^{3+} and pumped by blue LED chips.[2]

Acknowledgements

This research was supported by National Science Council of Taiwan, R.O.C. under contract No. NSC98-2113-M-009-005-MY3.

Notes and references

1 V. Bachmann, C. Ronda and A. Meijerink, *Chem. Mater.*, 2009, **21**, 2077.
2 H. S. Jang, Y. H. Won and D. Y. Jeon, *Appl. Phys. B: Lasers Opt.*, 2009, **95**, 715.
3 A. A. Setlur, W. J. Heward, Y. Gao, A. M. Srivastava, R. G. Chandran and M. V. Shankar, *Chem. Mater.*, 2006, **18**, 3314.
4 C. H. Huang and T. M. Chen, *Opt. Express*, 2010, **18**, 5089.
5 S. H. Lee, J. H. Park, S. M. Son and J. S. Kim, *Appl. Phys. Lett.*, 2006, **89**, 221916.
6 Y. C. Chiu, W. R. Liu, C. K. Chang, C. C. Liao, Y. T. Yeh, S. M. Jang and T. M. Chen, *J. Mater. Chem.*, 2010, **20**, 1.
7 J. S. Kim, K. T. Lim, Y. S. Jeong, P. E. Jeon, J. C. Choi and H. L. Park, *Solid State Commun.*, 2005, **135**, 21.
8 C. Guo, L. Luan, Y. Xu, F. Gao and L. Liang, *J. Electrochem. Soc.*, 2008, **155**, J310.
9 A. C. Larson and R. B. Von Dreele, *Generalized Structure Analysis System (GSAS)*, Los Alamos National Laboratory Report LAUR., 1994, 86–748.
10 Y. S. Tang, S. F. Hu, W. C. Ke, C. C. Lin, N. C. Bagkar and R. S. Liu, *Appl. Phys. Lett.*, 2008, **93**, 131114.
11 K. S. Shon, S. H. Cho, S. S. Park and N. Shin, *Appl. Phys. Lett.*, 2008, **89**, 051106.
12 N. Ruelle, M. P. Thi and C. Fouassier, *Jpn. J. Appl. Phys.*, 1992, **31**, 2786.
13 X. Zhang, H. Chen, W. Ding, H. Wu and J. Kim, *J. Am. Ceram. Soc.*, 2009, **92**, 429.
14 D. L. Dexter, *J. Chem. Phys.*, 1953, **21**, 836.
15 L. G. Vanuiter, *J. Electrochem. Soc.*, 1967, **114**, 1048.
16 T. W. Kuo, C. H. Huang and T. M. Chen, *Appl. Opt.*, 2010, **49**, 1.
17 G. Blasse, *Philips Res. Rep.*, 1969, **24**, 131.
18 C. H. Huang, W. R. Liu and T. M. Chen, *J. Phys. Chem. C*, 2010, **114**, 18698.

附錄四

Journal of Luminescence 131 (2011) 1346–1349

Contents lists available at ScienceDirect

Journal of Luminescence

journal homepage: www.elsevier.com/locate/jlumin

Novel green-emitting $Na_2CaPO_4F:Eu^{2+}$ phosphors for near-ultraviolet white light-emitting diodes

Chien-Hao Huang, Yen-Chi Chen, Te-Wen Kuo, Teng-Ming Chen*

Phosphors Research Laboratory and Department of Applied Chemistry, National Chiao Tung University, Hsinchu 30010, Taiwan

ARTICLE INFO

Article history:
Received 17 December 2010
Received in revised form
23 February 2011
Accepted 24 February 2011
Available online 3 March 2011

Keywords:
Phosphors
$Na_2CaPO_4F:Eu^{2+}$
Light-emitting diodes

ABSTRACT

In this study, green-emitting $Na_2CaPO_4F:Eu^{2+}$ phosphors were synthesized by solid-state reactions. The excitation spectra of the phosphors showed a broad hump between 250 and 450 nm; the spectra match well with the near-ultraviolet (NUV) emission spectra of light-emitting diodes (LEDs). The emission spectrum showed an intense broad emission band centered at 506 nm. White LEDs were fabricated by integrating a 390 nm NUV chip comprising blue-emitting $BaMgAl_{10}O_{17}:Eu^{2+}$, green-emitting Na_2CaPO_4F:0.02 Eu^{2+}, and red-emitting $CaAlSiN_3:Eu^{2+}$ phosphors into a single package; the white LEDs exhibited white light with a correlated color temperature of 5540 K, a color-rendering index of 90.75, and color coordinates (0.332, 0.365) close to those of ideal white light.

1. Introduction

In recent years, white light-emitting diodes (LEDs) have been in high demand for use in solid-state lighting technology applications [1]. At present, most white LEDs are fabricated by combining a blue-emitting InGaN chip and yellow-emitting $Y_3Al_5O_{12}:Ce^{3+}$ garnet phosphor ($YAG:Ce^{3+}$) [2,3]. However, the disadvantages of this method are a low color-rendering index (CRI, $Ra=75$) and a high correlated color temperature (CCT = 7756 K) [4]; these disadvantages can be attributed to the deficiency of red emission in the visible spectrum [5,6]. A high CRI and low CCT of white LEDs are required for general lighting applications. CRI and CCT properties can be improved using trichromatic phosphor blends and UV or near-UV (NUV) LEDs because near-UV or UV chip pumped trichromatic phosphors to white light provide great color stability and high CRI and do not suffer from the strong change in chromaticity [7]. According to Chiu et al. [8], an NUV LED chip combining trichromatic red-emitting $CaAlSiN_3:Eu^{2+}$, green-emitting $(Ba,Sr)_2SiO_4:Eu^{2+}$, and blue-emitting $Ca_2PO_4Cl:Eu^{2+}$ phosphors provides a relatively high CRI of Ra = 93.4 and low CCT of 4590 K.

To the best of our knowledge, there have been no reports yet on the luminescence properties of Eu^{2+}-activated Na_2CaPO_4F. In this paper, we report on the luminescence properties, thermal stability, and applications of NUV LEDs using green-emitting $Na_2CaPO_4F:Eu^{2+}$ phosphors. In addition, we fabricated white NUV LEDs and examined their optical properties.

2. Experimental

Green-emitting $Na_2CaPO_4F:Eu^{2+}$ phosphors were synthesized by carrying out solid-state reactions at high temperature. As our starting materials, Na_2CO_3 (ACROS, 99.95%), NaF (MERK, 99.99%), $CaCO_3$ (ALDRICH, 99.9%), $(NH_4)_2HPO_4$ (MERK, ≥99%), and Eu_2O_3 (ALDRICH, 99.99%) were employed within a stoichiometric molar ratio of $1/2:1.2:1-x:1:x/2$. After these powders were blended together and ground thoroughly in an agate mortar, the homogeneous mixture was placed into an alumina crucible and calcined in a muffle furnace at 800 °C for 8 h under a reducing atmosphere of 40% H_2 in an alumina boat, with excess 20 mol% NaF used as a flux.

The crystal structures of the as-synthesized samples were identified through powder X-ray diffraction (XRD) analysis using a Bruker AXS D8 advanced automatic diffractometer with Cu Kα radiation. The photoluminescence (PL) and photoluminescence excitation (PLE) spectra of the samples were measured using a Spex Fluorolog-3 spectrofluorometer equipped with a 450-W Xe light source. The diffuse reflectance (DR) spectra were measured using a Hitachi 3010 double-beam UV–vis spectrometer (Hitachi Co., Tokyo, Japan). The Commission International de l'Eclairage (CIE) chromaticity coordinates for all samples were measured using a Laiko DT-101 color analyzer equipped with a CCD detector (Laiko Co., Tokyo, Japan) and variable temperature PL spectra were measured using a Spex FluoroMax-3 spectrophotometer from Jobin-Yvon.

3. Results and discussion

A Na_2CaPO_4F compound has a rhombohedral crystal structure with a space group of R3m, and lattice parameters of

* Corresponding author. Tel.: +886-3-5731695; fax: +886-3-5723764.
E-mail address: tmchen@mail.nctu.edu.tw (T.-M. Chen).

0022-2313/$ - see front matter © 2011 Elsevier B.V. All rights reserved.
doi:10.1016/j.jlumin.2011.02.034

$a=7.0179(7)$ Å, $c=40.56(4)$ Å, $V=1730.21(1)$ Å^3, and $Z=15$. The Ca atom occupies five independent sites on the m plane with coordination number 6 (Ca1, Ca3, Ca4, Ca5) and coordination number 7 (Ca2). Each Ca cation has four (five for M2) oxygen and two fluorine ligands. The five independent P atoms are in 3*a* positions with 3m symmetry [9]. The ionic radii for six- and seven-coordinated Eu^{2+} are 1.17 and 1.2 Å; however, the ionic radii for six- and seven-coordinated Ca^{2+} cations are 1.0 and 1.06 Å, respectively. Therefore, based on a comparison of the effective ionic radii of cations with different coordination numbers, we have proposed that Eu^{2+} randomly occupies the Ca^{2+} sites in the Na_2CaPO_4F host structure. The powder XRD patterns of Na_2CaPO_4F and Na_2CaPO_4F:Eu^{2+} phosphors are shown in Fig. 1. The purity of each phase of the as-prepared phosphors was analyzed using ICSD:56962 [10] as a reference, indicating that neither the host nor the doped Eu^{2+} ions caused any observable changes in the Na_2CaPO_4F host structure, which is shown in the inset of Fig. 1.

The concentration dependence of the relative PL/PLE intensity of Na_2CaPO_4F:xEu^{2+} ($x=0.001$–0.05) under 390 nm excitation is demonstrated in Fig. 2. The PL spectrum exhibited a green broad emission band from 400 to 700 nm, centered at 506 nm, which was attributed to $4f^65d^1\rightarrow4f^7$ of the Eu^{2+} ion [11]. The PLE

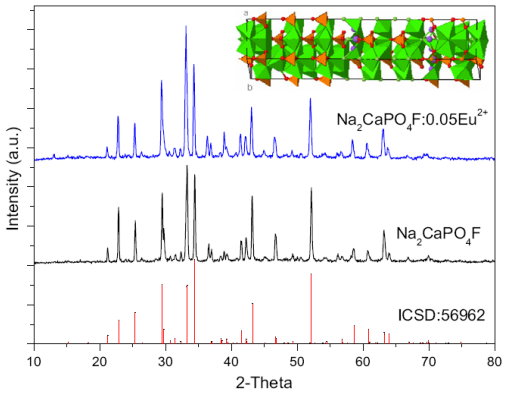

Fig. 1. Powder XRD patterns for Na_2CaPO_4F and Na_2CaPO_4F:Eu^{2+} phosphors.

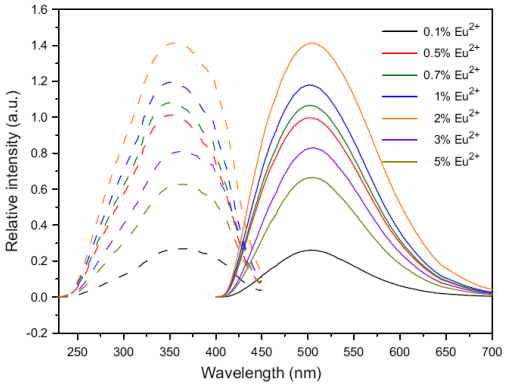

Fig. 2. Concentration dependence of relative PL/PLE intensity of Na_2CaPO_4F:xEu^{2+} ($x=0.001$–0.05) under 390 nm excitation.

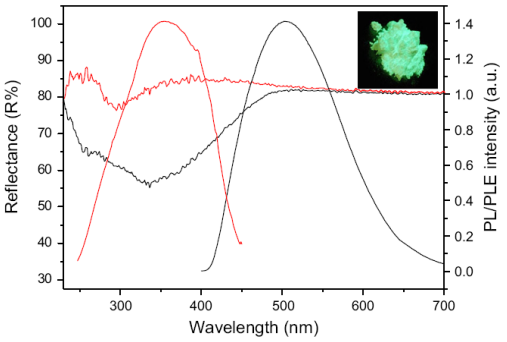

Fig. 3. Reflectance spectra of Na_2CaPO_4F host and Na_2CaPO_4F:$0.02Eu^{2+}$ phosphor, and PL/PLE spectra of Na_2CaPO_4F:$0.02Eu^{2+}$. The inset shows Na_2CaPO_4F:$0.02Eu^{2+}$ phosphor irradiated under a 365 nm UV lamp box.

spectrum showed broad absorption bands between 250 and 450 nm, which are attributed to the $4f^7\rightarrow4f^65d^1$ transition of the Eu^{2+} ions [12], and is well-matched with the emission from an NUV LED. The optimal concentration of the Eu^{2+}-doped content was found to be 0.02 mol, and the PL intensity was observed to increase when x is increased up to $x<0.02$ mol. Quenching was observed for samples with concentrations of Eu^{2+}-doped content higher than 0.02 mol, and the PL intensity was found to decrease with an increase in Eu^{2+}-doped content.

Fig. 3 shows the reflectance spectra of the Na_2CaPO_4F host and Na_2CaPO_4F:$0.02Eu^{2+}$ phosphor, along with the PL/PLE spectra of Na_2CaPO_4F:$0.02Eu^{2+}$. The reflection spectra for Na_2CaPO_4F and Na_2CaPO_4F:$0.02Eu^{2+}$ differ. The Na_2CaPO_4F host material demonstrates energy absorption within the $\leq$350-nm region [13], while a strong absorption of energy between 250 and 470 nm in the NUV range was observed for Na_2CaPO_4F:$0.02Eu^{2+}$. The PLE spectrum shows a broad hump between 250 and 450 nm, which matches well with the reflection spectrum. The PL spectra of Na_2CaPO_4F:$0.02Eu^{2+}$ show green broad emission bands centered at 506 nm ($4f^65d^1\rightarrow4f^7$ transition of Eu^{2+}). The inset of Fig. 3 displays a clear photograph of Na_2CaPO_4F:$0.02Eu^{2+}$ phosphor under a 365 nm UV lamp box. The broad and symmetric emission bands of Na_2CaPO_4F:$0.02Eu^{2+}$ are attributed to the transmission from Eu^{2+} occupying five crystallographically distinct Ca^{2+} sites in the host structure.

Thermal stability is very important for phosphor applications in white LEDs. The relative temperature-dependent emission intensities of Na_2CaPO_4F:$0.02Eu^{2+}$ and commercial BOS 507 phosphors under excitation at 390 nm are compared in Fig. 4. As can be seen in the inset, relative emission intensity decreases with an increase in temperature. We observed decays of 25% and 66% at 100 and 200 °C, respectively, for Na_2CaPO_4F:$0.02Eu^{2+}$, and decays of 9% and 49% for BOS 507. These results indicate that BOS 507 exhibits better thermal stability than Na_2CaPO_4F:$0.02Eu^{2+}$.

According to Lin et al. [14], the activation energy (E_a) can be expressed using the following equation:

$$I(T)\approx\frac{I_0}{1+c\exp(-E_a/k_BT)}$$

where I_0 and $I(T)$ are the initial PL intensity and the PL intensity at a given temperature T (K), respectively; c is a constant; k is the Boltzmann constant, 8.617×10^{-5} eV/K; and E_a is the activation energy for thermal quenching. This activation energy can be calculated from a plotting of $\ln[(I_0/I)-1]$ against $1/k_BT$, where a straight slope equals $-E_a$. The activation energy for thermal

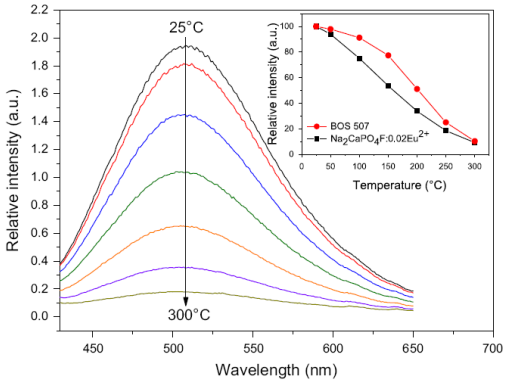

Fig. 4. Temperature dependence of PL spectra of $Na_2CaPO_4F:0.02Eu^{2+}$ phosphor under 390 nm excitation. The inset shows thermal quenching for the relative emission intensity of $Na_2CaPO_4F:0.02Eu^{2+}$ and commercial $Ba_2SiO_4:Eu^{2+}$ phosphors.

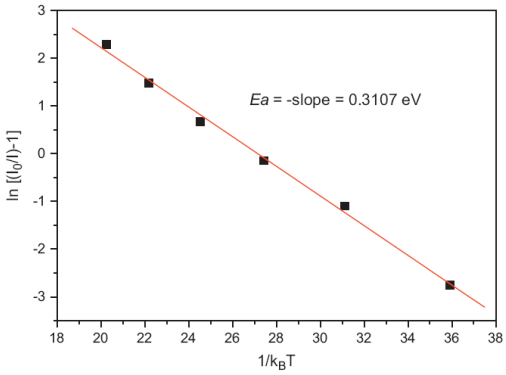

Fig. 5. A $\ln[(I_0/I)-1]$ vs. $1/k_BT$ activation energy graph for thermal quenching of $Na_2CaPO_4F:0.02Eu^{2+}$ phosphor.

quenching was found to be 0.3107 eV for $Na_2CaPO_4F:0.02Eu^{2+}$ as shown in Fig. 5.

Fig. 6 shows the electroluminescent spectrum of a white LED fabricated using a 390 nm NUV chip (AOT Product No.: C06HC, Spec.: 390V08C, wavelength peak: 385–390 ± 0.51 nm, chip size: 40 × 40 mil^2, forward voltage: 3.8–4.0 ± 0.02 V, power: 70–80 ± 2.32 mW) comprising blue-emitting $BaMgAl_{10}O_{17}:Eu^{2+}$, green-emitting $Na_2CaPO_4F:0.02Eu^{2+}$, and red-emitting $CaAlSiN_3:Eu^{2+}$ phosphors driven by a 350 mA current. The electroluminescent spectrum clearly shows four emission bands at 390, 460, 526, and 603 nm, which arise from the NUV chip and the $BaMgAl_{10}O_{17}:Eu^{2+}$, $Na_2CaPO_4F:0.02Eu^{2+}$, and $CaAlSiN_3:Eu^{2+}$ phosphors, respectively. The generated white LED shows CIE color coordinates of (0.332, 0.365), a CCT of 5540, a *Ra* of 90.75, and luminous efficiency of 20.6 lm/W under 350 mA driving current. The inset in Fig. 6 shows a white NUV LED driven by a 350 mA current. The 8 CRIs and average color-rendering index of *Ra*=90.75 are given in Table 1. These results demonstrate that our proposed phosphor blend has a higher *Ra* of 90.75 and lower CCT of 5540 K compared with a white LED fabricated using $YAG:Ce^{3+}$ phosphor pumped with a blue

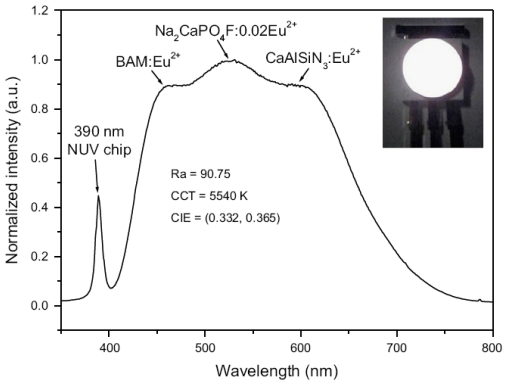

Fig. 6. EL spectrum of white LED from blue-emitting $BaMgAl_{10}O_{12}:Eu^{2+}$, green-emitting $Na_2CaPO_4F:0.02Eu^{2+}$, and red-emitting $CaAlSiN_3:Eu^{2+}$ phosphors using a 390 nm NUV chip. The inset shows a photograph of a LED lamp package driven by 350 mA current.

Table 1
Full set of 8 CRI and *Ra* values of blue-emitting $BaMgAl_{10}O_{12}:Eu^{2+}$, green-emitting $Na_2CaPO_4F:0.02Eu^{2+}$, and red-emitting $CaAlSiN_3:Eu^{2+}$ phosphors using 390 nm near-UV chip.

R1	R2	R3	R4	R5	R6	R7	R8	*Ra*
88	95	96	89	90	96	92	80	90.75

InGaN chip, which has a *Ra* of 75 and CCT of 7756 K. [4]. Therefore, $Na_2CaPO_4F:Eu^{2+}$ phosphor exhibits great potential for application in white NUV LEDs.

4. Conclusions

In summary, we have synthesized novel green-emitting $Na_2CaPO_4F:xEu^{2+}$ phosphors by carrying out solid-state reactions at high temperature, and investigated their optical properties. $Na_2CaPO_4F:xEu^{2+}$ phosphors have broad excitation bands between 250 and 450 nm with the green emission centered at 506 nm. The optimum concentration of Eu^{2+} in $Na_2CaPO_4F:Eu^{2+}$ is determined to be 0.02 mol. Moreover, trichromatic white LEDs, fabricated by integrating a 390 nm NUV chip comprising blue-emitting $BaMgAl_{10}O_{17}:Eu^{2+}$, green-emitting $Na_2CaPO_4F:0.02Eu^{2+}$, and red-emitting $CaAlSiN_3:Eu^{2+}$ phosphors into a single package, emit white light with a CCT of 5540 K, *Ra* of 90.75, and CIE of (0.332, 0.365). These results indicate that a 390 nm NUV LED chip coupled with $BaMgAl_{10}O_{17}:Eu^{2+}$, $Na_2CaPO_4F:0.02Eu^{2+}$, and $CaAlSiN_3:Eu^{2+}$ phosphors has a higher *Ra* and lower CCT compared to blue chips combined with a $YAG:Ce^{3+}$-based white LED.

Acknowledgment

This research was supported by the National Science Council of Taiwan under Contract no. NSC98-2113-M-009-005-MY3 (T.M.C.).

References

[1] S. Yuan, X. Chen, C. Zhu, Y. Yang, G. Chen, Opt. Mater. 30 (2007) 192.
[2] V. Bachmann, C. Ronda, A. Meijerink, Chem. Mater. 21 (2009) 2077.
[3] K. Zhang, W.B. Hu, Y.T. Wu, H.Z. Liu, Inorg. Mater. 44 (2008) 1218.
[4] H.S. Jang, Y.H. Won, D.Y. Jeon, Appl. Phys. B 95 (2009) 715.

[5] A.A. Setlur, W.J. Heward, Y. Gao, A.M. Srivastava, R.G. Chandran, M.V. Shankar, Chem. Mater. 18 (2006) 3314.
[6] M. Batentschuk, A. Osvet, G. Schierning, A. Klier, J. Schneider, A. Winnacker, Radiat. Meas. 38 (2004) 539.
[7] C. Guo, L. Luan, X. Ding, D. Huang, Appl. Phys. A 91 (2008) 327.
[8] Y.C. Chiu, W.R. Liu, C.K. Chang, C.C. Liao, Y.T. Yeh, S.M. Jang, T.M. Chen, J. Mater. Chem. 20 (2010) 1.
[9] E.V. Sokolova, Y.K. Kabalov, Can. Mineral. 37 (1999) 83.
[10] ICSD file no. 56962.
[11] T.W. Kuo, C.H. Huang, T.M. Chen, Opt. Express 18 (2010) A231.
[12] C.H. Huang, T.M. Chen, Opt. Express 18 (2010) 5089.
[13] C.H. Huang, T.M. Chen, W.R. Liu, Y.C. Chiu, Y.T. Yeh, S.M. Jang, Appl. Mater. Interface 2 (2010) 259.
[14] C.C. Lin, R.S. Liu, Y.S. Tang, S.F. Hu, J. Electrochem. Soc. 155 (2008) J248.